International Journal of Engineering Research and Applications (IJERA) ISSN: 2248-9622
National Conference on Advances in Engineering and Technology
(AET- 29th March 2014)

RESEARCH ARTICLE OPEN ACCESS

Thermal Performance of Flat-Plate Collector: An Experimental Study

Sunita Meena*, Chandan Swaroop Meena**, V.K.Bajpai***
* (Department of Mechanical Engineering, NIT Kurukshetra, Haryana-136119
Email: sunitameena2008@gmail.com)
** (Department of Mechanical Engineering, NIT Kurukshetra, Haryana-136119
Email: chandanswaroop2008@gmail.com)
*** (Professor, Department of Mechanical Engineering, NIT Kurukshetra, Haryana-136119
Email: vkbajpai@yahoo.com)

ABSTRACT
The analysis of thermal performance of the flat-plate collector includes parameters such as solar intensity, ambient temperature and configuration of flat-plate collectors etc. In this paper, the effect of the parameter $(T_i-T_a)/I_T$ on thermal performance of glazed flat-plate solar collector was experimentally analyzed for water heating application in winter climatic condition. The flat-plate collector consists of the total surface area 2.23 m^2 and the copper tubes are integrated beneath the absorber plate. The plate has a selective coating with high absorptivity of 92% and the heat transfer fluid flowing in the tubes is R-134a. In the paper, evaluation of useful heat gain or collector efficiency has been done. It is based on steady state analysis and by calculating the thermal performance of liquid flat-plate collector. Results show that the flat-plate collector gives good performance and provide a desire quantity of hot water.
Keywords **–** Flat-plate collector, solar energy, thermal performance, collector efficiency.

I. INTRODUCTION

Most domestic water heaters generate heat by consuming fuel or through electricity. These water heaters are usually simple, but not desirable in view of energy utilization efficiency as well as due to their environmental impact. Whereas the solar assisted heat pump (SAHP) is a promising means of reducing the consumption of none replenish able energy resources. The idea of the combination of heat pump and solar energy has been proposed and developed by many researchers around the world [1] [2] [3] [4]. The SAHPs that were proposed could be differentiated as direct expansion solar assisted heat pump and indirect solar assisted heat pump [5] [6] [7] [8]. The various parameters that could be assessed are solar intensity, ambient temperature, configuration of flat-plate collector etc. [9] [10] [11]. This paper is focused on estimating the effect of parameter, i.e. $(T_i-T_a)/I_T$ on the thermal performance of glazed flat-plate collector. Many theoretical and experimental studies have been reported in the literature [12] [13] [14] [15].

II. NOMENCLATURE

List of symbols
A_c- area of collector, m^2
C_b- bond conductance, mK/W
D_o- tube outside diameter, m
D_i - tube inside diameter, m
F - Fin efficiency
F'- collector efficiency factor
g - width of bond ,m
h_w -wind heat transfer coefficient, W/m^2K
I_T -total incident solar radiation on the collector, W/m^2
k_P- thermal conductivity of absorber plate, W/(m K)
M- number of covers
Q_u- useful heat gain by collector, W
S -net solar radiation on the absorber, W/ m^2 K
T_a- ambient temperature, ^oC
T_i -inlet fluid temperature, ^oC
T_p -temperature of absorber plate, ^oC
U_L -overall heat coefficient loss, W/ m^2K
U_t- top loss coefficient, W/m^2K
U_b- bottom loss coefficient, W/m^2K

U_e- edge loss coefficient, W/m^2K
V -wind velocity, m/s

Greek symbols
α -absorptivity
τ -transmissivity
η -efficiency
β -inclination angle of collector, ^{o}
ε_p -emissivity of absorber plate

ε_c -emissivity of glass cover

Subscripts
a -ambient
c -collector
f -fluid
i –inside/inlet
T- total
o- outside
u- useful

III. Experimental Setup

The main component of DX-SAHPWH is a single glazed flat plate collector which works as an evaporator, a reciprocating compressor, a condenser cum hot water storage tank and an expansion device. The schematic diagram of the experimental set up is shown in fig1.

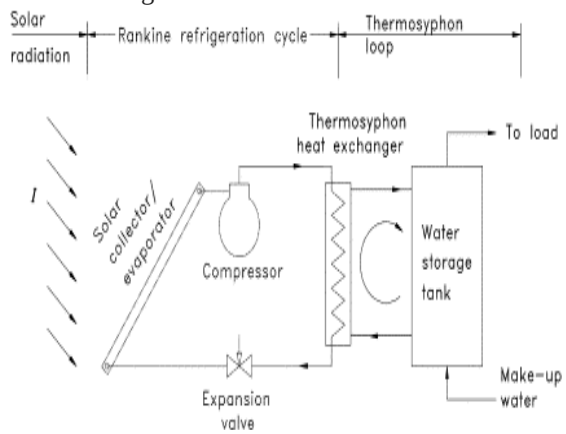

Fig.1: Direct Expansion Solar Assisted Heat Pump System

IV. Glazed Flat-Plate Collector

In this paper, the study is on a flat-plate collector having collector area as equal to 2.23 m^2. The geometric dimensions for the collector are 1.83m × 1.22m. The collector absorber plate is a copper plate, 0.3 mm thick, with its surface painted with high absorptive matt-black paint.

Fig. 2: Flat-Plate Collector Used in Experiment

The length of serpentine copper tube was 6.4 m. and outside diameter of 11 mm was soldered to the backside of the copper plate, with a pitch between tubes as 100 mm as shown in Fig 2. The absorber plate is encased in 50 mm resin bonded glass wool, retaining the collector's heat. The single-pane 4 mm tempered patterned or clear solar glass has a high solar transmittance up to 92% and excellent durability. The strength of toughened glass is about eight times of that of the common glass. The collector has faced south at an angle of inclination of 45°.

V. Energy Flow in The Collector

The efficiency of a solar collector depends on the ability to absorb heat as well as on the loss of heat from the absorber plate to ambient.

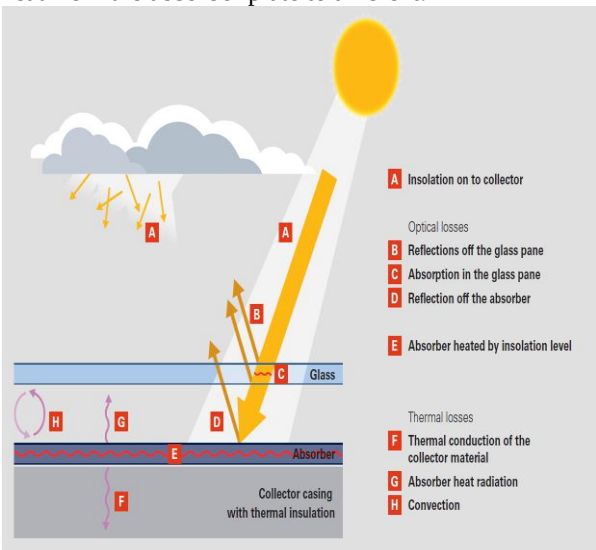

Fig.3. Energy Flow in the Collector [19]

The solar radiations are incident on the collector cover and then on absorber plate. Thus transmittance of heat is through the collector cover (glass cover) and the very same is absorbed by absorber plate as shown in Fig 3. Firstly the short wavelength radiation enters through the cover, then the convection losses occur between the plate and the glass cover, and after which conduction occurs due to the thickness of glass cover and finally radiation losses occur from the cover to the ambient. The distance between absorber and cover glass is important to minimize the heat losses due to convection and conduction.

VI. Thermal Performance of Flat-Plate Collector

The flat-plate collector, without any sun tracking utilizes beam and diffuse radiation. Thermal performance of flat plate collector can be evaluated by

$$Q_u = F'A_c\left[(\tau\alpha)I_T - U_L(T_i - T_a)\right] \quad (1)$$

Where A_c is the area of collector, F' is collector efficiency factor, τα transmittivity-absortivity product, I_T total solar intensity on flat plat collector, U_L overall heat loss coefficient, $(T_i-T_a)$is the temperature difference between inlet fluid temperature of collector and ambient temperature [16] [17].

$$U_L = U_t + U_b + U_e \quad (2)$$

The empirical relation of U_t is given by the klein [17].

$$U_t = \left[\frac{M}{\left(\frac{C}{T_P}\right)\left\{\frac{T_P - T_a}{M+f}\right\}^e} + \frac{1}{h_w}\right]^{-1} + \left[\frac{\sigma\left(T_P^2 + T_a^2\right)\left(T_p + T_a\right)}{\left(\varepsilon_p + 0.059Mh_w\right)^{-1} + \left\{\frac{\left(2N + f - 1 + 0.133\varepsilon_p\right)}{\varepsilon_g}\right\} - M}\right] \quad (3)$$

$$f = \left(1 + 0.089h_w - 0.116h_w\varepsilon_p\right)\left(1 + 0.07866M\right)$$

$$e = 0.43\left(1 - \frac{100}{T_P}\right)$$

$$C = 520\left(1 - 0.000051\beta^2\right) \quad for\, 0 < \beta < 70°$$

$$h_w = 5.7 + 3.8V \quad (4)$$

$$F' = \left[\frac{\frac{1}{U_L}}{W\left[\left(\frac{1}{U_L[D_o + (W - D_o)F}\right) + \frac{1}{C_b} + \frac{1}{\pi D_i h_{fi}}\right]}\right] \quad (5)$$

Where:

$$F = \frac{\tan h\left[m(W - D_o)/2\right]}{[m(W - D_o)/2]} \quad (6)$$

$$m = \sqrt{U_L / k_p\delta_p}$$

$$\eta = \frac{Q_u}{A_c I_T} \quad (7)$$

VII. Results

As shown in Fig 4, the solar radiation pattern for clear days increases from morning to noon and after that decreases from noon to evening. The experimental study revealed that with the decrease in parameter $(T_i-T_a)/I_T$ corresponding collector efficiency increases shown in Fig 5.

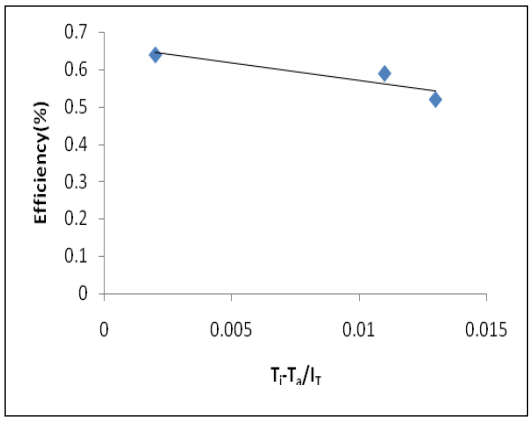

Fig. 4: Solar intensity Versus Time of The Day

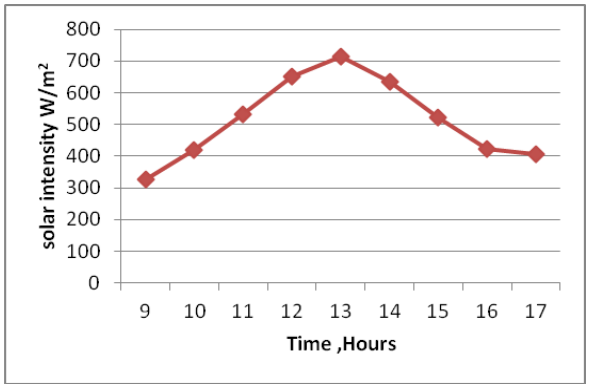

Fig. 5: $(T_i-T_a)/I_T$ versus Collector Efficiency

The collector efficiency η is plotted against $(T_i-T_a)/I_T$. The slope of this line (- F' U_L) represents the rate of heat loss from the collector.

VIII. Conclusion

This paper shows that Flat plate collector's efficiency is strongly influences by the parameter $(T_i-T_a)/I_T$, as this parameter increases collector efficiency decreases and in present study collector efficiency varies from 52%-64% with single glazed flat-plate collector when solar intensity varies from 523-710W/m^2.

References

[1] Freeman TL, Mitchell JW, Audit TE, "Performance of combined solar-heat pump systems", *Solar Energy, 22 (1), 1979, 125–135.*

[2] Macarthur JW, "Theoretical analysis of the dynamic interactions of vapor compression heat pump", *Energy Conversion Management, 24 (1), 1984, 49–66.*

[3] Duffie JA, Beckman WA, "Solar Engineering of Thermal Process", *Wiley, Inc. New York, 1991*.

[4] Kaygusuz K, Comaklio Ayhan T., "Solar-assisted heat pump systems and energy storage", *Solar Energy, , 47 (1), 1991, 383–391*.

[5] Chaturvedi SK, Chiang YF, Roberts AS, "Analysis of two-phase flow solar collectors with application to heat pumps", *Journal of Solar Energy Engineering, 104 (1), 1982, 358–365.*

[6] Morgan RG, "Solar assisted heat pump", *Solar Energy, 28(1), 1982, 129–135.*

[7] O'Dell MP, Mitchell JW, Beckman WA., "Design method and performance of heat pumps with refrigerant- filled solar collectors", *Journal of Solar Energy Engineering, Transaction of the ASME, 106 (1), 1984, 159–164*.

[8] Chaturvedi SK, James Shen Y, "Thermal Performance of a direct expansion solar-assisted Heat pump", *Solar Energy, 33 (1), 1984, 155–162.*

[9] Chaturvedi SK, Abazeri M., "Transient Simulation of a capacity-modulated, direct Expansion, solar-assisted heat pump", *Solar Energy, 39 (1), 1987, 421–428.*

[10] Morrison GL., "Simulation of packaged Solar heat-pump water heaters", *Solar Energy, 53 (1), 1994, 249–257*.

[11] Chaturvedi SK, Chen DT, Kheireddine A.,"Thermal performance of a variable capacity direct expansion Solar assisted heat pump", *Energy Conversion and Management, 39 (1), 1998, 181–191*.

[12] Axaopoulos P, Panagakis P, Kyritsis S.,"Experimental comparison of a solar-assisted heat pump and conventional thermosyphon solar system", *International Journal Energy Research 22 (1), 1998, 1107–1120.*

[13] Hawlader MNA, Chou SK, Ullah MZ., "The performance of a solar assisted heat pump water heating system", *Applied Thermal Engineering, 21 (1), 2001, 1049–1065.*

[14] Huang B. J., Chyng J. P., "Performance Characteristic of integral type solar-assisted heat pump", *Solar Energy, 71 (1), 2001, 403–414.*

[15] X.Q. Kong, D. Zhang, Y. Li, Q. Yang, "Thermal performance analysis of a direct-expansion solar-assisted heat pump water heater", *Energy, 36 (1), 2011, 6830-6838.*

[16] Hottel, H. C. and Whillier, A., "Evaluation of flat plate collector performance", *Trans. of the Conference on the Use of Solar Energy, 2 (1), 1958, 1- 14.*

[17] Bliss, R. W., "The derivations of several plate efficiency factor useful in the design of flat plate solar heat collectors", *Solar Energy, 3 (4), 1959, 55-64*.

[18] S. A. Klein, "Calculation of flat plate loss coefficients", *Solar Energy 17 (1), 1975, 79-80*.

[19] "Technical Guide – Solar Thermal Systems", *Viessmann GmbH, 2009.*

International Journal of Engineering Research and Applications (IJERA) ISSN: 2248-9622
National Conference on Advances in Engineering and Technology
(AET- 29th March 2014)

RESEARCH ARTICLE OPEN ACCESS

Comparative Investigation of Mechanical Properties of Aluminium Based Hybrid Metal Matrix Composites

Dinesh Kumar*, Jasmeet Singh**
*(Research scholar, Department of mechanical engineering, Punjab Technical University, Jalandhar-144601
Email: dineshranjha@gmail.com)
** (Assistant Professor, Department of Mechanical engineering, Punjab technical University, Jalandhar-144601
Email: jasmeet_singh23@rediffmail.com

ABSTRACT
Aluminium alloys are widely used in automobile industries and aerospace applications due to their great mechanical properties, low density, low coefficient of thermal expansion, better corrosion resistance and wear as compared with conventional metals and alloys. The low production cost and better mechanical properties of composites makes them very useful for various applications in many areas from technological point of view. The aim involved in designing aluminium based metal matrix composite by combining different percentage of particulates in the mixture. Present study is focused on the fabrication of two aluminium 6063 based metal matrix composites. One reinforced with silicon carbide, graphite and second reinforced with silicon carbide, boron carbide by stir casting technique. The percentage of each reinforcement particulate is kept 10% in two composites. The various mechanical tests like tensile strength test, ultimate tensile strength test, flexural test & hardness test performed on the samples obtained by stir casting technique for comparison purpose. The result indicated that the developed method is quite successful and there is an increase in the value of tensile strength, ultimate tensile strength, hardness value and flexural strength of newly developed composite having SiC and B4C particulates in comparison to the SiC, graphite reinforced composite.
Keywords **-** Aluminium 6063, SiC, B_4C, Graphite, Metal matrix composite, stir casting.

I. INTRODUCTION

The challenge and demand for developing metal matrix composites for use in high performance structural and functional applications including aerospace industries, automobile sector, defence etc. have significantly increased in the recent times [1]. The need to develop new materials with combinations of low density, improved stiffness and high strength in order to overcome the limitations of existing high-strength aluminum alloys and titanium alloys improved the design procedures and has resulted to achieve improvements in overall efficiency, reliability and performance by reducing either absolute weight or increases in strength-to-weight ratio. For this purpose the materials of high ultimate tensile strength, high stiffness, yield strength and low density is required.

Metal-matrix composites consist of at least two components. Among two components one is matrix phase usually a continuous phase like aluminium, magnesium & second component is discontinuous phase like fibers, whiskers or particles called reinforcement. The objective of developing metal matrix composite materials is to combine the desirable properties of metal and particulates. The matrix holds the reinforcement to form the desired shape & reinforcement improves most of the mechanical properties of composite. Aluminium metal matrix composites are preferred over other materials due to its properties like greater strength, improved stiffness, reduced density, improved temperature properties, controlled thermal expansion and improved wear resistance.

Based on the literature survey it has been observed that the application scope for aluminium based metal matrix composite is expanding. For the fabrication of AMCs on an industrial scale the technique used can be either solid state processing or liquid state processing. The liquid state processing technique especially stir casting is a promising method for the production of AMCs because of their simplicity and ease of manufacture [5]. The aim involving of this study are the fabrication of two hybrid composites and then investigating the comparative mechanical properties like tensile strength, ultimate tensile strength, hardness, flexural strength. Some of the authors have carried out the research work on different composites and their mechanical properties.

An experiment to investigate the mechanical behavior of aluminium 6063 reinforced with Al_2O_3 alumina fabricated by stir casting method is performed [3]. The reinforcement volume percentage was taken as 0%, 6%, 9%, 15% and 18% in the metal

matrix composites. The results revealed that the mechanical properties like tensile strength, yield strength, hardness values of composites increased with increase in alumina volume percentage while the fracture toughness was found to be decreased. Further the porosity level less than 3.6% was found in AL6063/Al_2O_3 metal matrix composites.

In [4], authors fabricate the aluminium based metal matrix composite by stir casting technique & further investigated the mechanical properties of composites. In this experiment aluminium 6063 was taken as base metal & aluminium oxide Al_2O_3 as reinforcement. The results showed that aluminium composite was superior to the base alloy AL6063. Further with increase in weight percentage of reinforcement particles in composite the mechanical properties like tensile strength, impact strength, hardness & yield strength improved and elongation decreased which confirms that alumina addition increases brittleness. A fairly distribution of reinforcement particles were found in the composite.

In [2], authors performed an experiment for the fabrication of aluminium-boron carbide metal matrix composite with stir casting technique & further investigated the mechanical properties. In this experiment aluminium LM6 alloy was taken as base metal & different percentage (0%, 2.5%, 5%, and 7.5%) of boron carbide as reinforcement. The results revealed that with increase in weight percentage of reinforcement particles in MMC, the ultimate compressive strength, hardness increased and density decreased.The scanning electron microscopy indicated the uniform distribution of reinforcement particles in the metal matrix composites.

II. MATERIALS USED

2.1 Metal Matrix Material: In the present experimental investigation the matrix material used is an aluminium alloy (6063) whose chemical composition (in weight %) is listed in Table 1. Al6063 is precipitation hardening aluminium alloy, containing Magnesium and Si as its major alloying elements. It has good mechanical properties. The melting point of aluminium 6063 is low (710°C).

Table 1: Chemical composition of AL 6063 Alloy

Constituents	%age
Si	0.45
Fe	0.22
Cu	0.02
Mn	0.03
Mg	0.50
Zn	0.02
Cr	0.03
Ti	0.02
Balance	Al

2.2 Reinforcement Material: The role of the reinforcement in a composite material is fundamentally to increase the mechanical properties of composite. The reinforcements used in the experimental investigation are:

Silicon Carbide: It is originally produced by a high temperature electro-chemical reaction of sand and carbon. The property of Silicon Carbide includes good mechanical properties with low density, high temperature strength and thermal shock resistance, highly wear resistant. Silicon carbide is a compound of silicon and carbon with chemical formula SiC. Silicon carbide is an excellent abrasive and has been produced and made into grinding wheels and other abrasive products. Today the material has been developed into a high quality technical grade ceramics. It is used in abrasives, refractories, ceramics, and other high-performance applications

Boron Carbide: The boron carbide is one of the hardest material [8]. It is produced by reacting carbon with B_2O_3 in an electric arc furnace. For commercial use the boron carbide powers are milled and then purified to remove the metallic impurities. The density of B_4C is 2.52 g/cm^3, melting point is very high up to 2445°C and hardness is 2900-3500.

Graphite: It is the most stable form of carbon under standard condition. Carbon exists in two crystalline allotropic forms one is diamond and second is graphite. The properties of graphite are listed in table 2.

Table 2: Properties of Graphite used as reinforcement

Properties	Porosity (%)	Bulk density (g/cm)	Flexural strength (mpa)
values	0.7-53	1.3-1.9	6.9-100

III. EXPERIMENTAL METHODOLOGY

The fabrication of metal matrix composite used in the present study is carried out by stir casting method. A stir casting setup consists of a resistance muffle furnace and a stainless steel stirrer which is connected to a variable speed vertical motor arrangement with range of 80 to 890 rpm by means of a steel shaft as shown in figure 1. Stir casting is the simplest and the most economical method for the fabrication of metal matrix composite [7]. In this present experimental method the molten aluminium matrix metal AL6063 is melted at a definite temperature nearby 710°C in the muffle furnace and then a preheated reinforcement material with a (wt %

of 10% each of SiC and Gr for first sample and SiC and B4C for second sample) is mixed with molten alloy & then stirrer is used to mix the mixture. In order to achieve the uniform properties of the composite, the distribution of the reinforcement material in the matrix alloy must be maintained.

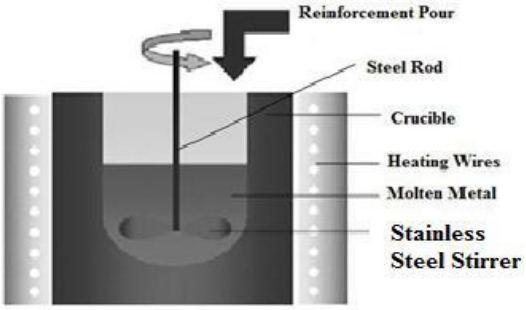

Fig.1: Stir Casting Technique

The inert gas (nitrogen) is used to prevent the oxidation of mixture. The mixed molten MMC is then poured into a mould & is then allowed for the solidification for some time. The schematic diagram shows various parts of stir casting machine as well as process.

IV. RESULT & DISCUSSION

For the nomenclature of samples the sample having composition Al6063/10% SiC/10% Gr is names as specimen A and the sample having composition Al6063/10% SiC/10% B_4C is names as specimen B

4.1 Tensile strength

The tensile testing was done on FIE make universal testing machine UTE-100 in Industrial Development Cum Facility Centre CITCO Chandigarh. For the identification purpose of two samples of composite materials the sample having AL6063/10%SiC/10%Gr composition is named as specimen A and sample having AL6063/10%SiC/10%B_4C composition is named as Specimen B. The tensile testing results are shown in the table 3 and figure 2.

Table 3: Tensile Testing Results of Two Composite Samples

Sr. No.	Samples	Tensile Strength (N/mm^2)	Percentage Elongation (%age)
1	Specimen A	10.4	31.250
2	Specimen B	11.8	12.500

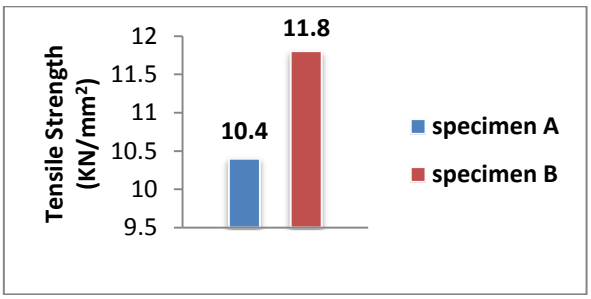

Fig 2: Comparison of Tensile Strength

4.2 Ultimate Tensile Strength

The ultimate tensile strength is the maximum engineering stress level in tensile test or it is the ability of material to withstand before fracture. The maximum load taken by the test specimen is measured in terms of its ultimate tensile strength against fracture. In stress-strain diagram the ultimate tensile strength is the highest point where curve line is flat and shown at the end of elastic portion or very close to the elastic limit. In case of ductile materials the stress hardening occurs and stress continue to increase until breaking of specimen but stress- strain curve may show decline in stress level before fracture. This is due to the reason that engineering stress is based on the original cross section and it commonly not accounts the fracture occurs in the specimen. For the design of components UTS is an important parameter [9]. It is easy to determine and is quiet reproducible. The ultimate tensile strength is useful for the specification and quality control of the components and parts in design problems. The ultimate tensile testing results are shown in table 4 and figure 3.

Table 4: Ultimate tensile strength results of two composites

Sr. No.	Nomenclature of samples	Maximum Force (KN)
1	Specimen A	22.450
2	Specimen B	28.250

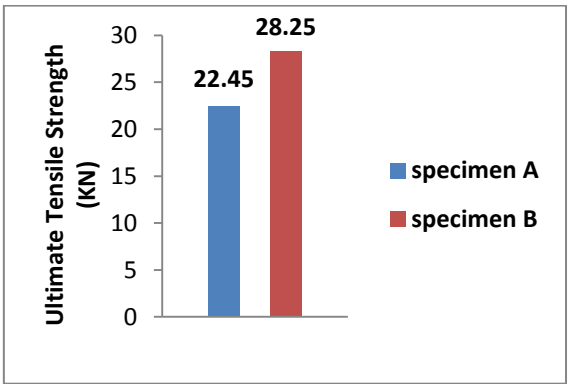

Fig 3: Comparison of Ultimate Tensile Strength

4.3 Hardness Measurement

Hardness test was carried out at room temperature using Vickers hardness tester with at least three indentations of each sample and then the average values were utilized to calculate hardness number [6]. Load used on Rockwell's hardness tester 150 Kg at dwell time of 20 sec. for each sample. The hardness of MMCs of specimen B increases with addition of SiC and B_4C of particulate in the matrix. The added amount of SiC & B_4C particles enhances hardness, as these particles are harder than Al alloy, which render their inherent property of hardness to soft matrix as shown in Table 5 and Figure 4.

Table 5: Hardness Test Results of Two composites

Sr. No	Samples	HV 1	HV 2	HV 3	Average HV
1	Specimen A	41.2	40.5	41.5	41.0
2	Specimen B	49.5	48.9	49.2	49.2

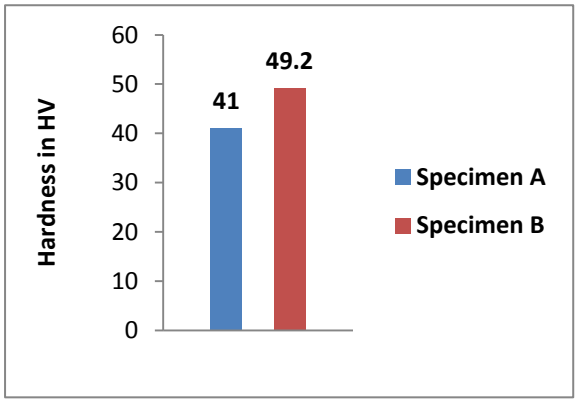

Fig 4: Comparison in terms of Hardness

4.4 Three Point Bending Test

In order to observe the fracture behavior of aluminium based metal matrix composites of different composition of reinforcement particulates the three point bending test or flexural test is performed. This method is also called transverse beam test for materials subjected to simple beam loading.

Table 6: Flexural Strength Test Results of two composites

Samples	Area of specimen mm^2	Max. Force KN	Flexural Strength KN/mm^2
Specimen A	160.14	22.450 KN	0.017
Specimen B	226.65	28.250 KN	0.030

The Flexural test measures the force required to bend the specimen under three point loading conditions as shown in Table 6 and Figure 5. The data is used to select those materials that will support loads without flexing. The specimen deflection is measured by crosshead position and results can also be plotted on stress-strain curve. This test includes flexural strength and flexural modulus. Flexural modulus is used as an indication of a material's stiffness when it is flexed.

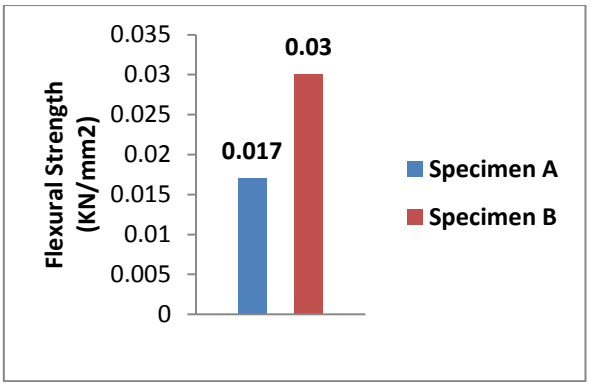

Fig 5: Comparison in terms of Flexural Strength

V. CONCLUSION

Aluminium based metal matrix composites are successfully fabricated by stir casting technique with fairly uniform distribution of Silicon Carbide, graphite in specimen A and silicon carbide, boron carbide in specimen B.

The tensile strength of specimen B is much greater than specimen A which revealed that specimen B is much stronger than specimen A

The ultimate tensile strength of specimen B is found to be more than the specimen A. it means that the load required to break the specimen having composition of silicon carbide, boron carbide is more than the specimen having composition of silicon carbide, graphite.

The hardness of specimen B is more than the specimen A. So the specimen B can be used where material hardness is an essential parameter.

The flexural strength of specimen B is more than that of specimen A. This indicated that specimen B can withstand against heavy loads conditions.

Applications of Aluminium MMCs: The composites can be used in automobiles parts of cars, trucks etc in the internal parts of engine. Also they can be used in turbines, aerospace industries, submarines in defence, tanks etc where high strength to weight ratio is an essential requirement.

REFERENCES

[1] Sandeep Kumar Ravesh , T.K. Garg , "Preparation And Analysis for Some

Mechanical Property of Aluminium Based Metal Matrix Composite Reinforced With Sic And Fly Ash", International Journal Of Engineering Research And Applications 2012, 2(6), 727-731.

[2] S Rama Rao , G Padmanabhan , Fabrication And Mechanical Properties of Aluminium-Boron Carbide Composites", International Journal Of Materials And Biomaterials Application, 2012, 2(3), 15-18.

[3] K. K. Alaneme K, M.O Bodunrin, "Mechanical Behavior of Alumina AA6063 Metal Matrix Composite Developed by Two-Step Stir Casting Processs", ACTA Technica Corviniensis-Bulletin of Engineering 2013, 3(1), 105-110.

[4] Ajay Singh, Love Kumar, Mohit Chaudhary, Om Narayan , Pallav Sharma , Piyush Singh, Kandpal Bhaskar Chandra Kandpal, Som Ashotosh, "Manufacturing of AMMCS using stir casting process and testing its mechanical properties", International Journal Of Advance Engineering Technology 2013, 4(3), 26-29.

[5] Bharath V, Mahadev nagaral, V Auradi , "Preparation, characterization and mechanical properties of Al_2O_3 reinforced 6061Al particulate MMC's", International journal of engineering research and technology, 2012,1(6), 1-6.

[6] Gopal Krishna, KV Sreenivas Rao, B vasudeva ,Effect of percentage reinforcement of B4C on the tensile property of aluminium matrix composites, International journal of mechanical engineering and robotics research 2012, 1 (3), 290-295.

[7] J Jenix rinol, D chandramohan , K.S sucitharan " An overview on development of aluminium metal matrix composites with hybrid reinforcement" International journal of science and research, 2012, 12 (3), 196-203.

[8] X.G Chen, M DaSilva , P Gougeon, L St-Georges, "Microstructure and mechanical properties of friction stir welded AA6063–B4C metal matrix composites", Journal of material science & engineering, 2009, 174-184.

[9] K Asif Chandra and P.S.Misra, "Development of aluminium based hybrid metal matrix composites for heavy duty applications", Journal of minerals & materials characterization & engineering 2011, 10 (14), 1337-1344.

International Journal of Engineering Research and Applications (IJERA) ISSN: 2248-9622
National Conference on Advances in Engineering and Technology
(AET- 29th March 2014)

RESEARCH ARTICLE OPEN ACCESS

Application of Taguchi Approach in the Optimization of Cutting Parameters in Micro-Ultrasonic Drilling Process

Vivek Jain
Mechanical Engineering Department, Thapar University, Patiala
E-mail: vivek.jain@thapar.edu,

ABSTRACT
In the present research work, effect of several process parameters on the machining characteristics of borosilicate glass has been reported. The machining characteristics that are being investigated are material removal rate (MRR) and tool wear rate (TWR). Four different process parameters were considered for this study - power rating of the machine, static load, slurry concentration and abrasive grit size. The optimal settings of parameters were determined through experiments using Taguchi method. The significant parameters were identified and their effects on MRR and TWR were studied. The analysis reveals that, in general, the MRR is most influenced by the static load while abrasive size mainly affects the TWR.
Keywords: micro ultrasonic drilling, glass, material removal rate, tool wear rate, optimization

I. INTRODUCTION

Glass, as a substance, plays an important role in modern civilization. High hardness and near inertness of this materials makes it extremely useful in numerous scientific and industrial applications. Its chemical, physical, and in particular optical properties make it suitable for applications such as flat glass, container glass, optics and optoelectronics material, laboratory equipment, thermal insulator (glass wool), reinforcement materials and glass art. Although vast majority of microdevices are made of silicon but for many applications silicon is not an appropriate base material where glass can be a suitable replacement. Owing to superior material properties of glass like transparency, mechanical robustness and chemical resistance the usage of glass for micro mechanical, micro fluidic and micro optical microelectro mechanical system (MEMS) devices is fast emerging [1]. MEMS applications where micro-machined glass is used include: sensors, such as those incorporating pressure, accelerometer, gyroscope transducers, BioMEMS devices enabled by lab-on-chip and micro fluidics technologies and spacers for cell phone cameras.

As the desire to use glass in the MEMS industry increases, the need to develop better processing/machining methods of this material in the micro domain also increases. In addition, as the diversity of MEMS applications expands, the desired features continue to get smaller, denser and more intricate. At present, the available processing technologies for structuring glass substrate are often restricted. In general, glass is considered as one of the difficult-to-cut material. Processing brittle glass with computer numerical control (CNC) supported cutting processes like scribing or milling leads to rough surfaces. Because of the small dimensions of microstructures subsequent polishing steps cause exceeding efforts. Photo resist structures can be transferred into the underlying glass substrate with reactive ion etching (RIE). Due to low etch rate, the structure depth is limited. Laser machining creates subsurface micro-cracks and also creates a HAZ (Heat Affected Zone) which results in a kerf or damaged area at the top surface of the hole [2]. Since it is a thermal process, laser machining can crack or break thin glass pieces. It is difficult to create blind holes or remove material with a fixed depth across a large area with a laser, as it creates an uneven etching as it progresses across the part.

Ultrasonic Machining (USM) could be another alternative machining process that can be applied commercially to machining of glass. The process is known to be free from major adverse effects associated with micromachining. The micron sized holes used in MEMS can be achieved with the help of micro ultrasonic drilling (MUSD). In MUSD, removal of material is accomplished by the abrading action of grit-loaded slurry circulating between the workpiece and a tool [3]. The contributing mechanisms in MUSD can be summarized into four categories as (i) micro chipping by impact of the free moving abrasive particles (ii) mechanical abrasion by the abrasive particles against the work piece surface (iii) cavitation effects in liquid agitated by ultrasonic vibration (iv) chemical actions associated with the liquid being employed. However, a reasonable understanding of the mechanisms is yet to mature. Influence of the whole range of parameters on the

process performance is also not explored exhaustively.

A well planned set of experiments in which all parameters of interest are varied over a specified range is a much better approach to obtain systematic data. Mathematically speaking such a set of experiments is complete and ought to give desired results. Taguchi has developed a method of conducting experiments based on "orthogonal array" which gives much reduced "variance" for the experiment with "optimum settings" of control parameters. Thus the marriage of 'design of experiments (DOE)' with optimisation of control parameters to obtain the best results is achieved in the Taguchi Method. Orthogonal Arrays (OA) provide a set of well balanced (minimum) experiments, while Taguchi's Signal-to-Noise ratios (S/N), as objective functions for optimisation, help in data analysis and prediction of optimum results [4].

The machining performance of ultrasonic machining has been investigated by a few researchers using DOE techniques. In [5], authors investigated the tool wear rate in ultrasonic drilling of engineering ceramics. The effect of five important process variables - workpiece material, tool material, grit size of the abrasive, power rating and slurry concentration on oversize, out-of-roundness and conicity of hole was computed using Taguchi's L-27 OA. It was concluded that all of these input variables significantly affect the quality characteristics except slurry concentration in case of out-of-roundness and conicity. In [6], authors modelled the material removal rate during ultrasonic machining of titanium and its alloys using Taguchi approach. Relationships between material removal rate and other controllable machining parameters (power rating; tool type; slurry concentration; slurry type; slurry temperature and slurry size) was deduced using Taguchi technique. The results suggested that ultrasonic power rating significantly improves the material removal rate with contribution of 28%, followed by type of tool with contribution of 24.6%. The third significant factor was type of slurry with contribution of 13.3%. The remaining three input parameters, namely slurry concentration, slurry grit size and temperature were in-significant. Same approach was used using different orthogonal arrays by other authors [7] [8] [9] [10] and results were discussed while machining with macro or rotary ultrasonic machining. With micro USM, the influence of machining load on machining rate and tool wear has been reported [11]. Machining rate as well as tool wears increases with the increase in machining load. This is because of debris accumulation at the bottom of the hole. Some studies on possible effect of tool geometries on machining rate and tool life were also carried out with micro USM [12]. The observed higher tool wear ratio in case of hollow tool is attributed to reduced contact area.

It has been observed from the published works that the Taguchi/DOE approach was used on macro USM and no effort has been made to investigate the machining performance on micro ultrasonic drilling process. The present work is an attempt to explore the machining characteristics of micro USD using Taguchi's L9 orthogonal array. Relationships between MRR, TWR and other controllable machining parameters (power rating; static load; slurry concentration and abrasive size) are deduced using Taguchi technique.

II. MACRO VS MICRO USD

Although micro USD germinated from macro USD, but the downsizing for micromachining requires exhaustive efforts and some changes in the process. This requires a micro sized tool (or tool feature), smaller amplitude, and micro sized abrasive particles. The static load should be in grams and vibration frequency must be more than 20 kHz. The major problem encountered with micro USD is the fabrication of micro tool and fixing it to the machine. Ultrasonic vibration of the machining head makes accurate tool holding difficult. Because of the size of the tool, the tool stiffness must be taken into consideration. 'Unit Removal' of sub-micrometer order is required when the object size is very small or when high precision of the product is required. Higher precision of the micromachining equipment is desired to reduce the dimensional error in proportion to the size of product [13]. A micro USD set up as shown in Figure 1 has been developed to investigate the feasibility of drilling on glass in micron domain. The micro tools are fabricated with the help of wire electric discharge grinding (WEDG) as shown in Figure 2. In WEDG the electrically conductive wire is travelling continuously and the cylindrical tool (workpiece) is rotating. Both the tool and workpiece are separated with a spark gap. Solid cylindrical tools having a circular cross section of 300 µm diameter made up of austenitic stainless steel were fabricated by this method.

III. EXPERIMENTAL PROCESS AND CONDITIONS

Ultrasonic machining is a non conventional process in which removal of material takes place mainly because of the impact forces generated by the vibrating tool on to the abrasive particles. The abrasives further hit the workpiece with high momentum energy and erode the surface. The frequency of the impacting tool head is above 20 kHz and amplitude is set in the range of 10 to 15µm. The

process is ideally suited for hard and brittle materials which are otherwise difficult to machine such as glass, ceramics etc.

Commercial borosilicate glass micro slides with 2 mm thickness were employed as workpiece material for the USD trials. Table 1 shows the experimental conditions and mechanical properties of the workpiece material. The experiments were carried out in an upgraded version of stationary Sonic- Mill machine (Model: AP-500) with a power output of 500 W and attached three axis motion controller unit. The power supply is equipped with an automatic frequency control and automatic load compensation unit that provides constant output amplitude at desired settings to meet the different energy requirement encountered during the operation cycles [14].

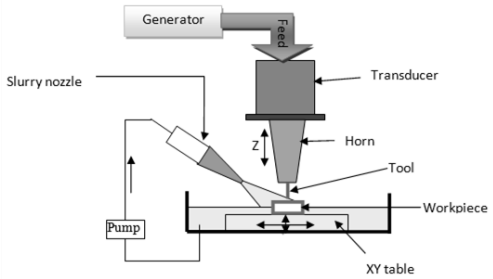

Fig 1: Schematic of A Micro USD Process

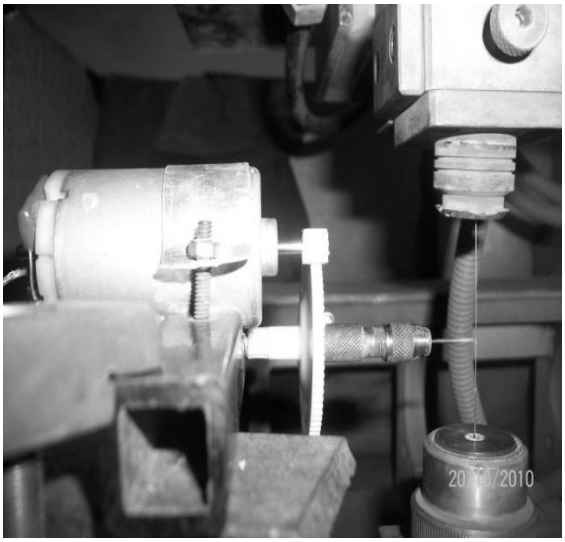

Figure 2: The Wedg Set-Up Used For Making Microtools

An electrostrictive PZT transducer converts the electric oscillations into mechanical vibrations in the frequency range of 20 kHz. Power rating in the range of 10% to 30% was used during the experiments. The static load applied on the horn was taken in the range of 100 g to 300 g throughout the experiments. A solid tool made up of austenitic steel having a circular cross section of 300 µm was used as cutting tool a schematic of which is shown in Figure 3. The material removal rate was determined by measuring reduction in weight of work piece and divided by time of drilling and respective densities of work piece. The tool wear rate was considered as the reduction in the length of tool in drilling the given depth of the hole to the time taken in drilling.

The tool wear length was calculated by the "Reference Point" method [15] and can be defined as the position difference in the Z axis when the reference point at the workpiece surface was touched by the tool tip before and after machining. Scanning electron microscopy was employed to characterize the micro mechanisms related to material removal under micro ultrasonic abrasion condition.

Table 1 Experimental Conditions

Work conditions		Description
Work material		Borosilicate glass micro slides 25 mm ⊠ 75 mm ⊠ 2 mm
Workpiece properties	Density (g/cm^3)	2.5
	E (GPa)	69
	H (GPa)	6.865
	K_{IC} ($MPam^{1/2}$)	0.7-0.8
Tool material		Austenitic steel, diameter 300 µm; length 7 mm
Abrasive used		Silicon carbide (SiC)
Frequency of vibration		20 - 30 kHz
Amplitude of vibration		10- 15 µm
Drilling Depth		2 mm
Tool Geometry		Conical with Straight cylindrical edge
Slurry Temperature		28° C (ambient room temperature)
Slurry Media		Water

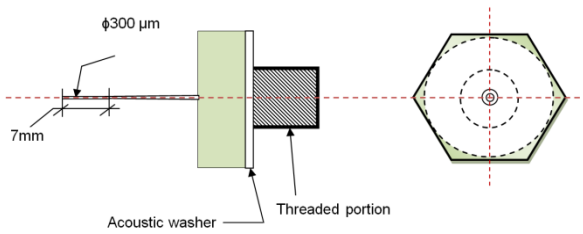

Figure 3: Schematic Of A Typical Micro Tool

IV. DESIGN OF EXPERIMENTS AND DATA ANALYSIS

The experimental layout for the machining parameters using Taguchi's L9 orthogonal array was used in this study. This array consists of four control parameters coded as A, B, C and D with three levels A_1, A_2, A_3, B_1, B_2, B_3, C_1, C_2, C_3 and D_1, D_2, D_3 as

shown in Table 2. In the method, most of the observed values were calculated based on 'higher the better' and 'smaller the better' criteria. Thus in this study, the observed values of responses MRR and TWR were set to maximum and minimum respectively. All the experiments were replicated twice; hence three trials were conducted at each experimental run. The output variables were recorded for each trial and then the results for each experimental run were averaged out to obtain the mean value of response variables (MRR, TWR) for that particular experiment. The experimental results are summarized in Table 3.

Optimisation of the observed values was carried out by comparing the standard analysis and analysis of variance (ANOVA) which was based on the Taguchi's method. In order to establish the relative significance of the individual factors, ANOVA was performed, both on raw data and on S/N data. Because of the ability of S/N data to reflect both the average effects and the variation in the results, ANOVA results based on S/N data are depicted here in Tables 4 and 5.

Table 2: Machining Parameters And Their Levels

Parameters	Factor	Level 1	Level 2	Level 3
Power rating (%)	A	10	20	30
Static load (g)	B	100	200	300
Slurry concentration (%)	C	30	35	40
Abrasive size (micron)	D	10	15	20

Table 3 Experimental Result/Matrix

S.NO.	MRR (mm^3/min)			S/N RATIO (dB)	TWR (mm/min)			S/N RATIO (dB)
	R1	R2	R3		R1	R2	R3	
1.	0.886	0.854	1.335	-0.29	0.191	0.193	0.198	14.25
2.	1.128	1.034	0.857	-0.12	0.305	0.302	0.302	10.38
3.	0.954	1.034	0.745	-1.07	0.328	0.285	0.265	10.64
4.	0.623	0.548	0.563	-4.80	0.267	0.267	0.269	11.45
5.	1.367	1.284	1.323	2.43	0.256	0.268	0.262	11.63
6.	0.879	0.895	0.979	-0.77	0.218	0.243	0.273	12.19
7.	0.942	0.989	0.953	-0.35	0.240	0.241	0.260	12.14
8.	1.756	1.241	1.412	3.08	0.331	0.288	0.301	10.24
9.	1.654	1.552	1.819	4.42	0.243	0.244	0.246	12.25

V. RESULTS AND DISCUSSION

5.1 Material removal rate

As S/N response takes into account both the magnitude as well as the variation in a response, the factor levels that correspond to the highest S/N ratio are termed as optimum. The main effects of four machining parameters (Power Rating, Static load, Slurry Concentration and Abrasive size) on MRR are shown in Figure 4. The variation of MRR with ultrasonic power rating is not uniform or linear; the MRR decreases with increase in power rating but after crossing certain level of power rating, MRR rises (corresponding to A_3=30%). This might be attributed to the relative low frequency of vibration at the starting which is insufficient to drag out the work material. Increased power causes high stresses in the impact zone and more material removal results.

The MRR increases with the increase in static load upto a value and then starts decreasing. This is in contrary with macro USM as in case of micro USM after a certain depth the cutting energy of abrasives diminishes because of insufficient recycling abrasive particles at the machining interface owing to accumulation of the debris (due to small size of the feature).

The use of high concentration of slurry and increase in abrasive size promotes the overall decrease in MRR. The reason lies in the puddle of slurry. The high concentration squeezes the movement of the tool and abrasive particles collide with each other causing loss of cutting energy and thus results in reduced MRR. The most important characteristic of the abrasive that highly influence the material removal rate is the grit size or grain size of the abrasive. Increase in abrasive size reduces the total number of abrasives in the cutting zone and thus reduces the MRR.

5.2 Tool wear rate

The machining characteristic TWR in micro ultrasonic drilling of glass have been found to be correlated and dependent upon the input parameters such as slurry concentration and grit size used. It can be observed (Figure 5) that TWR tends to increase sharply with a corresponding increase in the size of the grits. Coarser grits apply stronger impact on the surface of the tool and hence the rate of fracture increases. Use of high concentration of slurry results in high tool wear rate. Because of the choking of the tool movement at high concentration, the amputation of tool material starts instead of work piece material removal.

When tools of very small dimensions are used, the static load needs to be small to avoid breakage of the tool. The high static load imparts high pressure over the tool material and suppresses it.

As the load is increasing for a constant area, the stress produced will be more which results in easy and quick work hardening of the tool tip. This leads to an induced brittleness on the tool tip causing a favourable condition to be eroded by the deflected abrasives.

The tool wear rate (TWR) has been found to be nearly constant with a corresponding increase in power rating of the ultrasonic machine from 10% to 20%, the rate of increase being sluggish while the power rating is increased from 20% to 30%.

5.3 ANOVA Analysis

The ANOVA test summary for MRR and TWR has been recorded for S/N response Table 4 & Table 5. The percent contribution of each factor has been shown in Figure 6 & Figure 7.

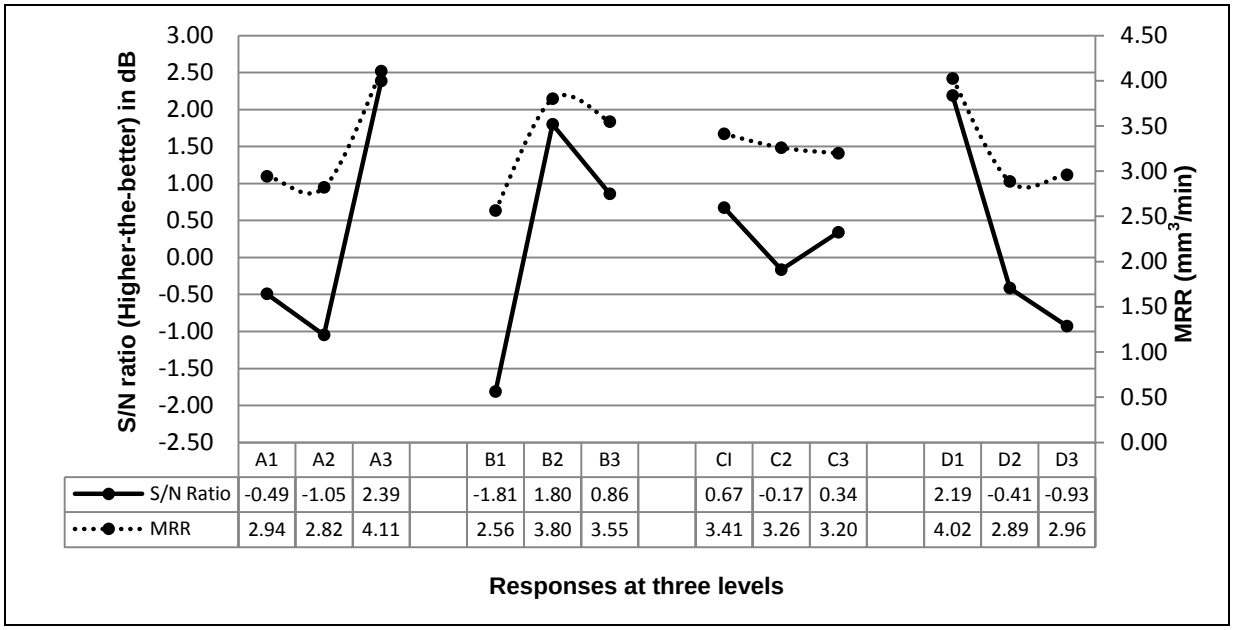

	A1	A2	A3	B1	B2	B3	CI	C2	C3	D1	D2	D3
S/N Ratio	-0.49	-1.05	2.39	-1.81	1.80	0.86	0.67	-0.17	0.34	2.19	-0.41	-0.93
MRR	2.94	2.82	4.11	2.56	3.80	3.55	3.41	3.26	3.20	4.02	2.89	2.96

Figure 4 Effect Of Process Parameters On Mrr Raw Data And S/N

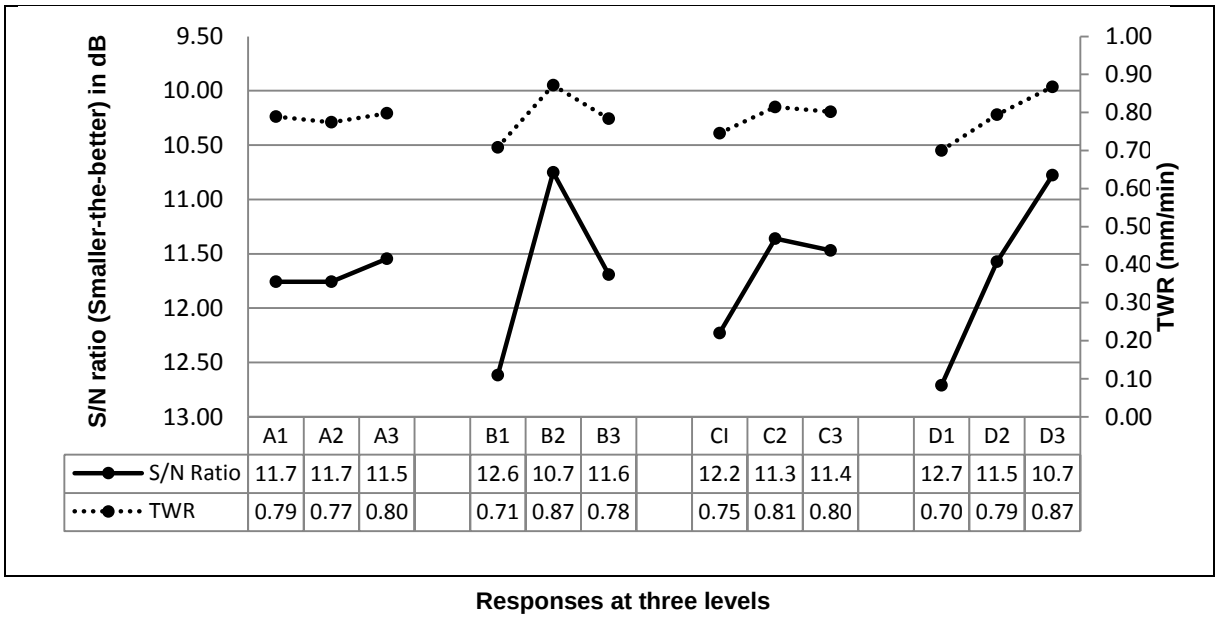

	A1	A2	A3	B1	B2	B3	CI	C2	C3	D1	D2	D3
S/N Ratio	11.7	11.7	11.5	12.6	10.7	11.6	12.2	11.3	11.4	12.7	11.5	10.7
TWR	0.79	0.77	0.80	0.71	0.87	0.78	0.75	0.81	0.80	0.70	0.79	0.87

Figure 5 Effect Of Process Parameters on TWR Raw Data And S/N

Table 4: MRR POOLED ANOVA RESULTS

Source	SS	DOF	V	Var ratio	SS'	P
Power rating	20.368	2	10.184	19.037	19.298	32.565
Static load	21.073	2	10.537	19.696	20.003	33.755
Slurry conc	1.070	2	**Pooled**	-	-	-
Abrasive size	16.749	2	8.375	15.655	15.679	26.459
Error	1.070	2	0.535	1.000	4.280	7.222

Table 5: TWR POOLED ANOVA RESULTS

Source	SS	DOF	V	Var ratio	SS'	P
Power rating	0.089	2	**Pooled**	-	-	-
Static load	5.220	2	2.610	58.513	5.131	41.653
Slurry conc	1.344	2	0.672	15.069	1.255	10.189
Abrasive size	5.665	2	2.832	63.494	5.575	45.261
Error	0.089	2	0.045	1.000	0.357	2.897

Static load emerges as the most significant factor at 95% confidence level with a percent contribution of 33.75. Power rating emerges as another highly significant factor, with a percent contribution of 32.56 in the variation of MRR, followed by Grit size with contribution of 26.49 percent. The relative influences are presented in Figure 6.

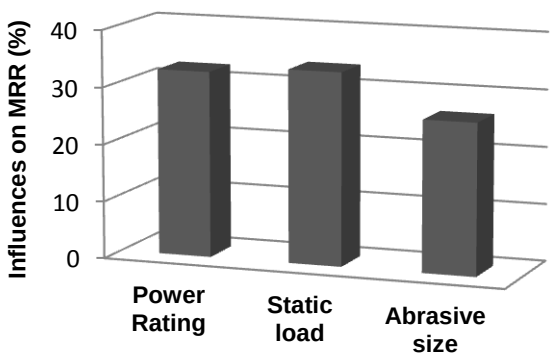

Figure 6 Percent Contributions For Mrr (S/N Data)

With regarding to the S/N response of TWR, grit size factor has emerged as the most significant factor with a percent contribution of 45.26% (Table 5) followed by the static load (41.65%). Slurry concentration factor can be termed as the least significant factor for TWR with a percent contribution of 10.18% (Figure 7).

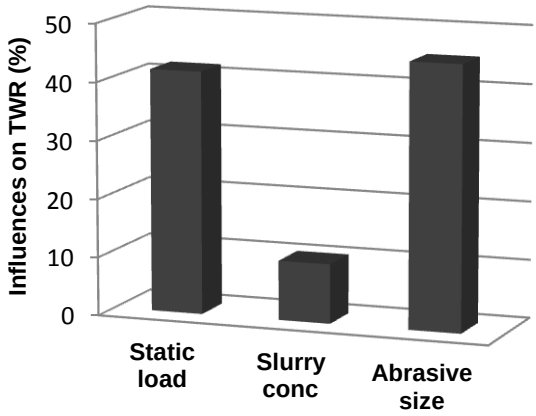

Figure 7 Percent Contributions For Twr (S/N Data)

VI. CONCLUSION

This paper has discussed the feasibility of drilling borosilicate glass by micro USM. Taguchi method has been used to determine the main effects, significant factors and optimum machining condition for both performance of micro USM. Some results found in case of MRR are differing with the nominal trend in macro USM. Based on the results presented herein, it can be concluded that, the MRR is most influenced by static load while abrasive size mainly affects the TWR.

REFERENCES

[1] Merz, P., Quenzer, H. J., Bernt, H., Wagner, B., and Zoberbier, M., "A Novel Micromachining Technology for Structuring Borosilicate Glass Substrates", Transducers '03, 1 (1), 2003, 258-261.

[2] Gad-El-Hak, M., 2006, MEMS: Applications. CRC Press, 2nd Edition.

[3] Jain, V., Sharma, A. K., and Kumar, P., "Investigations on Process Capabilities of Micro Ultrasonic Drilling", AFTMIE, 2010, 66-70.

[4] Ross, P.J., Taguchi Techniques for Quality Engineering, McGraw-Hill, New York, 1988.

[5] Jadoun, R. S., Kumar, P., and Mishra, B. K., "Taguchi's Optimization of Process Parameters for Production Accuracy in Ultrasonic Drilling of Engineering Ceramics", Prod. Eng. Res. Devel, 2009, 243–253.

[6] Singh, R., and Khamba, J.S., "Taguchi Technique for Modelling Material Removal Rate in Ultrasonic Machining of Titanium", Materials Science and Engineering, 2007, 365–369.

[7] Kumar, V., and Khamba, J.S., "An Investigation into the Ultrasonic Machining of Co-Based Super Alloy Using the Taguchi Approach", Int. J. of Machining and Machinability of Materials, 7 (3), 2010, 230 – 243.

[8] Lia, Z.C., Jiaoa, Y., Deinesa, T.W., Peia, Z.J., and Treadwell, C., "Rotary Ultrasonic Machining of Ceramic Matrix Composites: Feasibility Study And Designed Experiments", Int. J. of Machine Tools & Manuf., 2005, 1402–1411.

[9] Hu, P., Zhang, J.M., Pei, Z.J., and Treadwell, C., "Modeling of Material Removal Rate in Rotary Ultrasonic Machining: Designed Experiments", Journal of Material Processing Technology, 129 (1–3), 2002, 339– 344.

[10] Gauri, S.K., Chakravorty, R., and Chakraborty, S., "Optimization of Correlated Multiple Responses of Ultrasonic Machining (USM) Process", Int J. Adv. Manuf Technol, 53, 2011, 1115–1127.

[11] Egashira, K., Masuzawa, T., Fujino, M. and Sun, X. Q, "Application of USM to Micromachining by on-the machine Tool Fabrication", Int. J. of Electrical Machining, No. 2, 1997, 31-36.

[12] Jain, V., Sharma, A. K., and Kumar, P., "Recent Developments and Research Issues in Micro Ultrasonic Machining", ISRN Mechanical Engineering, 2011, 1-15.

[13] Masuzawa, T., "State of the Art of Micromachining", CIRP Annals - Manufacturing Technology, 49 (2), 2000, 473-488.

[14] Instruction Manual for Stationary SONIC-MILL 500W Model, 2002 (U.S.A).

[15] Jain, V., Sharma, A. K., and Kumar, P., "Investigations on tool wear in micro ultrasonic machining", MIMT 2011, Singapore, Proceedings IEEE, 2011, 222-225.

International Journal of Engineering Research and Applications (IJERA) ISSN: 2248-9622
National Conference on Advances in Engineering and Technology
(AET- 29th March 2014)

RESEARCH ARTICLE OPEN ACCESS

Pressure Drop Analysis of Water and Fly Ash Mixture Flow through Straight Pipeline

[1]Subhash Malik, [2]Lakshya Aggarwal, [3]Ankit Dua
[1,2,3] Department of Mechanical Engineering, M. M. University, Sadopur (Ambala), Haryana
[1]subhashmalik604@gmail.com, [2]lakskiet@gmail.com, [3]dua_ankit09@yahoo.co.in

ABSTRACT
Slurry transportation through pipeline provides better effect on material transportation system. Transportation of bottom and fly ash in thermal power plants through pipeline is best example of slurry transportation system. Transportation through slurry pipeline is a safe, pollution free and reliable method. In the present work, Rheological properties of bottom and fly ash are studied to know the flow behaviour of coal slurry. The Rheological properties of slurry depend on a number of factors such as particle size distribution, pH value and settling characteristics. Rheometer is used to know the shear rate and shear stress variation for the different concentrations of slurry. In this paper, computational simulation is performed on the slurry flow through pipeline for the analysis of pressure drop in pipeline. Modelling of pipeline developed in Gambit and Fluent is used for the numerical evaluation and the performance is analysed on various concentrations and flow velocities.
Keywords: - Computational Fluid Dynamics, Finite Volume Method, Slurry Transportation System.

I. INTRODUCTION

Fly ash is the finest of coal ash particles. It is called fly ash because it is transported from the combustion chamber by exhaust gases [1]. Fly ash is the fine powder formed from the mineral matter in coal, consisting of the non combustible matter in coal. Bottom and fly ash are quite different physically, mineralogical, and chemically [2]. The mixture of solids and liquids is known as slurry. The physical characteristics of slurry are dependent on many factors such as particle size distribution, solid concentration in the liquid phase, turbulence level, temperature, conduit size, and viscosity of the carrier [3]. Slurry is a mixture of a solid particles and fluid held in suspension [15]. Water is the most commonly used fluid. The speed of slurry flow is sufficiently high to maintain the particles in suspension [4]. Slurry transportation through pipeline provides better effect on material transportation system. This system has various advantages such as very less pollution and less noise. So, there is requirement of detailed study of pipeline slurry transportation system to improve its performance [5]. Slurry pipelines are used to transport solid materials using water for short or long distances. These pipelines are used in many industrial applications involving transportation of coal and disposal of slurry in thermal power plant [6]. In the present work, Rheological properties of bottom and fly ash are studied to know the flow behaviour of coal slurry [7]. The Rheological properties of slurry depend on a number of factors such as particle size distribution, pH value and settling characteristics. Rheometer is used to know the shear rate and shear stress variation for the different concentrations of slurry [8]. Computational simulation is performed on the slurry flow through pipeline for the analysis of pressure drop in pipeline [10]. Computational Fluid Dynamic [CFD] is the analysis of system involving fluid flow by means of computer based simulation [11]. Computational fluid dynamics is one of the branches of fluid mechanics that uses numerical methods and algorithms to solve and analyse problems that involve fluid flows [12]. It has become an indispensable tool in the design, development, evaluation and refinement of new industrial equipment and processes.

II. COMPUTATIONAL SIMULATION OF PIPELINE

Computational Fluid Dynamic (CFD) is the analysis of system involving fluid flow by means of computer based simulation. Computational fluid dynamics is one of the branches of fluid mechanics that uses numerical methods and algorithms to solve and analyse problems that involve fluid flows [13]. The use of computational fluid dynamic reduces the development cost of new products and cuts the time to market of these products [14]

III. METHODOLOGY

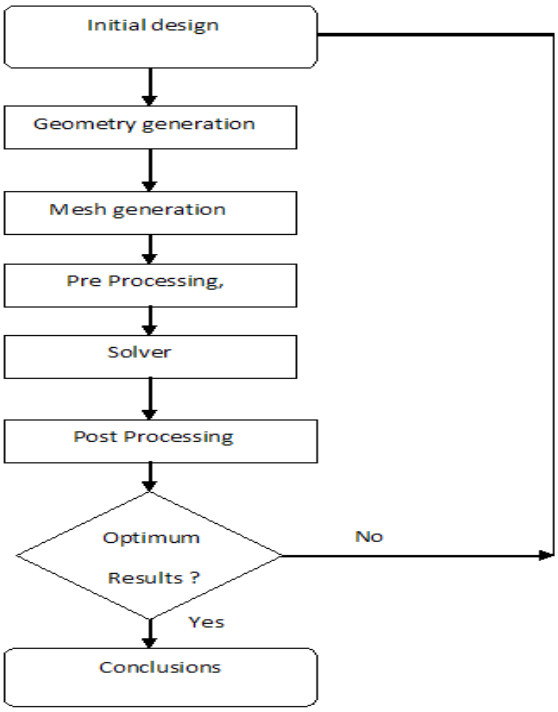

Figure 1: Methodology adopted

IV. SIMULATION RESULTS

Figure 2 shows that the pressure drop in 100 meter straight pipe is increased from inlet to outlet.

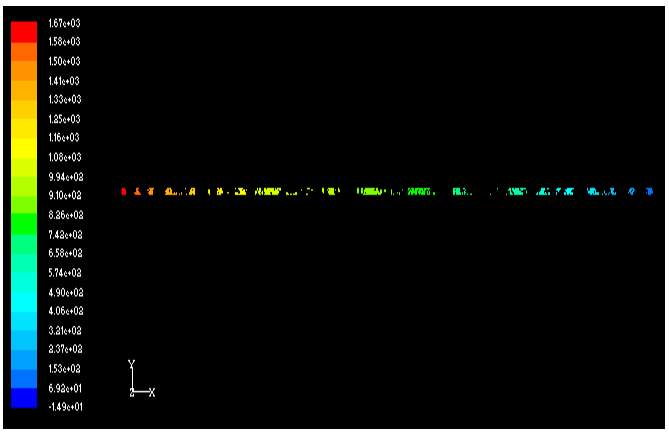

Figure 2: Pressure Display of Fly Ash at 50% Concentration in 100 meters Straight Pipe

When concentration of bottom ash is increased in slurry then pressure in pipe is also increased. Pressure will increase, when the velocity of slurry in straight pipe increases. It can be observed from Figure 3 that pressure loss difference at high velocities is considerably more than pressure loss difference at low velocities.

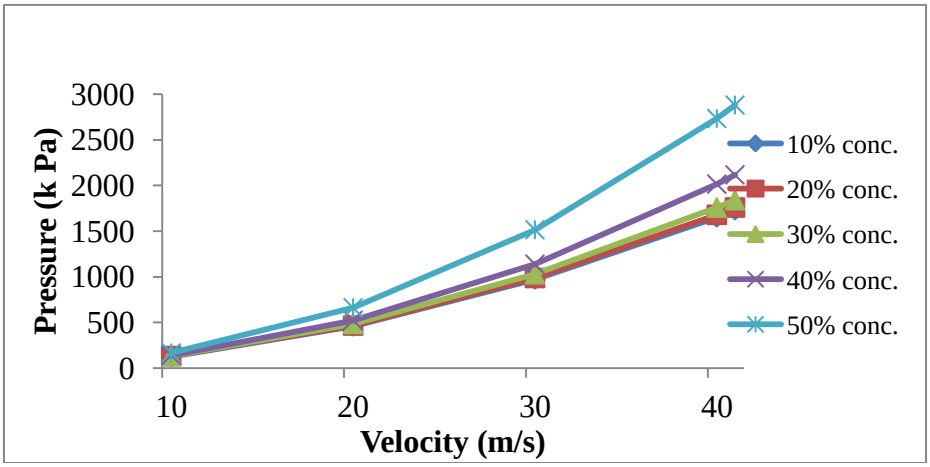

Figure 3: Pressure Drop per 100 meter Length with Different Flow Velocity and % Concentration (by weight) for Water and Fly Ash Mixture in Straight Pipe

Table 1: Pressure Drop per 100 meter Length with Different Flow Velocity and % Concentration

Velocity [m/s]	**Pr. Drop [k Pa] 10%**	**Pr. Drop [k Pa] 20%**	**Pr. Drop [k Pa] 30%**	**Pr. Drop [k Pa] 40%**	**Pr. Drop [k Pa] 50%**
10	126.94	132.79	133.34	139.87	167.31
20	460.04	466.85	484.72	524.09	661.98
30	972.50	986.82	1029.17	1138.65	1515.55
40	1651.19	1678.37	1757.71	201505	2732.48
41	1729.64	1758.56	1838.06	2116.06	2880.57

V. CONCLUSION

The simulation results show that the Pressure drop per 100 meter length across the straight pipe increases as increase in concentrations and flow velocities. Fluent results give the good agreement with analytical results for pressure drop in straight pipe for different concentrations of bottom ash slurry. It has been observed that the Slurry with 50% concentration can flow at velocity 41 m/s in straight pipe.

REFERENCES

[1] A. Mukhtar , S. N. Singh and V. Seshadri, "Pressure drop in a long radius 90° horizontal bend for the flow of multisided heterogeneous slurry", International journal multiphase flow, 21 (1), 1994, 329-334.

[2] C. Logos, Q.D. Nguyen, "Effect of particle size on the flow properties of South Austriala coal water slurry", Power technology, 88 (1), 1996, 55-58.

[3] Zeki Aktas, E.Ted Woodburn, "Effect of addition of surface active agent on the viscosity of a high concentration slurry of a low-rank British coal in water", Fuel Processing Technology, 62 (1), 2000, 1–15.

[4] Hiromoto Usui, Lei Li and Hiroshi Suzuki, "Rheology and pipeline transportation of dense fly ash-water slurry", Korea-Australia rheology journal, 13 (1), 2001, 47-54.

[5] E. Harmadi, Suwarmin, S. Machmudah, and S. Winardi, "Effect Of Particle Size Distribution On Rheology And Stability Of High Concentration Coal-Water Mixture (Cwm) With Indonesian Low Rank Coal", Jurnal teknik mesin, 2 (1), 2002, 3-98.

[6] F. Boylu, H. Dinc¸er, G. Atesok, "Effect of coal particle size distribution, volume

fraction and rank on the rheology of coal–water slurries", Fuel Processing Technology, 85 (1), 2003, 241–250.

[7] A. Al- Sarkhi and A. Solemani, "Effect of drag reducing polymers on two-phase gas – liquid flows in a horizontal pipe", Chemical engineering research and design, 82 (1), 2004, 1583-1588.

[8] Ibrahim Can, "Simplified equations calculate head losses in commercial pipes", The Journal of American Science, 1 (1), 2005, 1-3.

[9] Abhai Kumar Verma, S N Singh and Seshadri, "Pressure drop for high concentration solid-liquid mixture across 90° horizontal circular pipe bend", Indian journal of engineering & material sciences, 13 (1), 2006, 477-483.

[10] Wael H. Ahmed, Chan Y. Ching , Mamdouh Shoukri, "Pressure recovery of two-phase flow across sudden expansions", International Journal of Multiphase Flow, 33 (1), 2007, 575–594.

[11] K. Ekambara, R.S. Sanders, K. Nandakumar, J.H. Masliyah, "CFD simulation of bubbly two-phase flow in horizontal pipes", Chemical Engineering Journal, 144 (1), 2008, 277–288.

[12] Naik, H.K ,Mishra, M.K. and Roa Karanam, "Rhelogical characteristic of fly ash slurry at varying temperature environment with and without additive", world of coal ash conference, Lexington,KY, USA, 2009.

[13] P.K. Senapati , B.K. Mishra, A. Parida, "Modeling of viscosity for power plant ash slurry at higher concentrations: Effect of solids volume fraction, particle size and hydrodynamic interactions", Powder technology, 197 (1), 2010, 1–8.

[14] Naik, M.K.Mishra and Roa Karanam, "Evaluation of flow characteristics of fly ash slurry at 40% solid concentration with and without an additive", World of coal ash conference in Denver, CO, USA, 2011.

[15] Kunal Singh, Kundan Lal, "Effect of cetylpyridinium chloride,Triton x-100 and sodium dodecyl sulphate on rheology of fly ash slurry", International journal of scientific and research publications, 2 (1), 2012, 2250-3153.

International Journal of Engineering Research and Applications (IJERA) ISSN: 2248-9622
National Conference on Advances in Engineering and Technology
(AET- 29th March 2014)

RESEARCH ARTICLE OPEN ACCESS

Intelligent Equipment Health Monitoring System for Improving Availability of Remote Mining Equipment

V.M Kalra*,Tilak Thakur**, B.Spabla***
*(Department of Electronics and Communication Engineering, S.J.P Polytechnic Damla, Yamuna Nagar, India
Email: vmkalra@yahoo.com)
** (Department of Electrical Engineering, PEC University of Technology,Chandigarh, India
Email: tilak20042005@yahoo.co.in)
*** (Department of Mechanical Engineering, NITTTR Sector 26, Chandigarh, India
Email: pablabs@yahoo.com)

ABSTRACT

In today's era of competition the efforts are being made globally to reduce the mining production cost, one way to improve the mine productivity is to improve availability and Utilization of the mining Equipment by introducing a condition based preventive maintenance system. Real time monitoring system provides a cost effective mechanism to collect information from various sensors and measure the performance of the equipment which presently is taken care of by manual methods. Most of the Excavationma chinery in the underdeveloped countries is still operating without any monitoring system, as it is impossible to replace the machinery due to its high procurement cost. The sensors installed at different locations measure physical parameters such as pressure, temperature, oil levels and vibrations. Data acquired can be used to check if the acquired signal level is above or below the set values so that desired action is taken to avoid major breakdown of the equipment. Primary importance of sending the monitored data to the remote central computer with the help of network communication technology is that the timely action is taken by the managers and technicians to remove the faults to reduce downtime and improve Equipment Performance.

Keywords: Microcontroller, GSM Module, Sensors, Analog to Digital Converter, Fault Tree.

I. INTRODUCTION

It is observed that the maintenance cost of the mining equipment like Shovel and Dumper that work in poor and hazard conditions is around 35% to 50% of the total operating cost of the system [2] .The increase in automation with increase in the size and capacity of the equipment over the years has all caused concern over the ineffectiveness of the equipment. To stay competitive, mines are continuously pushing hard to increase productivity and reduce costs per ton of material moved. One way to improve productivity is to utilize equipment as effectively as possible. A low cost fault monitoring and diagnostic system has been developed to give a new lease of life to old shovels which are unable to perform due to poor feedback and with no equipment health monitoring. In addition to improved performance and availability, the mine enjoys reduced maintenance cost. The microcontroller with the help of software program checks the acquired signals with set values and issues alerts for the faults and the faulty stage. Maintenance personals can therefore take suitable action in time before the permanent failure of equipment, to improve performance and availability. The condition monitoring technology because of the various tools available has benefited to detect the fault before it happen [1]. These smart tools have the capability to handle the performance, decision making, alarm/ event handling and troubleshooting [6]-[7]. It is therefore possible to monitor the vital data for mining equipment health and safety of the workers.

II. Monitoring System Hardware

The hardware of the monitoring system mainly consist of sensors, signal conditioning circuits, analog multiplexer, Analog to Digital converter, Microcontroller and GSM module. The block diagram for acquisition of physical parameters of the mining shovel is shown in fig.1.

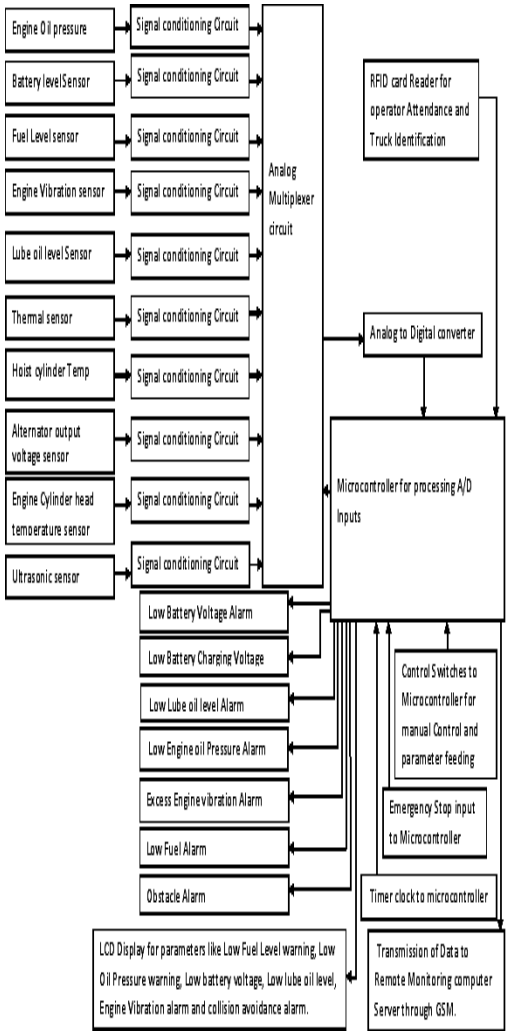

Fig.1 Data Acquisition system block diagram

2.1 Electronic Sensors

Engine Oil pressure level is checked with the help of Pressure Mems as sensor (F5) and is connected at pin no 4 mentioned as AN2, if the pressure level is low, operator can infer that the main cause of low oil pressure is due to non-operation of oil pump and engine can seize due to overheat in chamber. Hoist cylinder pressure is checked with the help of Pressure Mems as sensor (F1) to check if the pressure level is below the prescribed value, as lower limit will result into problem in the lift mechanism of the Bucket. Similarly the Hydraulic oil pressure sensor F4 gives indication if the Low Hydraulic oil level is due to broken Hose or leaking cylinder seal or damaged hydraulic pump. For vibrations sensing an accelerometer ADXL 105 is used to issue alerts to the operator if any mechanical assembly gets loose due to usage for long operating hours this can save the mining equipment from major breakdown and avoids accidents. For fuel level sensing resistive sensor is used to tell the operator that the fuel oil level has gone down the prescribed limits and refilling is desired. An alert can avoid wastage of time of the shovel and thus avoid production loss. Ultrasonic sensor is used to alert the operator if the dumper truck exceeds the set limit and come close to shovel and thus avoid accidents and safety of the driver. Thermal Sensor is used to pre warn the technicians if some circuit ambient temperature increase is detected on any electronic card, and the card is replaced before the failure of shovel machine. Inverter battery voltage level is checked so that various electronic circuits and the drive cards get the proper supply for operation of various motors in the shovel. Thermistor as sensor (F2) is used to issue alert if the Engine coolant temperature is above the set limits and maintenance personals can check if the Engine oil level is low due to some leakage or there is improper circulation of cooling fluid. All the variation in set limit is communicated to the remote supervisors through messages using GSM module SIMCON300 connected at Tx and Rx pin number 25 and 26 of the microcontroller. Actual specification for the sensors will depend upon the equipment. A prototype model of the system has been tested.

2.2 Signal Acquisition Module

The signal conditioning module and monitoring system as shown in Fig.1 mainly consists of filter circuits for filtering any noise present in the signal and amplifier to boost the signal to desired level. A 16 channels Analog multiplexer ADG 506A is used that accept many inputs but gives only single output works on +10.8V to 16.5V power supply. The availability of the output signal depends upon the selection bits issued by the microcontroller on select lines to the multiplexer at sampling frequency. The signal is converted from analog form to digital form using 16 bit AD976 for use by the microcontroller to process the signal. This ADC requires +5V Supply for operations. A PIC microcontroller (PIC18f46k22) is used for sensing, monitoring and control. The Microcontroller checks the acquired signal with the set values and issues the warning /alert messages to shovel operator on the LCD screen and also with the help of Buzzer [8], [9]. The LCD display show message for Low fuel level, Low oil Pressure warning, low Alternator output. Low battery level, Low lube oil etc. GSM technology is wireless technology and best suited for remote applications, Fiber optic technology has the drawback that it can break due to movement of trucks.

Condition monitoring [1] technology makes use of microcontroller to acquire signals from various sensors installed on the equipment to determine equipment present condition and predict the failure chances. Condition monitoring [10] [13] helps to

improve equipment availability with the help various notifications as messages in the form of alarms to the operator and the maintenance personals. The immediate attention of the servicing personals helps to maximize component life and thus improves the equipment performance. Fault tree [13] concept has been used as mentioned below to help detect the faulty stage and to further narrow down the defect to a specific component.

Table 1.Shovel Mechanical Fault Analysis

S. No	**Parameter Monitored.**	**Possible cause and Faulty stage.**	Fault Message to Maintenance Department
a.	Battery Charging voltage low.	Slipping or worn alternator belts or defective alternator.	DA
b.	Battery Charging voltage high.	Defective regulator in alternator.	DAR
c.	Engine difficult to start.	Empty fuel tank or cylinder head gasket leaking or faulty fuel pump.	FFP
d.	Cylinder head temperature high	Low engine oil level due to leakage ordirt on transmission or hydraulic coolers or improper circulation of cooling Liquid.	LEOICL
e.	Dump hoist pressure low.	Low hydraulic oil level due to broken hose or leaking cylinder seals.	LCS
f.	Engine difficult to start.	Empty fuel tank or cylinder head gasket leaking or faultyfuel pump.	FFP
g.	Engine Fuming.	Leakage in transmission or hydraulic oil cooler or overloading or Improper engine valve opening.	IEVP
h.	Lack of Engine power.	Air leakage in fuel suction line, defective Injector pump nozzle.	DIPN
i.	Excess Engine noise.	Broken engine mounts or restricted air supply.	BEM
j.	Excess Engine oil consumption.	Engine oil leakage due to worn piston rings or leaking filters.	EWPR
k.	Lack of dump power.	Low hydraulic oil level due to broken hose, leaking cylinder seals or worn hydraulic pump.	WHP
l.	Hydraulic pump noisy.	Low oil level or damaged pump.	WHP
m.	Breaks slowto apply.	Foot control valve Jamming.	FCJ
n.	Engine not starting.	Electrical problem due to low battery voltage or switches faulty or starter motor struck up.	BVSMS
o.	No Electricity to lights.	Damaged wiring or circuit breaker tipped due to excess Load.	CBT
p.	Crowd motor Noisy.	Broken crowd motor mounts.	CMM
q.	Excess heat on drive circuit.	Fault in Electronic Drive card.	FEDC
r.	Engine oil pressure low.	Damaged oil Pump, Low Engine oil level due to oil leakage or worn piston rings or fuel injector pump leaking.	DPPR

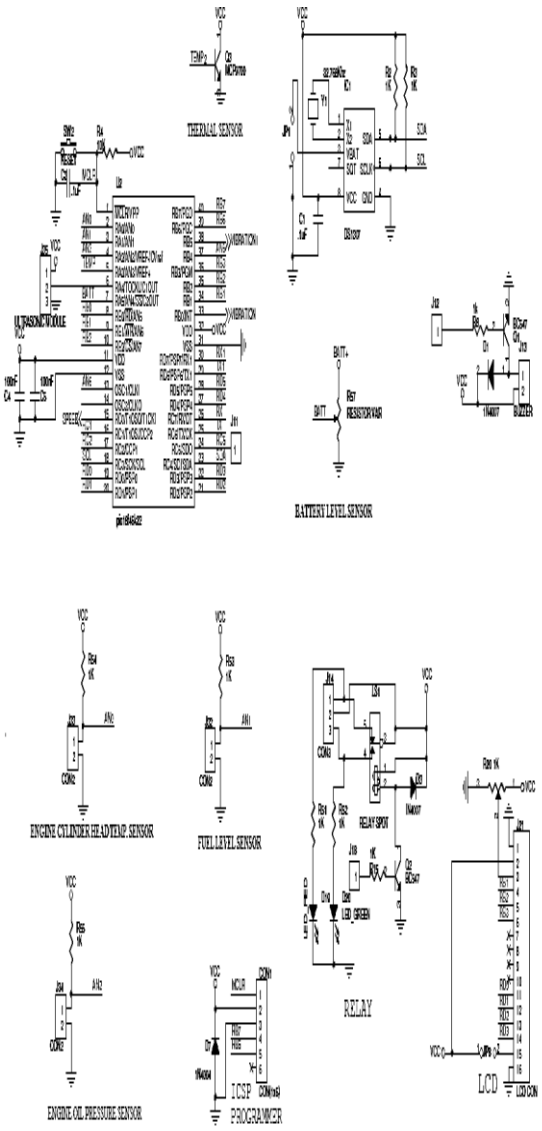

Fig 2. Microcontroller interfacing with sensors.

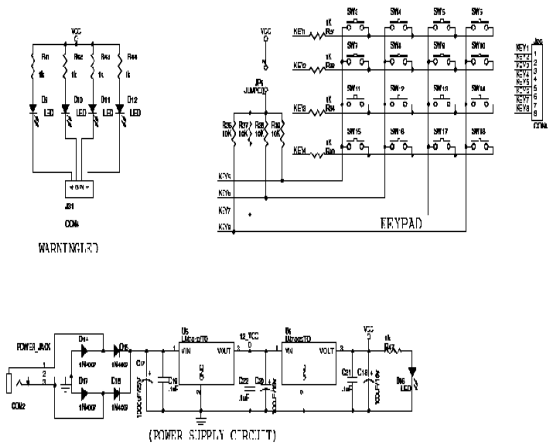

Fig 3. Power Supply Section, Warning LED's and Keyboard Section

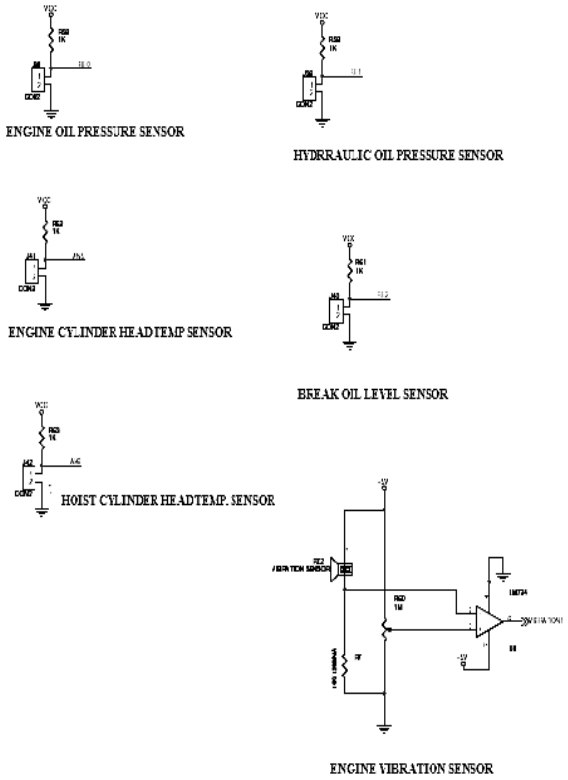

Fig 4. Sensors Interfacing

2.3 System Software

The following concept has been used for software development. The electronic Sensors acquire the data from the different sensors installed all through the equipment. The information from various sensors is checked using Logical AND, OR, NOR Gates [13] to detect the fault and the faulty state. The software compares the acquired data with the preset values using conditional statements and then issues the Alarm to the operator by ringing of the buzzer and also display the data on the operator Console. Any abnormality due to change in operating condition is also sent to the Supervisory maintenance staff with the help of GSM module Simcon300 interfaced with the Microcontroller in the form of SMS. The maintenance staff immediately knows the severity of the problem and the faulty stage and takes with them the required mechanical or electronic tools to rectify the Fault and set the equipment in the working order. These faults were previously known to the supervisors only at the end of the shift or when the equipment went out of order. Fault location time is considerably reduced to condition based preventive maintenance system, previously lot of time even many shifts were wasted due to no skill and capability of the servicing personal in locating the fault. The conditional based monitoring and communication technology has therefore helped rectify the fault immediately and has therefore helped

improving the availability, and better productivity of the mine. Inspection of the equipment that was carried out

Table 2. Availability with and without Monitoring System

Days	Down time in Hrs due to various Electromechanical Faults (F1-F6)						Down Time(Hrs)		%Availability	
	F1	F2	F3	F4	F5	F6	Without Monitoring	With Monitoring	Without Monitoring	With Monitor
1-7	96	48	0	0	0	0	144	80	14	52.38
8-15	149	0	14	0	0	0	163	72	2.9	57
16-23	0	0	9	14	0	2	25	18	85	89
24-30	2	0	0	32	32	0	66	40	60.7	76

manually previously has been replaced with intelligent automated system and therefore helps the operator to take preventive actions to avoid the equipment for major breakdowns. Information from the various hardware sensors for any change in Parameter is directly available to the operator on the screen and also communicated to the maintenance department for early action.

Software for checking the different mechanical faults [13] is based on the following Conditional statements as mentioned below:

1) If Engine oil_psi is low.
   Then mechanics are defective.
2) If Alternator is fail.
   Then electricity is low.
3) If battery voltages is low.
   Then electricity is low.
4) If electricity is low.
   Then drives are unable to work.
5) If oil _level is low.
   Then hydraulic pumps can be faulty.
6) If hydraulic pumps are unable to work.
   Then hydraulics is defective.
7) If cylinder head temperature is high.
   Then engine oil level may be low.
8) If dump hoist pressure is low.
   Then hydraulic oil level is possibly low
   Due to defective hose or leaking seal.
9) If charging voltage is low.
   Then alternator is defective.
10) If Battery charging voltage is high.
   Then regulator in alternator is defective.
11) If Engine is difficult to start.
   Then fuel tank can be empty or cylinder
   Head gasket leaking or faulty fuel pump.
12) If engine noise is excessive.
   Then engine mounts may be broken or
   Restricted air supply.
13) If engine oil level is low (high consumption)
   Then piston rings may be damaged.
14) If hoist cylinder temp is high. Then hoist holding power is low.

Maintenance, Breakdown and Idle condition data for the month of April 2013 of DEMAG H55 Mining Shovel operating in the Eastern Coal fields at Gopinath Pura Dhanbad Open cast mine has been used for analysis as shown in table 2.

III. Fault & Availability Analysis

F1-Hoist cylinder Pressure low, F2-Engine Cylinder head Temperature High, F3-Hour Meter Fault, F4-Hydraulic Oil Pressure Low, F5-Engine Oil pressure Low, F6-Low Battery output Voltage.

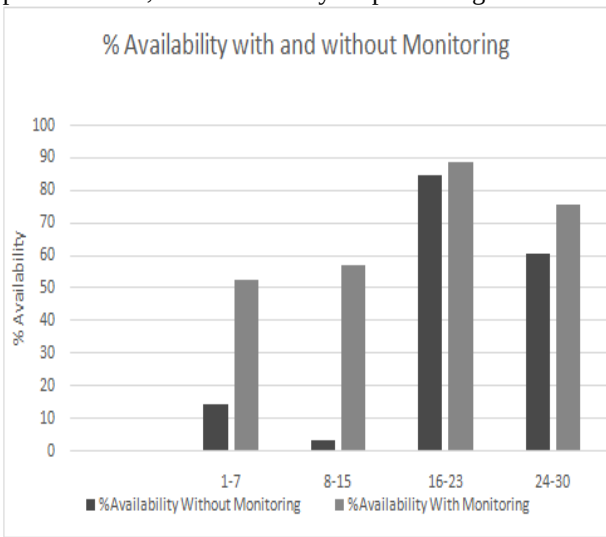

Fig 5: Availability Chart

Availability of the equipment is mainly affected by the down time, this factor indicates that

the equipment is in working state and can be used for the intended purpose [4].

Total Hours
= (Total Hours –Downtime Hours)*100%

Total operating time (hrs) for one month's period
=1*30*24=720hrs
Down time hours without monitoring
=144+163+25+66
=398hrs.
Availability without monitoring system
= (720-398)/720
=44.7%
Down time hours with monitoring
=80+72+18+40
=210hrs.
Availability with monitoring system
= (720-210)/720)* 100
= 70.8%

As the repair time to bring the mining shovel back into working state mainly depends upon the maintenance skill and capability of maintenance personnel's, there is expected average improvement of 26% in Availability of Mining shovel from 45% to 70.8% with Equipment Health Monitoring System as shown in Fig 5. The international standards have suggested that the Availability of mining equipment should be above 85%. Availability and Utilization of the equipment indicates that that achieving high equipment availability is a Maintenance responsibility and while achieving high utilization is a production responsibility, therefore if equipment utilization and availability are maintained high, maximum productivity can be achieved from the mining Equipment.

IV. System Benefits

The proposed system therefore helps monitor the physical parameters and helps the operator and the servicing personnel's to immediately know the equipment healthy state for operations, as he gets the information from the various sensors immediately on startup. The time for detection of fault and the faulty stage is drastically reduced from days to few hours. The part procurement time due to instant information in the form of messages to the servicing department and the purchase Managers also helps bringing the equipment to the up state at the earliest. Therefore there is an inherent benefit in case of monitoring system, that the mining workforce take with them the necessary tools and the part to be repaired or replaced in the shovel immediately on receipt of message and thus helps minimizing the down state. Previously these Parameters were monitored manually and therefore standby time is reduced considerably. Since the equipment failures are addressed properly by preventing major Failures and have therefore resulted into improving the equipment life. Due to shifting of unscheduled downtime to Scheduled downtime, operational impact is minimized and production goals can be easily achieved. Most of the Excavating machinery in the open cast mines in the underdeveloped countries is still operating without any monitoring system, as it is impossible to replace the machinery due to its high procurement cost, the proposed can be fitted in the old shovels at fractional cost to improve their availability and utilization to achieve the desired production goals.

REFERENCES

[1] Ni News,"Increasing Equipment Uptime and Reliability with Condition Monitoring", National Instruments, Sept, 2011, from http://www.ni.com/newsletter/51426/en/.

[2] Bin Guang-fu, Li Xue-Jun,Balbir S Dhillon, Huang Zhen-Yu, GuoDengta, "The integrated monitoring system for running parameters of key mining Equipment based on condition monitoring technology", China Journal of coal science & Engineering, 2010, 16 (1), 108-112.

[3] John Chadwick, "The Autonomous mine", The international mining magazine, 2010, 46-57.

[4] Sermin Elevli ,Birol Elevli, "Performance Measurement of Mining Equipments by Utilizing OEE", ACTA Montanistica Slovaca, 15 (2), 2010, 95-101.

[5] Li X J,Qiu W L, Chu F L, "Remote monitoring and control system for key Equipment in coal-mine based on signal acquisition and data analysis". China Journal of scientific instrument, 2009, 126-133.

[6] Shi Wei, Li Li-li, "Multi-Parameters monitoring system for coal mine based on wireless sensor network technology", China International Conference on Industrial Mechatronics and Automation, 2009, 225-227.

[7] Zhichang ,Zhangeng Sun and Junbao Gu, "Study on the technology of the Coal Mining Safety monitoring system," China Journal of Applied science, 3 (8), 2009, 95-99.

[8] Heyes A. L, Feist J P, Chen X,MutasimZ,Nicholls J R, "Optical Nondestructive condition monitoring of thermal barrier coatings," Journal of

Engineering for gas turbines and power, 130 (6), 2008, 1- 9.

[9] R. L Himte, A. PKedar, P. V Washimkar, M. V Wakhare and P. N Belkhode, "An Approach to Improve the Productivity of Dumper by Preventive Maintenance", International Conference on Emerging trends in Engineering and Technology, 2008, 735-738.

[10] Werner J, Lewis M W, "The integration of condition monitoring into the maintenance process", CIM/ICM Bulletin technical papers, 124, 163-168, 2006.

[11] Zhang W M, ''Configuration software control technology", Beijing, **B**eijing Jiaotong University Press, 2006.

[12] M.D Kuruppu, "New technologies available to maximizing equipment reliability", Taylor Francis group London, 2004.

[13] A Ursenbach, Qun Wang and Ming Rao, ''Intelligent Maintenance support System for mining truck conditioning monitoring andtroubleshooting", International journal of surface mining, Mining Reclamation and environment, 8 (1), 1994, 73-81.

RESEARCH ARTICLE OPEN ACCESS

Numerical Simulation of Drag Reduction in Formula One Cars

A.Muthuvel *, N. Prakash **, J. Godwin John***
*(Department of Automobile Engineering, Hindustan University, Chennai-603103
Email: muthuvelcfd@gmail.com)
** (Department of Automobile Engineering, Hindustan University, Chennai-603103
Email: nprakrao1@gmail.com)
** (Department of Automobile Engineering, Hindustan University, Chennai-603103
Email: godwinjohn18@gmail.com)

ABSTRACT
Today, it is very usual to see numerous cars, from commercial cars to sports cars fitted with different types of spoilers on them. The exterior fashioning and aerodynamically well-organized design for reduction of engine load which reflects in the reduction of fuel consumption and producing the down force for the stability are the two essential factors for an effective operation in the modest world. The adding of rear spoiler to an aerodynamically optimized car body will result in a change of lift and drag forces the car experiences and thus influence the cars overall performance, fuel consumption, safety, and stability. This paper presents a discussion on the results obtained from numerical simulation of airflow over a F1 car for various speeds like 80m/sec, 100m/sec and 120m/sec with and without a rear spoiler for 0^0 and 5^0 angle of attack of the spoiler. The influence of rear spoiler on the generated lift, drag, and pressure distributions are investigated and reported.
Keywords – Aerodynamics, Drag, Fuel consumption, Lift, Spoilers.

I. INTRODUCTION

Flow over body has been a subject of great number of investigation mainly because of wider engineering applications. Some examples are flow over car, buildings, flight-deck of a ship, underwater appended vessels like submarine, torpedo, automated underwater vehicle (AUV), remotely operated vehicle (ROV) etc. In [1] author described the identification of aerodynamic noise source around a coupe passenger car and rear spoiler is added to the vehicle and acoustic effects are investigated. It is found that installing a rear spoiler can change the dominant noise source (location) from front bumper to the rear spoiler. Subsequent to noise source identification, the effect of different angles for rear spoiler is studied in order to recognize the case that gives the minimum acoustic power level of the dominant source (rear spoiler). By increasing the vehicle cruise, the aerodynamic noise rises significantly (e.g. the maximum acoustic power level increases around 3%). Size of the wake formed behind the rear spoiler and the turbulent intensity distribution on it, confirms that there exists a case that generates lower air-born noise. A pressure-based implicit procedure to solve Navier-Stokes equations on a unstructured polyhedral mesh with collocated finite volume formulation is used [2] to simulate flow around the smart and conventional flaps of a spoiler section under the ground effect. The agreement between presented predation and experimental data is for smart flap is smoother than conventional flap. In [3], authors carried out the work for numerical simulation of airflow over a passenger car without a rear spoiler and compares these with results obtained for a passenger car fitted with a rear spoiler and he suggested a rear spoiler on the generated lift, drag, and pressure distributions are investigated and reported. Two different types of simulations are performed [4] for the flow around a simplified high speed passenger car with a rear-spoiler and the other for the flow without a rear-spoiler. The standard k-ε model is selected to numerically simulate the external flow field of the simplified Camry model with or without a rear-spoiler. Through an analysis of the simulation results, a new rear spoiler is designed and it shows a mild reduction of the vehicle aerodynamics drag. This leads to less vehicle fuel consumption on the road. In [5], authors presented a comprehensive study for realistically predicting airflows around cars. The focus is on high fidelity road vehicle simulations, but with as short as possible turnaround time as prerequisite for aerodynamic optimization and innovation at lower development cost. The airflow is modeled using different commercial CFD packages, i.e. Ansys Fluent, CFX, Open FOAM and Power FLOW. Furthermore, recommendations for geometry preparation, grid and case set-up are given. Results for a road vehicle indicate that the best solver from an accuracy point of view is Star-CCM+. In [6] authors described about the drag reduction by checking car models with the installation of external devices and without the

devices. After validating it is found that the LES gave the good results. By installing the devices it is found the drag coefficient variation is about average of 18%. These were for tractor trailer. One SUV model was also simulated. A rear wing modeled by NACA 0015 was attached at 10 degrees from the rear slant angle which lowered the drag-by-area of the Ahmed car model by 10%.All results were compared against experimental results. Tractor trailer RANS results showed an error of 12% while LES results showed an error of 4.9% in comparison with the paper's results. The SUV model showed an error of 5.7% in comparison with the experimental results for a small scale Hummer model in a wind tunnel.

A detailed discussion about the drag reduction by means of using rear spoilers is carried out [7]. Adding a spoiler at the very rear of the vehicle makes the air slice longer, gentler slope from the roof to the spoiler, which helps to reduce the flow separation. Reducing flow separation decreases drag, which increases fuel economy. In [8], author highlighted the turbulence areas and how to reduce it and he suggested that real trouble is that the winglets and the lower rear wing element, which are in interaction with the diffuser, produce the most turbulence. The spallartallmaras based DES of Ahmed reference model with the slant angles 25 ° and 35^0 is discussed [9]. At 25 ° RANS gives relative results for it is in good agreement as flow is attached and is no good in the wake region. At 35° slant angle DES is in good agreement with the experimental analysis in the wake region. DES is also good with the drag as in experimental analysis. They suggested that des gives good result in the wake region. **Nari Krishnani**[10]discusses about the drag reduction in the vehicle and checked the feasibility of using the external devices for reducing drag on large size SUV. The study suggests that STARCCM+ software gives the better result than other software and by using the spoiler we will get the less drag force and better stability.

II. ANALYTICAL RESULTS AND ANALYSIS OF F1 CAR

Three dimensional numerical analysis of the flow over F1 car is carried out with the general purpose Reynolds Averaged Navier-Stokes Equations (RANSE) solver STAR-CCM+. Steady analysis is carried out with unstructured polyhedral mesh with AKN k-ε model turbulence models. For all the cases, the maximum residual from continuity, x-momentum, y-momentum and z-momentum is restricted to 1e-4 as convergence criteria. Initially, 300 iterations are carried out with first-order upwind scheme and relaxation factor for velocity as 0.3 and pressure as 0.1 to guard against divergence of the solution. Later, till the convergence criteria are met, iterations are carried out with second-order upwind scheme with velocity relaxation factor as 0.5 and pressure relaxation factor as 0.3 to obtain higher accuracy and also to accelerate the convergence.

III. GEOMETRICAL MODELING

Three dimensional F1 CAD models of front view is shown in Fig.1 its side view is shown in Fig. 2 and top view is shown in Fig.3 by using the Solid works CAD software with its actual dimensions.

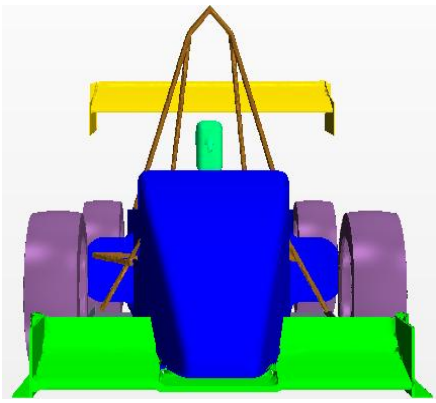

Figure 1: Front View

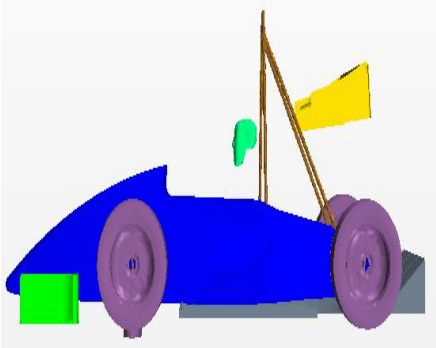

Figure 2: Side View

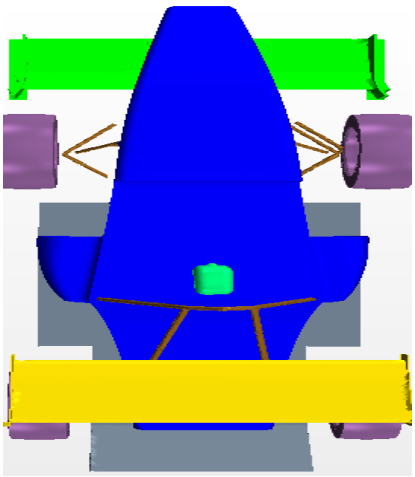

Figure 3: Top View

IV. GRID GENERATION

Unstructured polyhedral mesh is chosen while generating the grid. During generation of the meshes, attention is given for refining the meshes near the F1 car so that the boundary layer can be resolved properly. The typical mesh for car is shown in Fig.4 its sectional view is shown in Fig.5 and a magnified view near the solid wall of car is shown in Fig.6.

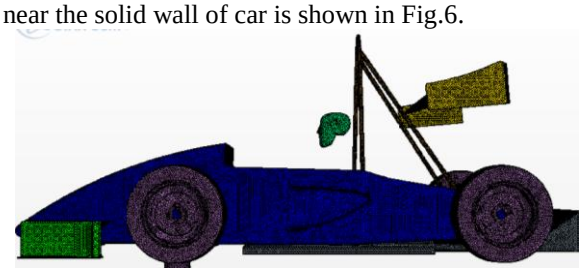

Figure 4: Mesh on Car

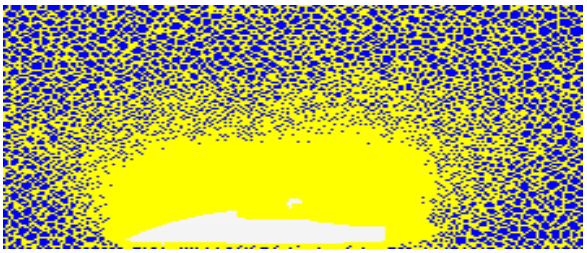

Figure 5: Sectional View of Polyhedral Mesh

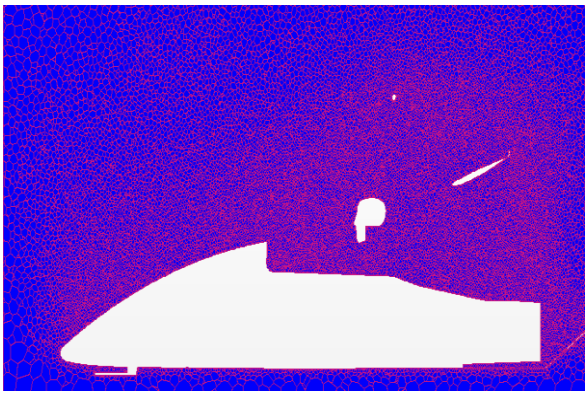

Figure 6: Magnified View of Polyhedral Mesh

V. BOUNDARY CONDITIONS

Boundary conditions were applied on the meshed model using the STARCCM+ CFD software. The analysis was carried out in moving road and rotating wheel condition. In the simulation only straight wind condition was considered at 3 different vehicle speed of 80, 100,120 m/sec. Constant velocity inlet condition was applied at the inlet to replicate the constant wind velocity conditions same as wind tunnel tests. Zero gauge pressure was applied at the outlet with operating pressure as atmospheric pressure. All the boundary conditions used in the analysis are listed in Table 1 and its computational domain for numerical simulation is shown in Fig. 7.

TABLE 1: BOUNDARY CONDITIONS

BOUNDARY	BOUNDARY CONDITIONS	VALUES
Inlet	Constant velocity	V=80,100 & 1200m/sec
Outlet	Pressure outlet	Constant pressure= 0 N/m2
Bus body	No slip – stationary wall	-
Domain	Constant velocity	V=80,100 & 1200m/sec

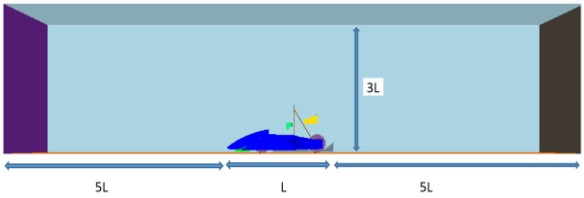

Figure 7: Computational Domain for the F1 Car Analysis

VI. RESULTS FOR UNSTRUCTURED MESH

Grid independent test is carried out for the F1 car for 1.52 million, 2.47million and 3.54 million cells. AKN k-ε two layer models were used for the test. The drag coefficient values along the surface are measured. From Fig. 8 it can be seen that the values at 1.52 million is deviating from the values obtained with 2.47 million cells. However, difference between the values obtained from 2.47 million cells with those 3.54 million cells is very less (less than 5%).Hence, 2.57 million cells is considered for further analysis for F1 car. The CFD analysis of flow over the F1 car is made for various speeds with 0^0 and 5^0 angle of attack for spoiler. Drag force is measured for various speeds like 80,100 and 120m/sec are shown in Table 2 and Table 3.The drag force and normal force are gradually increasing w.r.t to high speed.

Table 2: Results For 0^0 Angle Of Attack

Speed	Pressure Force	Shear Force	Total Axial Force	Pressure Force	Shear Force	Total Normal Force
80	190.85	6.05	196.90	-184.43	0.72	-183.711
100	299.81	9.52	309.33	-306.50	1.28	-305.22
120	422.08	13.24	435.36	-443.44	1.79	-441.69

Table 3: Results For 5^0 Angle Of Attack

Speed	Pressure Force	Shear Force	Total Axial Force	Pressure Force	Shear Force	Total Normal Force
80	196.33	5.75	202.09	-175.01	0.65	-174.39
100	306.38	9.36	315.75	-276.83	1.30	-275.50
120	443.50	13.12	456.60	-373.49	1.72	-371.77

The velocity contour and pressure contour diagram for AKNk-ε two layer model is shown is shown in Fig. 11 and Fig 12 for velocity 80/sec. From the velocity contour and pressure contour diagram, the variation of the velocity and pressure of flow over the F1 car are seen. At the bow of the AUV, stagnation condition is clearly captured. Also, boundary layer formation is seen near the walls. As the flow advances over the body, the velocity increases gradually and then reduces in the rear region due to curvilinear nature of the rear geometry. Similarly for 100 m/sec is shown in Fig. 16-17 and for 120 m/s is shown in Fig. 21-22.The vortices are formed behind the front part and rear of the spoiler is shown in Fig.8, 13 and 19. Pressure and velocity path lines are clearly showing the stagnation points and high stream flow area are in Fig. 9 -10 for 80m/sec, Fig. 14 - 15 for 100m/sec and Fig. 19-20 for 120 m/sec.

Analytical results for 80 m/sec

0 Degree **5 Degree**

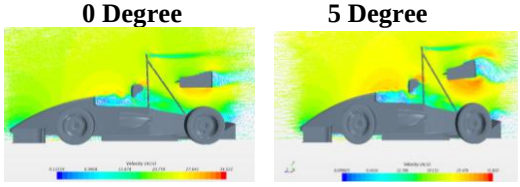

Figure 8: Velocity Vectors on The Body

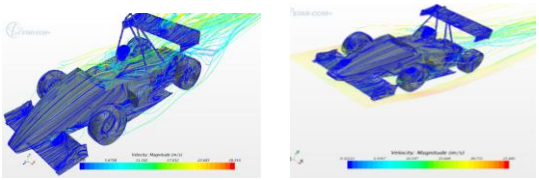

Figure 9: Velocity Path Line on The Body

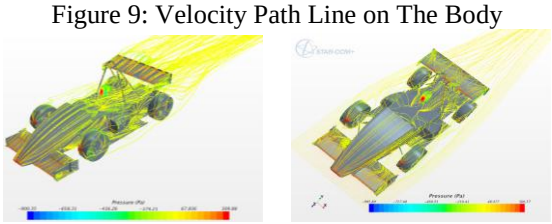

Figure 10: Pressure Path Line on The Body

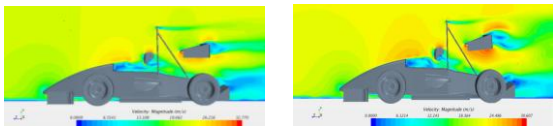

Figure 11: Velcity Contours on The Body

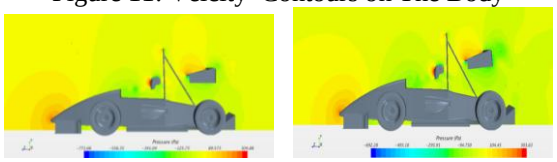

Figure 12: Velcity Contours on The Body

Analytical results for 100 m/sec

0 Degree **5 Degree**

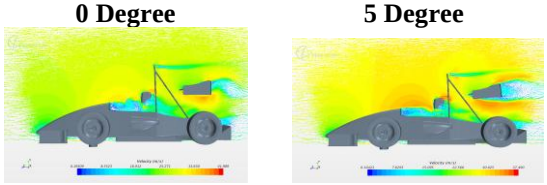

Figure 13: Velocity Vectors on The Body

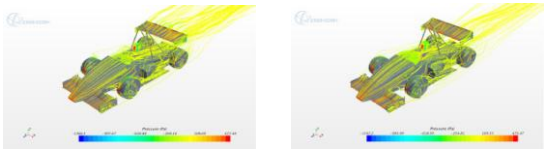

Figure 14: Pressure Path Line on The Body

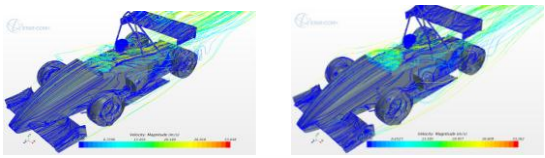

Figure 15: Velocity Path Line on The Body

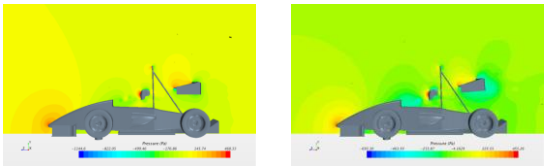

Figure 16: Pressure Contours on The Body

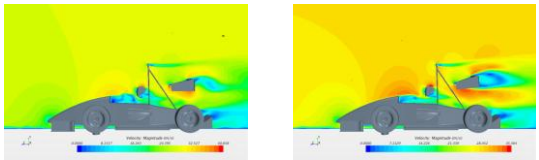

Figure 17: Velcity Contours on The Body

Analytical results for 120 m/sec

0 Degree **5 Degree**

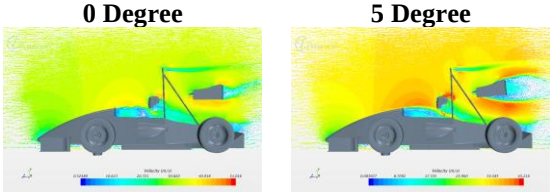

Figure 18: Velocity Vectors On The Body

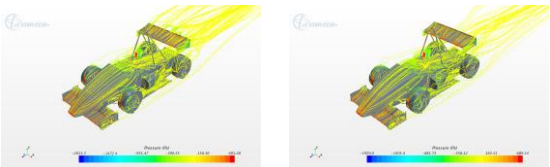

Figure 19: Pressure Path Line On The Body

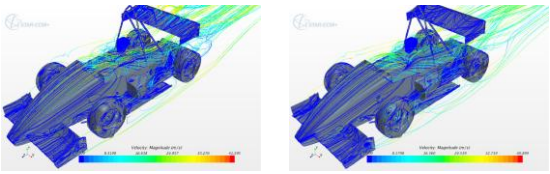

Figure 20: Velocity Path Line On The Body

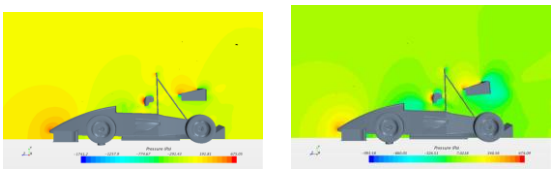

Figure 21: Pressure Contours On The Body

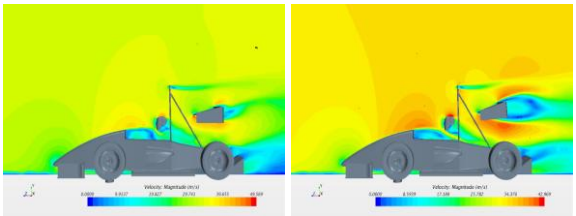

Figure 22: Velcity Contours On The Body

VII. CONCLUSION

In this paper, analysis is carried out for F1 car with commercial code STAR-CCM+. Analysis is carried out for F1 car with spoiler for unstructured to 0^0 and 5^0drift angles of spoiler. In this analysis, AKN k-ε turbulence model is used. The normal and axial forces are obtained from the present analysis.

It is seen that pressure force and shear forces are gradually increasing w.r.t to speed due to this drag and normal forces are increasing for 0^0 and 5^0 spoiler drift angles. For this F1 car at 0^0 spoilers gives less drag then 5^0 spoilers.

REFERENCES

[1] SajjadBeigmoradi, KambizJahani, Arash Keshavarz and Mohsen BayaniKhaknejad, "Aerodynamic Noise Source Identification for a Coupe Passenger Car by Numerical Method Focusing on the Effect of the Rear Spoiler", SAE International, 2013.

[2] M.H. Djavareshkian, A. Esmaeli, "Optimization of Smart Spoiler for Race Car", International Conference on Fluid Dynamics and Thermodynamics, Dubai, January 25-27, 2011, 1-8.

[3] Shyam P. Kodali and SrinivasBezavada, "Numerical Simulation Of Air Flow Over A Passenger Car and The Influence of Rear Spoiler Using CFD", International Journal of Advanced Transport Phenomena, 1(1), 6-12, Jan-Dec, 2012.

[4] Xu-xia Hu, Eric T. T. Wong, "A Numerical Study On Rear-spoiler Of Passenger Vehicle", World Academy of Science, Engineering and Technology, 57, 636-641, 2011.

[5] ŞtefanBordei, Florin Popescu, "Aerodynamic results for a notchback race car", The Annals of "Dunărea De Jos", University of Galați Fascicle, Technologies in Machine Building, ISSN 1221- 4566, 2011.

[6] Walid Ibrahim Mazyan, "Numerical simulations of drag-reducing devices for ground vehicles", 2013.

[7] Mustafa Cakir, CFD study on aerodynamic effects of a rear wing/spoiler on a passenger vehicle, Dec 2012, Santa Clara University, School of Engineering, 2012, 1-124.

[8] MiladMafi, "Investigation of turbulence created by formula one cars with the aid of numerical fluid dynamics and optimization of overtaking potential", Ansys Conference and 25th CADFEM's User Meeting, 21-23 Nov, 2007.

[9] Sagar Kapadia and Subrata Roy, Matthew Vallero, KennethWurtzler and James Forsy, "Detached-eddy simulation over a reference Ahmed car model", from http://cpdl.kettering.edu/ahmed-dles.pdf.

[10] Pramod Nari Krishnani, "CFD Study of Drag Reduction Of A Generic Sport Utility Vehicle", 2006.

International Journal of Engineering Research and Applications (IJERA) ISSN: 2248-9622
National Conference on Advances in Engineering and Technology
(AET- 29th March 2014)

RESEARCH ARTICLE OPEN ACCESS

FEA Analysis to Study the Influence of Various Forming Parameters on Springback Occurs In Single Point Incremental Forming

Ravinder Pal Singh*, Ghansham Goyal**
*(Research Scholar, Department of Mechanical Engineering, MM University, Mullana-Ambala
Email: ravinderpalsingh89@yahoo.com)
** (Assistant Professor, Department of Mechanical Engineering, MM University, Mullana-Ambala
Email: ghansham_goyal2000@yahoo.com)

ABSTRACT
The involvement of computer in manufacturing had result in the development of many modern manufacturing processes, among which one is the Incremental sheet metal forming (ISMF). ISMF is a modification of conventional sheet metal forming process, in which a hemispherical tool which is in the regular contact with the sheet metal moves under a control in three dimensional space and produces the plastic deformation of sheet layer by layer in incremental steps. Previous researches have shown that in ISMF, springback is major factor that affects the accuracy of the job. Controlling of springback is essential to improve the geometrical accuracy of the job. In the present work, the effect of various forming parameters like forming angle (α), tool diameter (*td*), step size (*dz*), sheet thickness (T_s) on the local springback in ISMF is studied..
Keywords – Geometric Accuracy, Increment Sheet Metal forming, Springback.

I. INTRODUCTION

Incremental sheet metal forming (ISMF) is a new innovative combination of computer technology with machine, and this makes it a flexible process. The complicated geometry information is resolved into a series of two-dimensional layers, and then the plastic deformation is carried out layer-by-layer through the CNC controlled movements of a simple hemispherical forming tool to get the desired part [1]. Springback is one of the sheet metal forming defects, which is the most difficult to control and results in geometrical inaccuracy. Many researchers committed to find an effective method to reduce the springback. Trial-and-error, as a traditional method, has been used to compensate the springback.

There have been many researches about springback prediction in ISMF processes. In [2], authors investigated investigated springback prediction in the ISMF process using a genetic neural network. However, the optimization speed was slow, and the accuracy was not very high. In [3], authors investigated material formability in incremental forming and, in particular, the evaluation and compensation of elastic springback through experimental investigation and explicit FEM analysis. In [4], authors investigated the negative springback phenomenon in sheet metal obtained by the incremental forward stretch forming operation, both experimentally and numerically.

Numerical simulation method can be used to save Cost for mold repairing in the process of compensation and to reduce new product development cycle. A spring forward method, which uses the finite element method to calculate the amount of springback accurately, is proposed [5]. The process can also be used for rapid prototyping of new products [6]; but also its well suitable to make old parts which have to be rebuilt, like automotive parts whose dies are today out of service.

1.1 INCREMENTAL SHEET METAL FORMING (ISMF)

Several new metal forming techniques have been developed in the last few years due to advances in:
1) Computer controlled machining and
2) The development of toolpath postprocessors in CAD software packages.

One significant outcome of this technology is the ability to form asymmetric shapes at low cost, without expensive dies. In ISMF, the blank remains stationary and rigidly holds the sheet and forming occurs with the CNC control of the tool in a CNC mill. The toolpath code is feed in the machine and the machine forces the tool to move along the desired path. The tool which is in continuous contact of the sheet and controlled by the computer forces the plastic deformation of sheet layer by layer and result in the required shape.

1.2 DEFINITION

Incremental Sheet Metal Forming (ISMF) is a process which:

- is a innovative sheet metal forming process,
- has a solid, hemispherical forming tool,
- does not requires large, dedicated dies,
- consist a forming tool which is in continuous contact with sheet metal,
- has a tool that moves under control, in three dimensional space,
- can manufacture axis symmetric sheet metal shapes [1].

1.3 ELEMENTS OF INCREMENTAL SHEET METAL FORMING

Incremental Sheet Metal forming has four basic elements:

1) A sheet of material like aluminum, steel, brass etc 2) A blankholder for rigidly hold the sheet
3) A single point hemispherical forming tool,
4) CNC Control and tool path planning as shown in Fig 1.

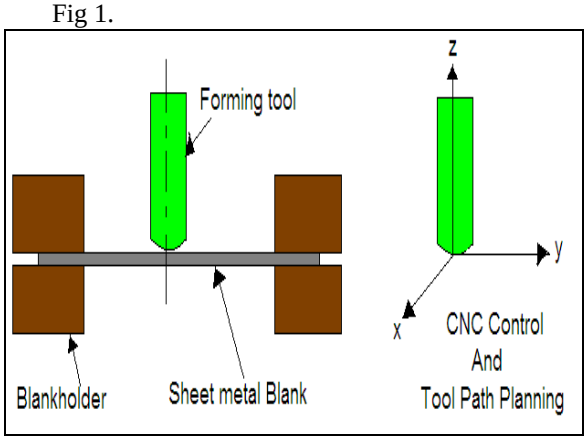

Figure 1: The basic elements needed for Incremental Sheet Metal Forming (ISMF)

1.4 TYPES OF INCREMENTAL SHEET METAL FORMING

ISMF is further categorized in two common types

1) Two Point Incremental Forming (TPIF)
2) Single Point Incremental Forming (SPIF)

These are discussed in the chronological order in which they appeared, historically. In TPIF, the blankholder moves vertically on the bearing i.e. along the Z axis, and at the same time forming tool pushes on to the sheet metal plate as shown in Fig 2. The process consists of two points where the sheet metal is pressed. Hence at a given time interval the sheet metal experiences forces at two points, therefore it is called two point incremental forming. One point is where plastic deformation occurs which is directly below the forming tool and the other point is a static post that creates a counter force on the sheet metal. At one point tool presses into the sheet and other act as a partial die. Hence TPIF is not purely dieless. TPIF consist of:

1) A sheet metal blank holder which moves down with the tool path increments.
2) A stationary post provided at the centre of the blank.
3) A forming tool
4) CNC programming.

To avoid the twisting of shape along the partial die and to provide the backpressure on sheet, there is a backing plate underneath the blank. The partial die in TPIF can also be replaced by a mould which acts as a full die.

In SPIF the opposite surface of the sheet being deformed is free and hence it is a pure dieless process. The apparatus of SPIF is simpler than TPIF as there is no stationary post and the blankholder remains stationary. But as the sheet is completely free from one side it creates different strain and stress patterns in the sheet, in comparison to TPIF.

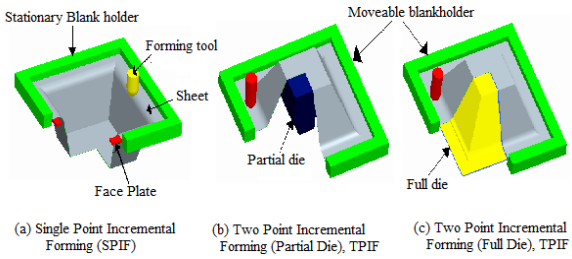

Figure 2: Types of Incremental forming

II. TOOLPATH GENERATION

Effective toolpath generation is very important for incremental forming. Normally two types of toolpath trajectory are used in incremental sheet forming as shown in Fig 3 and Fig 4. These are:

1. Contour toolpath
2. Spiral toolpath

2.1 Contour toolpath

Contour toolpath is defined by fixed step size increments (*dz*) between consecutive contours.

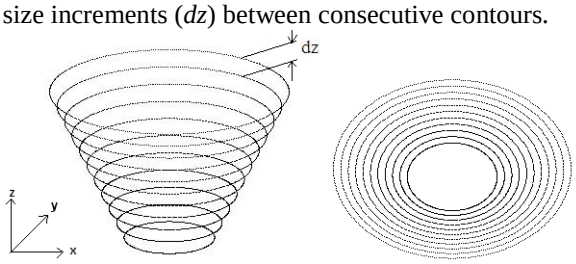

Figure 3: Contour Toolpath

2.2 Spiral toolpath

Spiral toolpath is continuous with incremental drop of the tool distributed over the complete contour of the part.

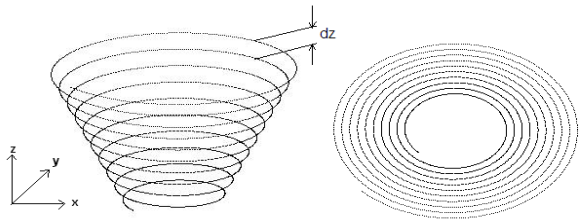

Figure 4: Spiral Toolpath

III. ACCURACY IN ISMF

There are three different types of error which affects the geometrical accuracy of the forming process. First includes the bending of sheet which occurs at the major base of the job. But this defect can be solved by using the backing plate which avoids the over bending of the sheet. Secondly when the tool moves from one part to the other part of the sheet, the sheet bounces back and this result in the distortion of the final shape of the part, this distortion is called springback. Third is a 'pillow effect' which occurs at the minor base of the job and represents the concave curvature on the undeformed material Micari [9]. All these defects are illustrated in Fig 5. Pillow effect can be overcome by just modifying the toolpath trajectory.

Out of the above three error, springback is the major error which effect the geometrical accuracy of part. Lack in geometrical accuracy is basically the difference between the ideal profile and obtained profile. To avoid the effect of springback, proper tradeoff should be made between various process parameters including the use of backing plate and definition of toolpath.

Three types of springback which exist in ISMF are:

- A continuous 'local springback' that occurs on every node at the displacement of the tool toward and away from the sheet element.
- A global springback that occurs at unloading and when the sheet is removed from the blankholder after the job has been made, this result in the change of final shape to some extent.
- A global springback which occurs when the job is trimmed or cut after the job is released from blankholder.

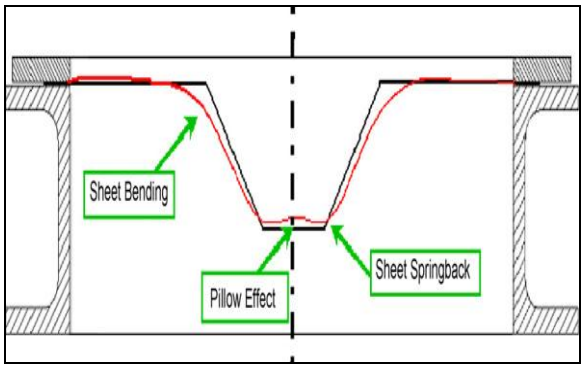

Figure 5: Geometrical error in SPIF process.

IV. FINITE ELEMENT MODELING

The FEA analysis was carried out using a variety of process parameters on CAD Software i.e. ABAQUS (version 6.10). The sheet used for model was Al5052 of young's modulus 70GPa and Poisson ratio 0.3, as Al alloy is the most commonly used in ISMF, mainly because of reduced forming forces as shown in Fig 6. The sheet size was of 75x75 mm and 100x100 mm and the other process parameters i.e. tool diameter (td) was 8 mm, 10 mm, 12.7 mm, the thickness of sheet for various simulation was 0.5 mm, 0.88 mm, 1.2 mm. The sheet was meshed in rectangular linear elements of 1 mm x 1 mm for all simulation. Three step down (dz) size were used i.e. 0.6 mm ,0.8 mm, 1 mm. Higher value of dz were avoided as it effect the surface roughness and lower value results in high simulation time [7] [8] [9] [10]. A truncated conical shape was taken for FEA simulation with the upper diameter of 65 mm and forming angle i.e. draw angle (α) for the two simulations was 45 and 60 degree. The higher value of draw angle was avoided as it leads to sheet thinning and cracks. The depth of cone for the simulation was taken to be 25 mm and 20 mm.

Reliable result was obtained for all simulation consisting of 5625 elements. The final model was cut along the X-plane and the displacement of each node was calculated from the simulation results. The result of all simulation was calculated and analyzed.

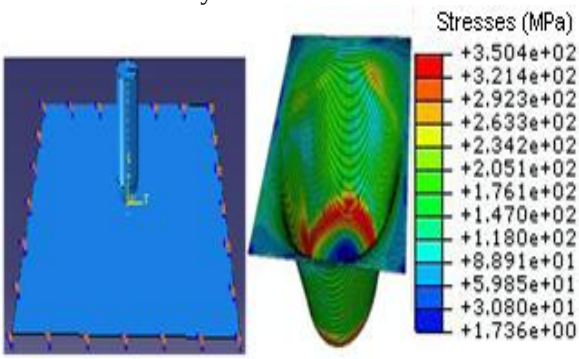

Figure 6: Initial and final stages of sheet metal simulation in ABAQUS

Springback analysis is generally composed of two steps: loading and unloading. The behavior of the nodes was studied with respect to the tool movement along the generated tool path. The displacement of tool towards and away from the sheet element results in the displacement of node, As shown in below Fig 7 and its was found that the crest and trough found in graph are due to the loading and bounce back of sheet which finally results in spring back

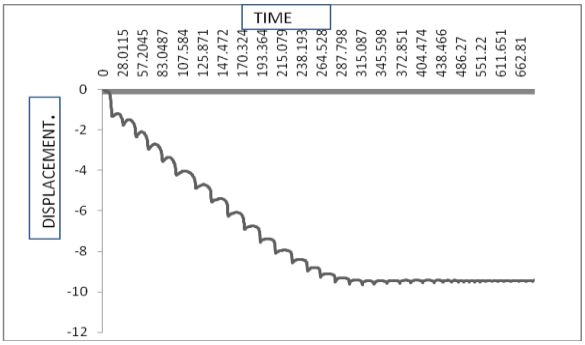

Figure 7: Displacement behavior of node with time

Springback in forming is of three types:
1) Local springback of sheet after force exerted by tool is removed. 2) Global springback, which changes the shape of sheet when it is unclamped and 3) springback which occurs when the sheet is trimmed or cut, if desired. In this paper the effect of various parameters on the local springback was studied. To calculate the local springback occurred in the model the node displacement result obtained from simulation was plotted with ideal curve generated from MATLAB and then the displacement was measured. Fig 8 shows the difference between the simulated and ideal curve.

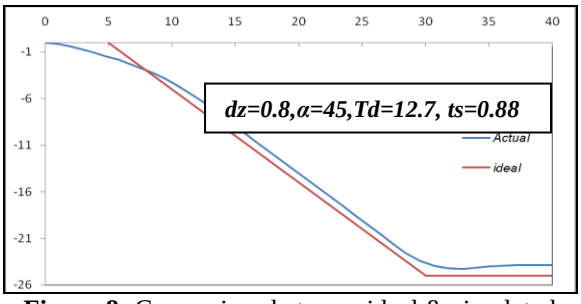

Figure 8: Comparison between ideal & simulated result

V. RESULT AND DISCUSSIONS

5.1 Influence of draw angle (α):

Draw angle has a direct effect on the thickness of sheet, as draw angle (α) increases, more decrease in sheet thickness. The simulation results for draw angle 45 and 60 degree corresponding to step size of 0.6 and 0.8 mm was compared and given Table 1. It was clear from simulation results that the springback increases with increase in draw angle.

Table 1: Local springback results for varied draw angle (α)

dz(mm)	*T_d(mm)*	*T_s(mm)*	*α*	*Springback (mm)*
0.8	12.7	0.88	45	0.7
0.8	12.7	0.88	60	1.4
0.6	12.7	0.88	45	0.64
0.6	12.7	0.88	60	1.3

5.2 Influence of tool diameter (T_d):

Tool diameter affects the surface quality and manufacturing time. The minimum diameter used depends upon the smallest radius required in the part. The most commonly used tool diameters are 12 and 12.7 mm [1]. Three simulations for tool diameter of 8 mm, 10 mm, and 12.7 mm were carried out and the springback obtained are shown in Table 2. It clearly indicates that increase in tool diameter, increases the springback.

Table 2: Local springback results for varied tool diameter (T_d)

dz(mm)	*T_d(mm)*	*T_s(mm)*	*α*	*Springback(mm)*
0.8	8	0.88	45	0.45
0.8	10	0.88	45	0.5
0.8	12.7	0.88	45	0.7

5.3 Influence of Step size (dz):

High value of Step size (dz) results in surface roughness and lower value results in longer simulation time. Therefore for the simulation test the preferable values of dz are 0.6, 0.8 and 1 mm are taken, and results corresponding to variation in step size for springback are shown in Table 3. It can be said that the value of dz has little effect on springback but it has much effect on surface quality.

Table: 3 Springback results for varied step size **(**dz**)**

dz(mm)	*Td(mm)*	*Ts(mm)*	*α*	*Springback(mm)*
0.6	12.7	0.88	45	0.64
0.8	12.7	0.88	45	0.7
1	12.7	0.88	45	0.75

5.4 Influence of Sheet thickness (T_s)

Thickness of sheet depends on the nature of job; it has a direct effect on the forming angle, higher sheet thickness is avoided as they require high forces for deformation. In ISMF, the thickness of sheet varies from 0.3 to 3 mm. In present study simulation on thickness of 0.5 and 0.88 were carried out and results corresponding to variation in sheet thickness for springback are shown in Table 4. It was observed that change in sheet thickness has less impact on variation of spring back.

Table: 4 Local springback results for varied sheet thickness **(**Ts**).**

dz(mm)	*Td(mm)*	*Ts(mm)*	*α*	*Springback(mm)*
0.8	12.7	0.5	45	0.4
0.8	12.7	0.88	45	0.5

VI. CONCLUSION

A study was carried out in order to evaluate the influence of various forming parameters on local springback in forming components. Based on simulation results, the local springback was calculated for different process parameter which include tool diameter (Td), Draw angle (α), step size (dz), and sheet thickness (Ts).The node displacement from simulation result were compared with the ideal curve geometry and it was obtained that springback increases with increase in tool diameter (Td), draw angle (α) and sheet thickness (Ts). The vertical step size (dz) has little effect on springback which increases with increase in dz, but higher value of incremental step size (dz) results in surface roughness and cracks. It is clear from present study that forming angle (α) has a major effect on the springback, and the geometrical accuracy of the formed part can be improved by making necessary tradeoffs between above parameters.

For future work a generalized mathematical formulation can be made between these parameters to indicate the springback and global springback can be investigated for different shapes and parameters like material, lubrication, tool rotation etc.

REFERENCES

[1] Jeswiet J, Micari F, Hirt G, Bramley A ,Duflou J ,Allwood J. Asymmetric single point incremental forming of sheet metal [J]. Annals of CIRP, 2005, 54(2): 623−649.

[2] Han Fei, MO Jian-hua, Gong Pan. Incremental sheet NC forming springback prediction using genetic neural network [J]. Journal of Huazhong University of Science and Technology: Nature Science Edition, 2008, 36(1): 121−124.

[3] Ambrogio G, Costantino I, de Napoli L, Filice L,Muzzupappu M. Influence of some relevant process parameters on the dimensional accuracy in incremental forming: A numerical and experimental investigation [J]. Journal of Materials Processing Technology, 2004, 153−154: 501−507.

[4] Tanaka S, Nakamura T, Hayakawa K, Nakamura H, Motomura K. Experimental and numerical investigation on negative springback in incremental sheet metal forming [C]//12th International Conference on Metal Forming. Cracow: Verlag Stahleisen MBH, 2008: 55−62.

[5] Karafillis A P, Boyce M C. Tooling and binder design for sheet metal forming processes compensating springback error [J]. Int J Mech Tools Manufact, 1996, 36(4): 503−526

[6] H. Amino, Y. Lu, T. Maki, S. Osawa, K. Fukuda, Dieless NC forming, prototype of automotive service parts, in: Proceeding of the Second International Conference on Rapid Prototyping and Manufacturing (ICRPM), Beijing, 2002.

[7] Filice, L., Fantini, L., Micari, F. Analysis of Material Formability in Incremental Forming, Annals of the CIRP, vol. 51/1/2002: 199-202.

[8] Hirt, G., Ames, J., Bambach, M., Kopp, R. Forming Strategies and Process Modelling for CNC incremental Sheet Forming. Annals of CIRP vol 53/1/2004; p 203

[9] F. Micari , G. Ambrogio, L. Filice . Shape and dimensional accuracy in Single Point Incremental Forming: State of the art and future trends. Journal of Materials Processing Technology 191 (2007) 390–395

[10] Hagan, E. and Jeswiet, J. Analysis of surface roughness for parts formed by CNC incremental forming". IMECHE part B, J. of Engineering Manufacture. Vol. 218 No. B10, 2004. pp 1307 –1312.

International Journal of Engineering Research and Applications (IJERA) ISSN: 2248-9622
National Conference on Advances in Engineering and Technology
(AET- 29th March 2014)

RESEARCH ARTICLE OPEN ACCESS

Noise Reduction Technique in Synthetic Aperture Radar Datasets using Adaptive and Laplacian Filters

Sakshi Kukreti*, Amit Joshi*, Sudhir Kumar Chaturvedi*
*(Department of Aerospace Engineering, University of Petroleum and Energy Studies, Dehradun -07
(E-mail: sudhir.chaturvedi@ddn.upes.ac.in)

ABSTRACT

Presence of salt and pepper noise in Synthetic Aperture Radar (SAR) raw image datasets of coastal and sea areas makes it very difficult to detect the targets in it. Adaptive filters are known for their remarkable filtering of those signals which are a result of unknown terrain mapping and which has a non-stationary surface. Whereas a Laplacian filter is known for its edge marking and enhancing the processed image. Hence both the filters were used together to produce an enhance image having target with clear boundaries. The processed image has a substantial reduction in the value of salt and pepper noise. The computing power used in this filtering technique is very less as compared to other filtering methods and the results obtained are better than other methods. The position of the target can be calculated afterwards by measuring the centroid of the geo-referenced image.

Keywords – SAR, Laplacian Filter, Adaptive Filter, Enhance, Image enhancement technique

I. INTRODUCTION

An image can be represented as a function of $f(x,y)$ where (x,y) are spatial (plane) coordinates. The amplitude of the function $f(x,y)$ gives the intensity of image at coordinates(x,y). Images provided by SAR systems have very high resolution and are of wide area, hence sub images or regions of interest are carved out from the original image. As an image is nothing but a matrix, hence it is easy to extract a sub image from an original image matrix. After the sub images have been extracted the noise can be removed from them using an adaptive filter first and then a Laplacian filter to enhance the target position. The noise present in the SAR dataset is due to high amount of backscatter from the sea surface [1] The waves having crust and trough produce the noise known as salt and pepper noise and it makes the detection of actual target i.e. ship very difficult. A digital filter is a system which uses certain mathematical operations to reduce or discretize certain aspects of the input data which is noise in the case of SAR dataset. Every signal processing system has a filter to its core and it helps remove noise, unnecessary clutter data and enhance the final image. The adaptive filter is a special type of filter which adapts itself according to the characteristics of the image and removes the noise accordingly [2]. Adaptive noise smoothing filter for images with signal-dependent noise [5] whereas Laplacian filter is used to mask the resultant image from adaptive filtering and then remove the remaining noise and enhancing the target object [3].

1.1. Filters

1.1.1. Averaging Filter

Averaging filter replaces each element of image matrix (pixel value) with average of pixels in a square window surrounding pixel. In a large window of operation it can remove noise more effectively but it blurs the details. Instead of averaging all pixel values in an image matrix, closer pixels can be given higher weighting and far away pixels can be given lower weighting [4].
The function for a weighted averaging filter can be given as:

$$g(m,n) = \sum_{l=-L}^{L} \sum_{k=-L}^{L} h(k,L) S(m-k, n-l)$$

Where $g(m,n)$ is output image, $h(k,L)$ is the transfer function or the weight given to an element and $S(m-k, n-l)$ is the input image.

1.1.2. Adaptive Filter

An Adaptive filter is a linear filters which is capable of changing their behavior depending upon the region of the image being filtered. These are special type of filters which are applied on the images

where image characteristics vary drastically form point to point [2]. An adaptive filter is as follows:

$$g(x,y) = f(x,y) - (\sigma_n^2/\sigma_l^2) * (f(x,y) - m(x,y))$$

Where $f(x,y)$ is the input image, $g(x,y)$ is the output, $m(x,y)$ is the mean image value, σ_n *and* σ_l are constants with value respectively 4 and 3. The adaptive filter given above is known as Willis filter and used in the image processing of non-stationary surfaces and targets [4].

Laplacian Filter Algorithm

Laplacian of an image $f(x,y)$ can be denoted as $\nabla^2 f(x,y)$ and expressed as

$$\nabla^2 f(x,y) = \frac{\partial^2 f(x,y)}{\partial x^2} + \frac{\partial^2 f(x,y)}{\partial y^2}$$

Digital approximation of second derivative can be done in two ways. According to the first method

$$\frac{\partial^2 f(x,y)}{\partial x^2} = f(x+1,y) + f(x-1,y) - 2f(x,y)$$
$$\frac{\partial^2 f(x,y)}{\partial y^2} = f(x,y+1) + f(x,y-1) - 2f(x,y)$$

The above expression can be realized at all the elements of an image by convolving the image with following spatial mask

$$\begin{bmatrix} f(x-1,y-1) & f(x,y-1) & f(x+1,y+1) \\ f(x-1,y) & f(x,y) & f(x+1,y) \\ f(x-1,y+1) & f(x,y+1) & f(x+1,y+1) \end{bmatrix}$$

Or

$$\begin{bmatrix} 0 & 1 & 0 \\ 1 & -4 & 1 \\ 0 & 1 & 0 \end{bmatrix}$$

Another approach of digital second derivatives takes into account of diagonal elements and can be implemented as

$$\begin{bmatrix} 1 & 1 & 1 \\ 1 & -8 & 1 \\ 1 & 1 & 1 \end{bmatrix}$$

Enhancement of the image using Laplacian filter is based on following equation

$$g(x,y) = f(x,y) + c[\nabla^2 f(x,y)]$$

Where $\nabla^2 f(x,y)$ is the filter mask, $f(x,y)$ is the input image, $g(x,y)$ is the output image and the value of c is 1 when center coefficient of filter mask is positive and -1 when center coefficient is negative [5].

II. METHODOLOGY

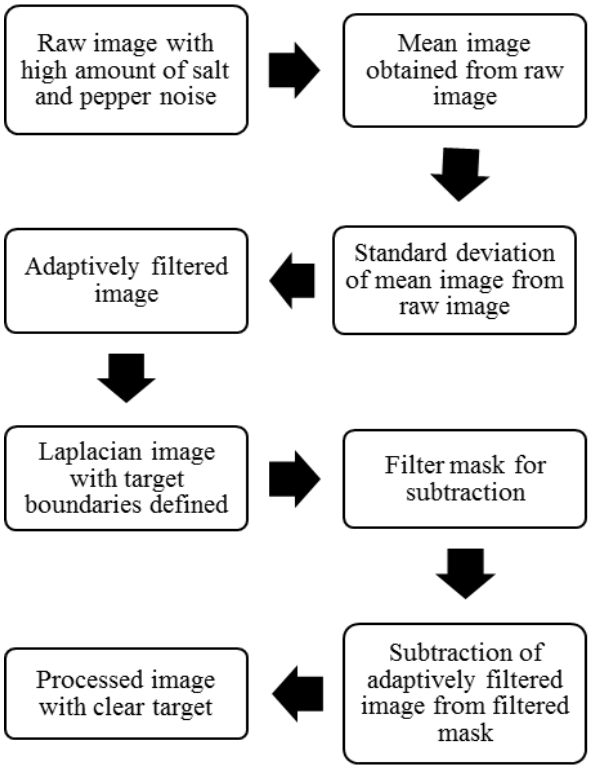

Figure 1: Flow Chart for Noise Reduction Technique And Methodology

Figure 1 shows the methodology of the research work to obtain the final image which contains a clear target with defined boundaries. At first the noise present in the raw image is smoothed out using an adaptive filter. Due to the filter target gets blurred which is not intended. To reduce this blur and produce a clear image, a Laplacian filter is then used to produce a boundary mask which is when subtracted from adaptively filtered image produces an enhanced and clear image of the target.

III. RESULTS

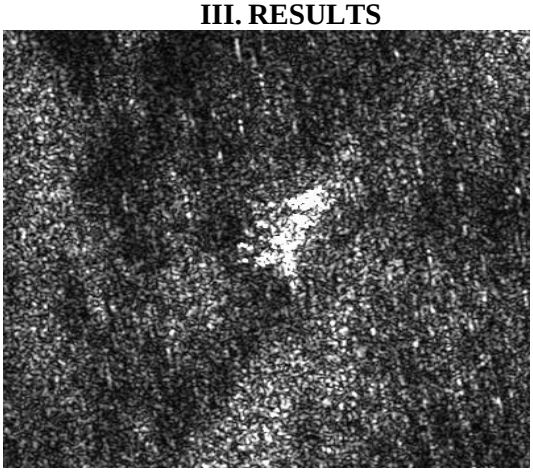

Figure 2: Original Raw Image

The raw image of the region of interest obtained from TERRASAR-X is shown in Fig. 2. It is clearly visible that the presence of noise (because of sea backscatter), has made the target very less identifiable. This noise is also known as salt and paper noise and it is induced because of the sea surface movements. To remove the noise a systematic approach of filtering was used in which an adaptive filter was first used to suppress the noise elements present in the raw image data and then the image was enhanced using Laplacian filter. The histogram of original image in Fig 3 displays the gray level value of pixel in x axis and pixel count containing that gray level value in y axis.

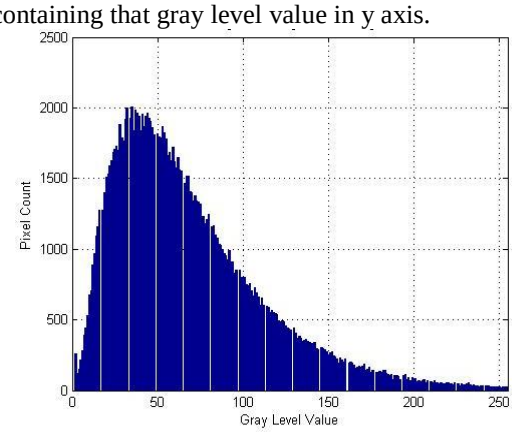

Figure 3: Histogram of Original Image

The mean image is the generated from the original image to smooth out the noise elements however in this process some details get blurred. To get a mean image each element is replaced by the mean value of its surrounding MXM matrix which is in this case matrix of 5X5 matrix. The resultant image thus produced is shown in Fig 4.

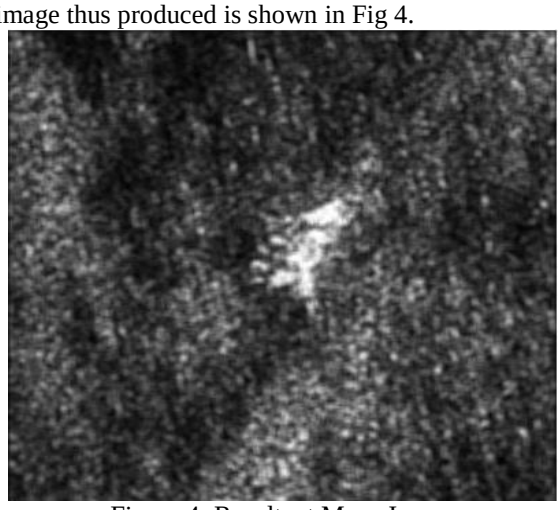

Figure 4: Resultant Mean Image

The loss of clear edges and induction of blur can be clearly seen between original and the local mean image. The histogram of the mean image shows the clear difference between the gray level value and pixel count from the original image.

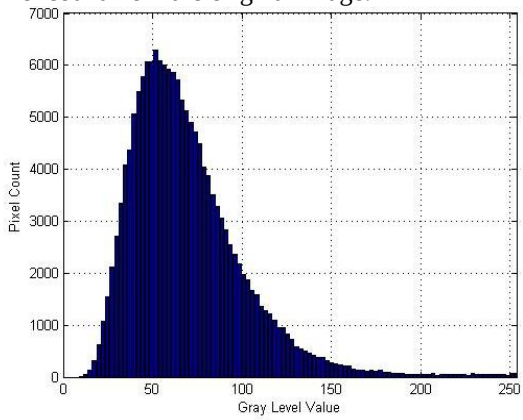

Figure 5: Histogram of Local Mean Image

After the mean image has been obtained another image showing standard deviation from the original image is obtained which is only used to find out maximum possible value of grey level of the target. From Fig 5, it can be seen that now the grey level value of majority of pixels have been shrunk to the region 10 to 100.

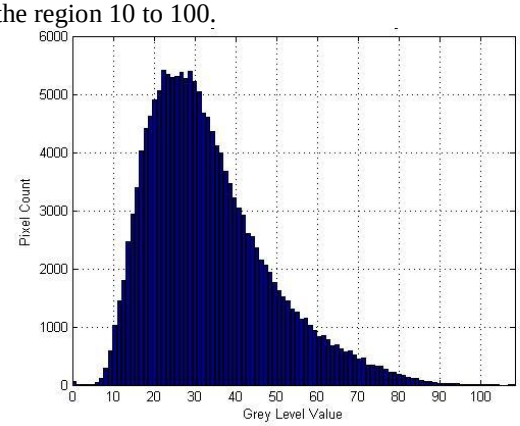

Figure 6: Histogram of Standard Deviation Image

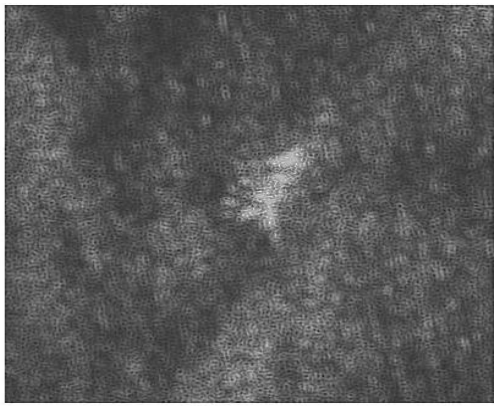

Figure 7: Result Obtained From Adaptive Filtering Technique

The histogram of standard deviation image is shown in Fig 6. It can be clearly seen that the pixels have been even further shrunk to the grey level value ranging between 10 to 70. This will help us derive the final filtered image as shown in Fig 7 which is shown below with its histogram. In the final filtered image, the histogram has been spaced between 40 to 100 giving a clear region of target as shown in Fig 8. Rest of the noise has been reduced to a minimum level, which will be masked by a laplacian filter and then will be removed by subtracting it from the original image.

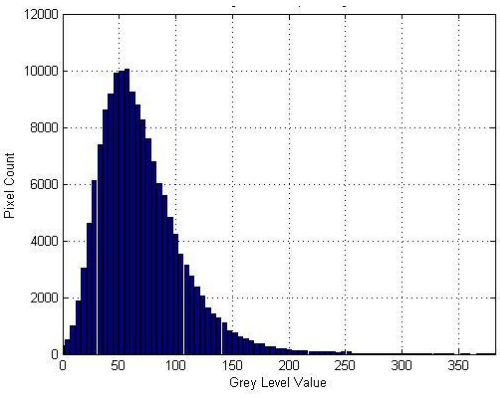

Figure 8 : Histogram of Adaptively Filtered Image

After the final filtered image has been achieved, a laplacian filter is used to mask the remaining noise and target as shown in Fig 10. The mask creates the boundaries for the target and the noise which is then subtracted to get the final enhanced image of target with noise reduced to maximum.

The masked image obtained in MATLAB computation as shown in Fig. 9.

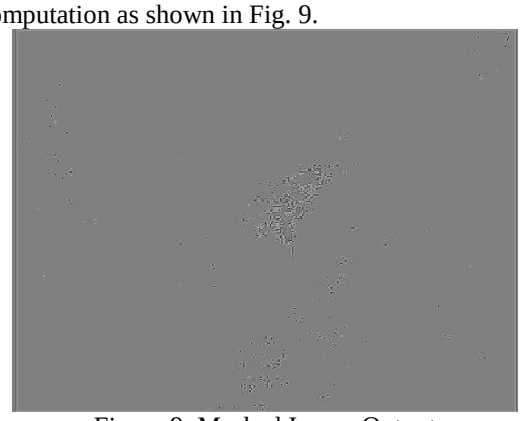

Figure 9: Masked Image Output

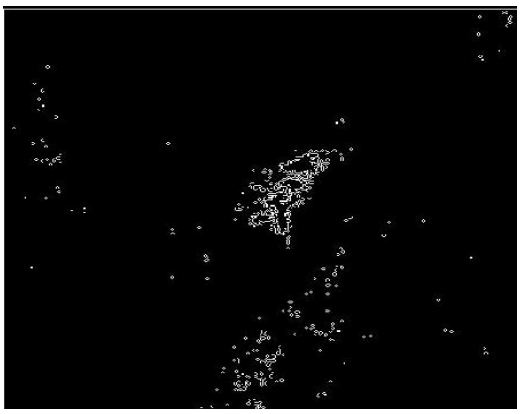

Figure 10 : Laplacian Mask of the Target

In the image the boundaries of the target can be clearly seen. The purpose of defining the boundaries is to eliminate the target from the blurred noise obtained from adaptively filtered image. However in this process some part of noise is also inserted as target boundaries because of its size. After the boundaries have been defined, a filter mask is produced which is used for the subtraction of noise from adaptively filtered image and enhance the target edges.

Fig 11 shows the original image is then subtracted from this filtered image to get the enhanced output image of the target. Area inside the target boundaries as well as some bigger chunks of noise are retained whereas rest of the noise is completely removed making those pixels value to be zero. Thus a final enhanced image is obtained as shown in Fig 12, with clear edges of the target situated at the center of the image. The coordinates of the target can be calculated by measuring the centroid of the image as the target lies at the center itself.

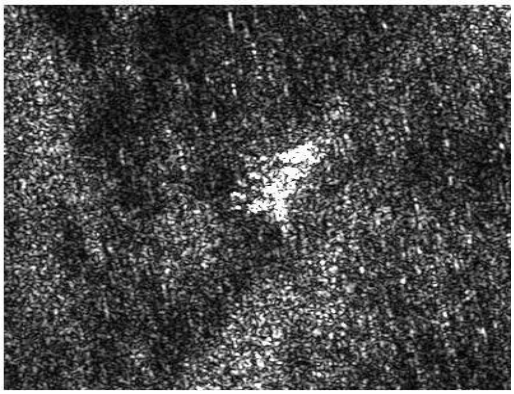

Figure 11: Original Raw Image of The Target

Figure 12 : Result Shows the Enhanced Image with Target in the Center of an Image with Certain Amount of Noise.

IV. CONCLUSION

The difference between the clearness of targets can be clearly seen from the comparison of above two images. In the original image, there is no exact distinction of target boundaries because of the presence of salt and paper noise. In the final image the target can be seen at the center of the image with very less noise. This process consumes very less amount of computing power than the other filtering techniques and produces very sharp, enhanced images also reduces the noise to a significant level. The study of various filters over the SAR image data were carried out to provide the result for the image enhancement. The technique provides the exact methodology and study of image enhancement in presence of salt and pepper noise using the filters algorithm.

V. ACKNOWLEDGEMENT

Authors would like to thank University of Petroleum & Energy Studies for utilizing the computation facility. Also, presenting author would like to thank Prof. S.K. Chaturvedi for his continuous support and guidance towards this work.

REFERENCES

[1] Soumekh, “Synthetic Aperture Radar Signal Processing”, Mehrdad (1999), New York, Wiley.

[2] Kuan, Darwin T., “Adaptive Noise Smoothing Filter For Images With Signal-Dependent Noise, Pattern Analysis and Machine Intelligence”, IEEE Transactions on 2, 1985, 165-177.

[3] Paris, Sylvain, Samuel W. Hasinoff, and Jan Kautz, “Local Laplacian Filters: Edge-Aware Image Processing With A Laplacian Pyramid”, ACM Trans. Graph, 2011, 30 (4), 68.

[4] Haykin, Simon S., “Adaptive Filter Theory”, 2005, 4/e, Pearson Education, India.

[5] Huertas, Andres, and Gerard Medioni, “Detection of intensity changes with subpixel accuracy using Laplacian-Gaussian masks, Pattern Analysis and Machine Intelligence”, IEEE Transactions on 5, 1986, 651-664.

RESEARCH ARTICLE OPEN ACCESS

Review of the High Vacuum Metal-Metal and Metal-Ceramic Brazing Process

Mohit Srivastava*, Bir Bahadur Sherpa**
*(PEC University Of Technology, Chandigarh, India
Email: mohit.10989@gmail.com)
** (PEC University Of Technology, Chandigarh, India
Email: sherpa7419@gmail.com)

ABSTRACT
Brazing is a joining process which is extensively used for components fabrication. The significance of this process lies in its ability to join similar or dissimilar metals to metals and metals to non-metals with close coefficient of thermal expansion (CTE). High vacuum brazing is carried out at high temperature to obtain hermetically sealed joints. This technical paper emphasizes on various parameters governing the brazing process, significance of contact angle in promoting wetting and spreading, strength obtained by mechanical testing and braze joint design. Furthermore it discusses various designs of metal-ceramic joining.
Keywords – Active, CTE, hermetically sealed, high vacuum and parameters.

I. INTRODUCTION

The American Welding Society (AWS) defines brazing as "a group of welding processes" which produces coalescence of materials by heating to suitable temperature and using a filler metal having a liquidus above 450^0C and below solidus of base metal [1].It differs from welding as it takes place at temperatures below the melting points of the base materials to be joined. Parts that may not be joined at all by other methods can be joined by brazing. The nature of the interatomic (metallic) bond is such that even a simple joint, when properly designed and made, will have strength equal to or greater than that of the as-brazed parent metal or non-metal. Metal as thin as 0.01mm and as thick as 150 mm can be brazed. There are infinite numbers of possible parent metal brazing alloy combinations. The phenomena of wetting and flow of a liquid on the surface of a solid are basic to most models developed to describe the formation of a braze joint. Wetting of the base materials by the braze filler metal is required to provide the bonding needed and is characterized through the thermodynamic concept of capillarity [2]. The braze filler metal is distributed between the closely fitted surfaces of the joint by capillary attraction. The capillary flow depends on the ability of the brazing alloy to wet the parent metals. This property is determined by the relative characteristics of the solid and liquid phases, its measure being the magnitude of the contact angle. The lower the contact angle, the better are the wetting and spreading properties of the brazing alloy, and no capillary flow can take place unless the contact angle is less than 90^0 [3]. Brazing generally generates much less thermally-induced distortion or warpage since a part can be uniformly heated to brazing temperature and therefore, minimizes any type of distortion. Load carrying capacity of the brazed joint is affected by the dimensions of the joint gap and by the design of whole assembly. Brazing processes are employed where welding processes cannot be used viz. value added components, high quality RF systems, carbide tools, UHV components of high energy [4].

1.1 SIGNIFICANCE OF VACUUM FURNACE BRAZING

It is usually a high temperature (typically 927^0C to 1232^0C), fluxless process using nickel-base, pure copper and less frequently precious BFM.

(i) Advantages of brazing under vacuum conditions Purity level of atmosphere (vacuum) can be precisely controlled. There is less residual oxygen to contaminate the work piece. The vacuum condition at high temperature results in a decomposed oxide layer, and by doing so improves the base metal wetting properties. It results in minimum distortion because all parts are heated and cooled uniformly at precisely controlled rates. Furthermore, it provides repeatability and reliability of the brazing process.

1.2 MANDATORY CONDITIONS FOR BRAZING

(i) Joining must be without melting the base metal.
(ii) Braze filler metal (BFM) must have melting temperature above 450^0C.

(iii) BFM must wet the base metal surfaces and be drawn into or held in the joint by capillary attraction.

1.3 REASONS OF VARIOUS BRAZING PROBLEMS

Violation of one of these fundamentals of brazing causes brazing problems:

(i) Proper design of brazed joint.
(ii) Cleaning and surface preparation of work pieces prior to brazing.
(iii) Proper joint fit up (gap clearance at brazing temperature, flatness, etc.)
(iv) Braze filler metal selection.
(v) Properly designed vacuum furnace brazing cycle (brazing temperature and time, heating and cooling rates, etc.)

1.4 WETTING AND ADHESION

Joining of two materials together requires bonding. The nature of this interaction can be chemical, physical or simply mechanical. Joining processes resulting in physical or chemical bonding such as brazing is ruled by thermodynamic principle of energy reduction. The elimination of two surfaces to form an interface reduces the total energy of the system. When the materials to be joined are dissimilar, there also exists a chemical potential gradient at the interface. Ceramic/metal brazing relies on the ability of a filler metal or alloy to wet the ceramic surface. The wetting by a liquid metal/alloy depends on the magnitude of the surface tension and the reactivity of the species involved. Surface properties, microstructure of the ceramic material and reactivity of the filler alloy in the brazing atmosphere are the main aspects that control wetting. The magnitude of wetting can be evaluated from the contact angle [5].

1.5 BRAZE JOINT DESIGN

1.5.1 Clearance for Vacuum Furnace Brazing: It is the distance between the surfaces of the joint at brazing temperature. Required clearance for silver, gold, copper and nickel braze filler metals at brazing temperature lies between 0.0005 to 0.004 inch. Vacuum brazing requires lower clearances than atmospheric brazing. For vertical joints, clearance should be less than 0.002 inches.

1.5.2 Differential Metal Expansion (DME): With dissimilar metals, the one with the highest expansion coefficient may tend to increase or decrease the clearance.

Calculation of Room Temperature Clearance: Knowing the DME rates for the metals being joined, back calculate from the brazing temperature down to room temperature, to find room temperature clearance.

1.5.3 Effect of Surface Roughness: It may be 32 RMS, 64 RMS or even 125RMS or greater. It adds surface area to the joint which provides countless extra capillary paths for BFM to follow [1].

1.5.4 Design of Joints:

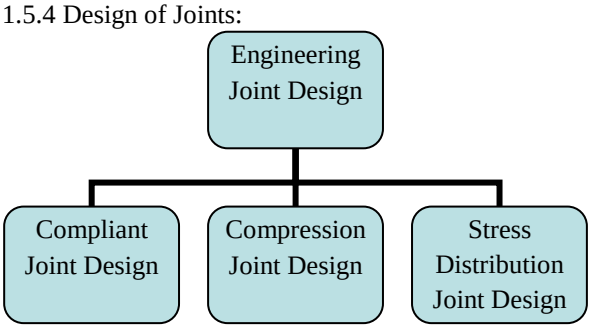

Fig. 1: Taxonomy of Joint Design

Compliant Joint Design (Fig.1): Edge brazing of a metal cylinder to a ceramic face is a popular form of compliant joint. In this case, thermal expansion mismatch is accommodated by the concentric distortion of the metal cylinder. This design can also be obtained by using an interlayer that has a thermal expansion coefficient between those of the ceramic and the metal. This distributes the thermal expansion mismatch and reduces the thermal stress.

Compression Joint Design: In this design, thermal expansion mismatch is used to obtain a reliable joint. This can be obtained by brazing the ceramic member into the metal member. During cooling from brazing temperature to room temperature, the metal member (outside) contracts more than the ceramic member (inside).This results in compressive stress in the ceramic as well as in the joint and the joint strength is increased.

Stress Distribution Joint Design: A ceramic backup can be used to distribute tensile loading on the metal diaphragm [6].

1.6 METAL CERAMIC JOINING

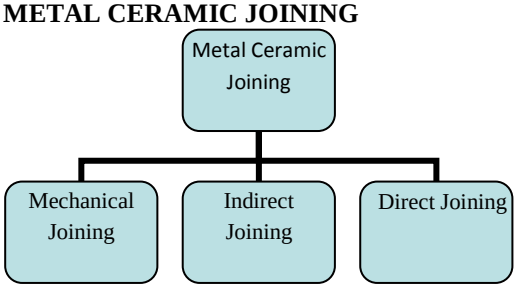

Fig. 2: Taxonomy of Metal Ceramic Joining

Mechanical Joining (Fig 2): It can be done by 3 ways:

(i)Screwing (ii) Fitting (iii) Clamping

Mechanical strength of the metal-ceramic joint in mechanical joining lies between 10 to 50 MPa.

Indirect Joining is classified into two categories viz. Adhesive and Brazing [8]. Structural ceramics which have been brazed are Si_3N_4, SiC, Al_2O_3, AlN and ZrO_2.Mechnical strength of metal-ceramic joint in brazing is approximately 100MPa.

Direct joining of metal-ceramic is carried out by solid state diffusion. Friction welding is an example of solid state joining. Fusion welding is based on localized melting of the metallic component. A laser beam is commonly used as a heating source. Mechanical strength of the joint in fusion welding lies between 50 to 200 MPa .

Problem in Joining of Ceramics by Brazing: Usual BFM do not wet surface of ceramics. The difference in coefficient of thermal expansion of metal and ceramics induces tremendous stress which can lead to cracking of brazed joint [7].

II. ANALYTICAL ANALYSIS

Young's equation is given as

$$\cos \Theta = (Y^{SV} - Y^{SL}) / Y^{LV} \quad (1)$$

Where,

Θ = contact angle

Y^{SV} = solid vapor interfacial energy

Y^{SL} = solid liquid interfacial energy

Y^{LV} = liquid vapor interfacial energy

Average velocity, V, of capillary flow between parallel horizontal surfaces, is given by

$$V = D \gamma \cos \Theta / 6 \eta S \quad (2)$$

where,

D = joint gap

γ= surface tension of BFM

η= viscosity of BFM

Θ = contact angle

S = distance through which the metal has flowed.

Time, t, in which the brazing alloy will flow through the distance S is given by

$$t = 3 S^2 / D \gamma \cos \Theta \quad (3)$$

where, t = time taken by BFM to flow through distance S.

III. OBSERVATIONS

An example of the edge brazing where a copper-clad 430- stainless- steel cap has been brazed on an alumina cylinder is shown in Fig. 3.

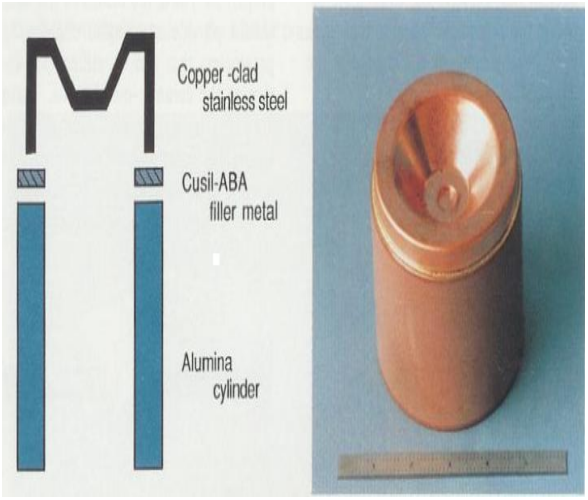

Fig. 3 A schematic cross section of the assembly (left) and the actual brazed sample (right)

An example of the compression joint where a silicon nitride rod is brazed into a hole machined in a 410 stainless steel with Cusil- ABA is shown in Fig. 4.

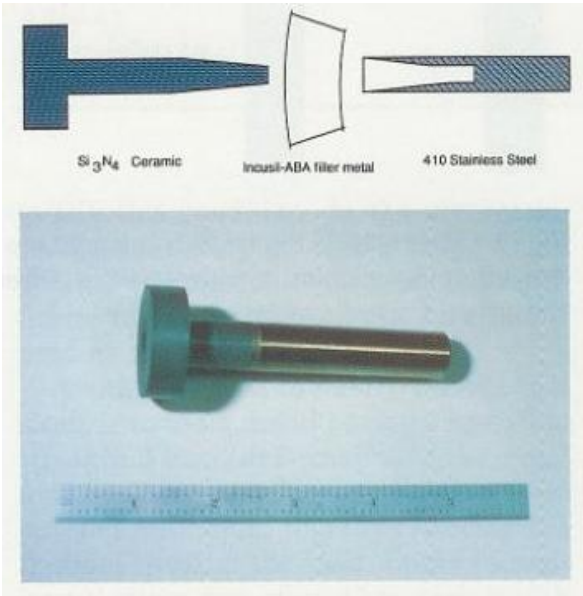

Fig. 4 A schematic cross section of the joint (top) and the actual compression joint (bottom)

An example of the stress distribution joint design where Alloy 42 sheets are brazed on both ends of an alumina cylinder with alumina backup rings is shown in Fig. 5.

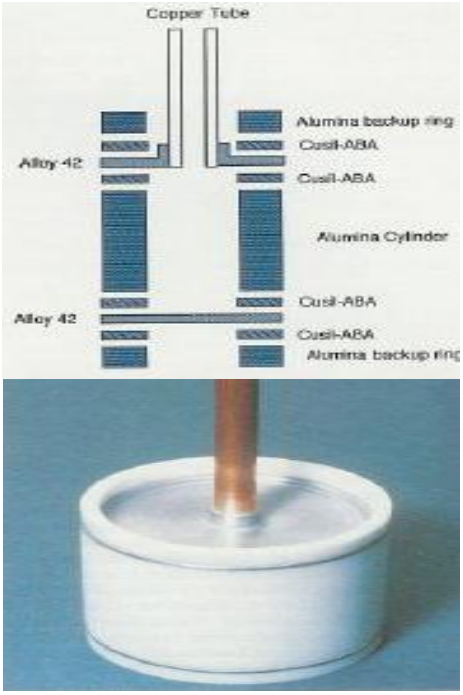

Fig. 5 A schematic cross section of the joint (top) and actual stress distribution joint (bottom).

IV. CONCLUSION

Brazing is a versatile joining process which can be used for joining dissimilar materials. The quality of brazed joints depends strongly on the combination of filler and component materials and also on the processing conditions that are used.

There is a difficulty in joining of metal with ceramics due to large difference in coefficient of thermal expansions (CTE). But this CTE mismatch can be used to obtain a strong joint by selecting proper joint design.

The strength of brazed joint depends upon the wetting of base metal by braze filler metal which in turn depends upon the contact angle.

REFERENCES

[1] Janusz Kowalewski and Janusz Szczurek, "Issues in Vacuum Brazing," *Proc. International Brazing and Soldering Conference*, 2006, 326-333.

[2] Mel M. Schwartz, *"Brazing," ASM International (Second Edition)*, 2003

[3] M.H. Sloboda, "Design And Strength Of Brazed Joints," *Johnson Matthey & Co Limited London*, 1961.

[4] Rajvir Singh, Kamlesh Yedle, A.K Jain, *Development of Vacuum Brazing Furnace*, Accelerator Component Engineering & Fabrication Centre for Advanced Technology, 2010, 1- 4.

[5] R.M. do Nascimento, A.E. Martinelli, A.J.A Buschinelli, "Review Article: Recent advances in metal-ceramic brazing," *Ceramica, 49 (1), 2003, 178-198.*

[6] Howard Mizuhara, E.Huebel and T.Oyama, "High-Reliability Joining Of Ceramics To Metal," *Cremica Bulletin, 68(9), 1591-1599*

[7] H.R Prabhakara, "Vacuum Brazing of Ceramics and Graphite to Metals," *Bangalore Plasmatek Pvt. Ltd.*

[8] David M. Jacobson, "Principles of Brazing," *ASM International*, 2005.

International Journal of Engineering Research and Applications (IJERA) ISSN: 2248-9622
National Conference on Advances in Engineering and Technology
(AET- 29th March 2014)

RESEARCH ARTICLE OPEN ACCESS

Experimental Study on Direct Expansion Solar Assisted Heat Pump System

Chandan Swaroop Meena*, Sunita Meena**, V.K.Bajpai***
* (Department of Mechanical Engineering, NIT Kurukshetra, Haryana-136119 Email: chandanswaroop2008@gmail.com)
** (Department of Mechanical Engineering, NIT Kurukshetra, Haryana-136119 Email: sunitameena2008@gmail.com)
*** (Professor, Department of Mechanical Engineering, NIT Kurukshetra, Haryana-136119 Email: vkbajpai@yahoo.com)

ABSTRACT
In this paper, an experimental study for heating of domestic water using direct expansion solar assisted heat pump (DX-SAHP) was carried out. The refrigerant R-134a was expanded in the glazed solar collector which also plays the role of the evaporator in a conventional vapor compression heat pump device. The experiment on the above mentioned system was performed for four different days which were chosen depending upon the clear day. The average coefficient of performance (COP) of heating for this system under winter climatic conditions was found to be about 2.91. The parameters like refrigerant mass flow rate, temperature and pressure have been measured at different point in the system. It was concluded that the time taken for heating 30 liters of water from 15°C to 50°C is about 75 minutes for this system. At that time solar intensity varies from 523-710 W/m^2.
Keywords – solar energy, direct expansion solar assisted heat pump, coefficient of performance, heat transfer fluid.

I. INTRODUCTION

Among the alternative energy sources in nature, solar energy is free, easily available and non-polluting which could be used in domestic or industrial low temperature applications. The idea of the combination of heat pump and solar energy known as SAHP has been proposed and developed by many researchers [1] [2] [5]. The SAHP that were proposed could be differentiated as direct expansion solar assisted heat pump and indirect solar assisted heat pump. This paper is focused on estimating the performance of DE-SAHPWH system where DX-SAHPs integrate directly Reverse-Rankine refrigeration device with solar collector that also serves as evaporator. In the direct-expansion solar-assisted heat pump water heater (DX-SAHPWH) system, the refrigerant in solar collector absorbs the incident solar energy and ambient energy and in condenser, it contributes to water heating by heat rejection. In this regard, many theoretical and experimental studies have been reported [3] [4] [11] [12]. A review on such a field of work has indicated that the COP values of the DX-SAHP systems range from 2 to 9, where the experiment was carried out under different climate conditions. Since the overall performance of a solar system is influenced significantly by the changes in climatic conditions and load, it describes the variation in COP.

II. NOMENCLATURE

C_p --heat capacity of refrigerant, [kJ/kg-K]
C_{pw} –heat capacity of water, [kJ/kg-K]
COP -- coefficient of performance of DX-SAHP
h_1-- the enthalpy of the refrigerant exiting evaporator, [kJ/kg]
h_2-- the enthalpy of the refrigerant exiting compressor, [kJ/kg]
h_3 --the enthalpy of the refrigerant exiting condenser, [kJ/kg]
h_4-- the enthalpy of the refrigerant exiting capillary tube, [kJ/kg]
$\dot{m}_r$ -- the mass flow rate of the refrigerant (R-134a), [kg/s]
Q_e--the heat transfer rate through the evaporator, [kW]
Q_c--the heat transfer rate through the condenser, [kW]
T_1 --the temperature of the refrigerant exiting evaporator / entering compressor, [^{o}C]
T_2 --the temperature of the refrigerant exiting compressor / entering condenser, [^{o}C]
T3 --the temperature of the refrigerant exiting condenser / entering capillary tube, [^{o}C]
T4 --the temperature of the refrigerant exiting capillary tube / entering evaporator, [^{o}C]
Tw-- the temperature of water in condensor, [^{o}C]

U_L --the overall heat transfer coefficient, [kW/^{o}C]
W_{comp}-- the electrical power consumption of the compressor, [kW]

III. Literature Review

An analytical and experimental studies on direct-expansion solar-assisted heat pump (DX-SAHP) in Shanghai where the effects of various parameters under the constant compressor speed were performed [1]. In [2], authors carried out preliminary theoretical performance studies concerning a direct expansion solar-assisted heat pump that uses a bare collector as an evaporator for the heat pump. In [3], authors further developed a multi-functional domestic DX-SAHP system, which was able to offer multi-fold functions to residences at low costs, including space heating in winter, space cooling in summer, and hot water supply for the whole year.
A system that uses two-phase solar energy collector in conjunction with a heat pump is developed [4] [5]. Their results indicate that the system merits further investigation. Theoretical and experimental studies were made [6] on the thermal performance of a heat pump that used a bare flat plate collector as the evaporator. Experimental investigations were conducted on the direct expansion solar assisted heat pump (DX-SAHP) [7].

IV. Direct Expansion Solar Assisted Heat pump

In a direct-expansion solar assisted heat pump system, heat pump refrigerant is directly circulated through a solar collector that acts as the system's evaporator. This collector evaporator absorbs the heat transferred by convection and solar radiation. Solar energy absorbed in the collector/evaporator is transferred to the load via the heat pump's condenser. The condenser can be arranged as an external heat exchanger supplying a hot water tank or arranged as an immersed coil in the hot water storage tank. The concept of the Direct Expansion SAHP as shown in Fig 1 was firstly considered in 1955 [8] and several authors has followed this study [9] [10] [11]. In [12], authors published an experimental validation of the work [13], with the COP ranging from 2 to 3.

V. Experimental Setup

5.1 Flat plate collector

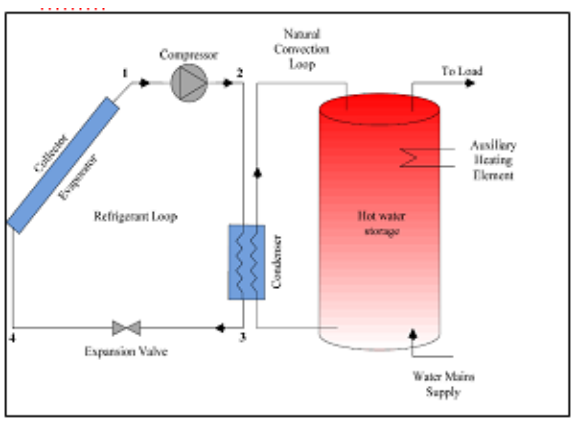

Fig.1. Schematic of a direct expansion SAHPWH

In the present study, a glazed solar collector of an area of 2.23m^2 was used. The solar collector has 0.3-mm thick copper fins attached with copper tube. The fins are coated with matt black paint to absorb the maximum incident solar radiation falling on the surface. The tubes along with fins are placed directly behind the glazing surface of 4 mm thickness with an air gap of 3 cm from the cover. Bottom side of the collector was insulated with a glass wool of 25 mm thickness, to avoid the back losses. The temperature of the air in the gap between the absorber and the glazing surface increases because of the greenhouse effect .The solar collector (evaporator) was tilted to an angle of about 45 degrees with respect to a horizontal surface. The solar collector was oriented to face south to maximize the solar radiation incident on the solar collector.

5.2 Reciprocating compressor

R-134a hermetically sealed reciprocating compressor with rated input power 245 W is used. To avoid the overload, high pressure cut-off switch was connected to the compressor. Compressor work is found by energy meter reading. A small R134a reciprocating-type hermetic compressor with piston swept volume 5.79 cc, and rated input power 245 W is adopted. R134a or 1, 1, 1, 2-tetrafluoroethane is the working fluid in this system. The refrigerant mass flow rate can be evaluated from the volumetric efficiency of the compressor given by Huang B. J. and Chyng J. P. (1999).

$$\dot{m}_r = \frac{\eta_v \times V_D}{v}$$

Where:

$$\eta_v = -0.0163 \times \left(\frac{P_2}{P_1}\right) + 0.6563$$

5.3 Storage tank

Hot storage water tank is assumed to be non-stratified i.e. neglect losses for finding out the coefficient of performance. The condenser is made up of copper tubes of outer diameter 9.5mm with length 9.7m which is immersed in the domestic hot water tank.

$$Q_w = m_w C_{pw} \left(dT_w / dt \right)$$

5.4 Capillary tube

Capillary tube is the throttling devices in the refrigeration and the air conditioning systems. The capillary tube is a copper tube of very small internal diameter. It is of very long length and it is coiled to several turns so that it would occupy less space. The internal diameter of the capillary tube used for the refrigeration and air conditioning applications varies from 0.5 to 2.28 mm. Capillary tube used as the throttling device in the heat pump is of 3 meter in length. When the refrigerant leaves the condenser and enters the capillary tube its pressure drops down due to very small diameter of the capillary.

The Coefficient of performance is defined as the ratio of heat gain Q_w in the condenser to the compressor work

$$COP = \frac{Q_w}{W_{cm}}$$

VI. Instrumentation and other Measuring Devices

In order to determine the performance of the prototype under various conditions of the DX-SAHP, The apparatus is equipped with necessary instrumentation.

Properties measured mainly includes temperature, pressure and radiation and these parameters were measured by respective devices as mentioned in table.1

Table 1: Conventions

Label	Instrument
T	Thermocouple [Range: -50 to +99°C in 1 deg. Resolution]
P	Pressure gauge [bourdon type]
W	Wattmeter / Energy meter

A schematic diagram with measuring devices is shown in fig.2

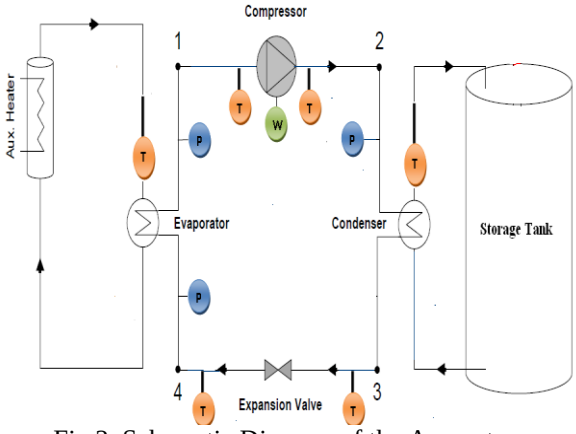

Fig.2. Schematic Diagram of the Apparatus Highlighting Instrumentation

VII. Results

The experimental tests of DX-SAHPWH with glazed evaporator/Flat-plate collector have been conducted on different time of different days. Data was recorded for all tests. Out of that recorded data a single test data has been taken in which heat pump is giving best performance using a glazed evaporator. As Shown in Fig.3. Heat pump gave the best performance between 15:20 pm to 16:45 pm. At that time the coefficient of performance was 3.

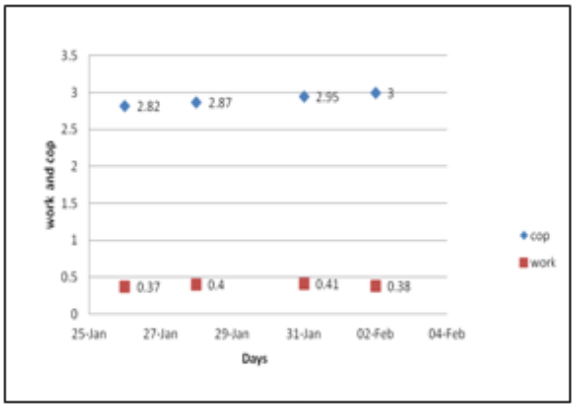

Fig 3: COP verses Work

VIII. Conclusion

The Coefficient of Performance of DX-SAHPWH is strongly influenced by the solar intensity and compressor work. The experiment on the above mentioned system was performed for four different days which were chosen depending upon the clarity of sky. The average coefficient of performance (COP) of heating for this system under winter climatic conditions was found to be 2.91. The parameters like. refrigerant mass flow rate, compressor work, temperature and pressure have been measured at different point in the system.

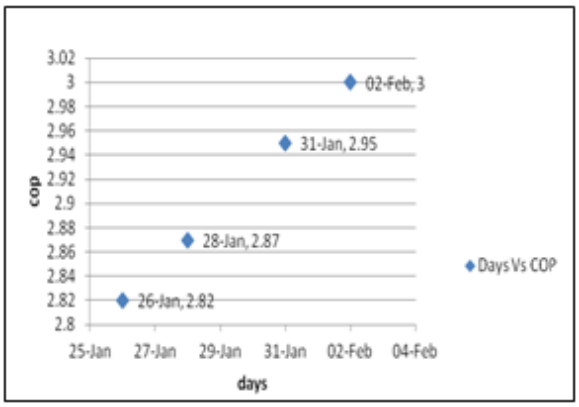

Fig 4: COP measured for different days

References

[1] Kuang YH, Sumathy K, Wang RZ. Study on a direct-expansion solar-assisted heat pump water heating system. Int J Energy Res 2003;27:531–548.

[2] Chaturvedi, S. K., Roberts, A. S., and Mei, V., Solar Collector as Heat Pump Evaporator, Proceedings of 13th Intersociety Energy Conversion Conference, Boston, Mass., Aug. 4- 9, 1979.

[3] Kuang YH, Wang RZ. Performance of a multi- functional direct-expansion solar assisted heat pump system. Sol Energy 2006;80:795–803.

[4] Franklin, J. L., Saaski, E. W., and Yamagiwa, A., A High Efficiency, Direct Expansion Solar Panel, Proceedings of 1977 Flat-Plate Solar Collector Conference, Orlando, Fla., Feb. 28- March 2, 1977, pp 197-195.

[5]. Franklin, J. L., Saaski, E. W., and Yamagiwa, A., DOE Heating and Cooling Contractor Conference,Reno, Nevada, March 1980.

[6] Ito S., Miura N., and Wang K., Performance of a Heat Pump Using Direct Expansion Solar Collectors, Solar Energy Vol. 65. No. 3, pp.189-196, 1999.

[7] Abdesselam Hamlaoui, Performance of a Direct Expansion Solar Assisted Heat Pump, Thesis Submitted for the degree of Master of Engineering Science in the Faculty of Engineering, University of Malaya, July, 1998.

[8] Sporn P, Ambrose ER. The heat pump and solar energy. Proceedings of the world symposium on applied solar energy, Phoenix, Arizona;1955.

[9] Sushil K, Chaturvedi SK, Shen JY. Thermal performance of a direct expansion solar assisted heat pump. Solar Energy 1984:155e 62.

[10] Ito S, Miura N, Wang K. Performance of a heat pump using direct expansion solar collectors. Solar Energy 1999:189-196.

[11] Kuang YH, Sumathy K, Wang RZ. Study on a direct-expansion solar-assisted heat pump water heating system. International Journal of Energy Research 2003; 27:531-148.

[12] Sushil K, Chaturvedi SK, Shen JY. Thermal performance of a direct expansion solar-assisted heat pump. Solar Energy 1984:155-162.

[13] Chaturvedi SK, Chiang YF, Roberts AS. Analysis of two-phase flow solar collectors with application to heat pumps. ASME Paper 80-WA/Sol-32;1980.

International Journal of Engineering Research and Applications (IJERA) ISSN: 2248-9622
National Conference on Advances in Engineering and Technology
(AET- 29th March 2014)

RESEARCH ARTICLE OPEN ACCESS

Quantitative Analysis for Effect of Copper on Various Mechanical Properties of Ductile Iron during Austempering

Ankit Dua[1*], Bikram Jit Singh[2], Subhash Malik[3]
[1]*Department of Mechanical Engineering, M.M. University, Sadopur, Ambala - 134007, India, email: dua_ankit09@yahoo.co.in*
[2]*Department of Mechanical Engineering, M.M. University, Sadopur, Ambala - 134007, India, email:chann461@yahoo.com*
[3]*Department of Mechanical Engineering, M.M. University, Sadopur, Ambala - 134007, India, email: subhashmalik604@gmail.com*

Abstract
Aim of this study is to perform relevant quantitative analysis of the observations during austempering of with or without copper in ductile iron. Ductile iron is a group of materials having wide range of properties and possessing controlled microstructure. Austempered-Ductile-Iron (ADI) is a relatively new material having exceptional combinations of mechanical properties and having potential applications. Researchers had tried to customize its properties mainly; yield strength (YS), percentage of elongation, ultimate tensile strength (UTS) and hardness by doping materials like copper in its microstructure. The present work highlights impact of austempering temperature and time on various mechanical properties of ductile iron and further emphasis to execute quantitative analysis for uncovering the affect of copper, effectively. Next General-Regression is applied to find relation of various properties with given Austempering metrics. High R (sq) value (0.80) signifies strong relations of properties with temperature and time, respectively and demonstrated empirically in terms of linear equations for drawing necessary implications for future research. The paper does not cover the images of microstructure or change in micro structural behavior during the austempering process of ductile iron. The paper also not covers the fractural behavior of ADI.
Keywords : Austempered-Ductile-Iron (ADI), Yield Strength (YS), Percentage of Elongation, Ultimate tensile strength (UTS), hardness, quantitative analysis, General regression analysis, regression equations, Scatterplot

I. INTRODUCTION

The process of alloying is used to change the chemical composition of steel and improve its properties over carbon steel or adjust them to meet the requirements of a particular application. Every steel is truly an alloy but not all steels are called "alloy steels". Even the simplest steels are iron (Fe) (about 99%) alloyed with carbon (C) (about 0.1% to 1%, depending on type) [1] [2]. Precipitation of Cu in iron and steel is a well-known phenomenon and it might have a potential to achieve better strength-ductility balance than conventional high-strength steels because of a different nature of Cu precipitates from other precipitates like carbides and nitrides [3]. The introduction of copper into an iron–carbon melt coarsens the microstructure of the particles and increases the grain size [4]. With an increasing copper content, the elongation of steel monotonically decreases and its thermal conductivity grows [5]. The austenitizing temperature controls the carbon content of the austenite which, in turn, affects the structure and properties of the austempered casting. Austenitizing time should be the minimum required to heat the entire part to the desired austenitizing temperature and to saturate the austenite with the equilibrium level of carbon. Once the austempering temperature has been selected, the austempering time must be chosen to optimize properties through the formation of a stable structure of ausferrite [6].

II. METHODOLOGY ADOPTED

In the paper, data obtained from the previous research work [1] is further analyzed by quantitative approaches. Tests were executed by using Minitab-16 software and the effect of copper addition along with austempering temperature and time is considered.

III. RESULTS AND DISCUSSIONS

The results obtained are displayed by multi- vari chart (Fig. 1) which shows with the addition of 0.49% copper [1] percentage of elongation decreases at each stage of austenisation.

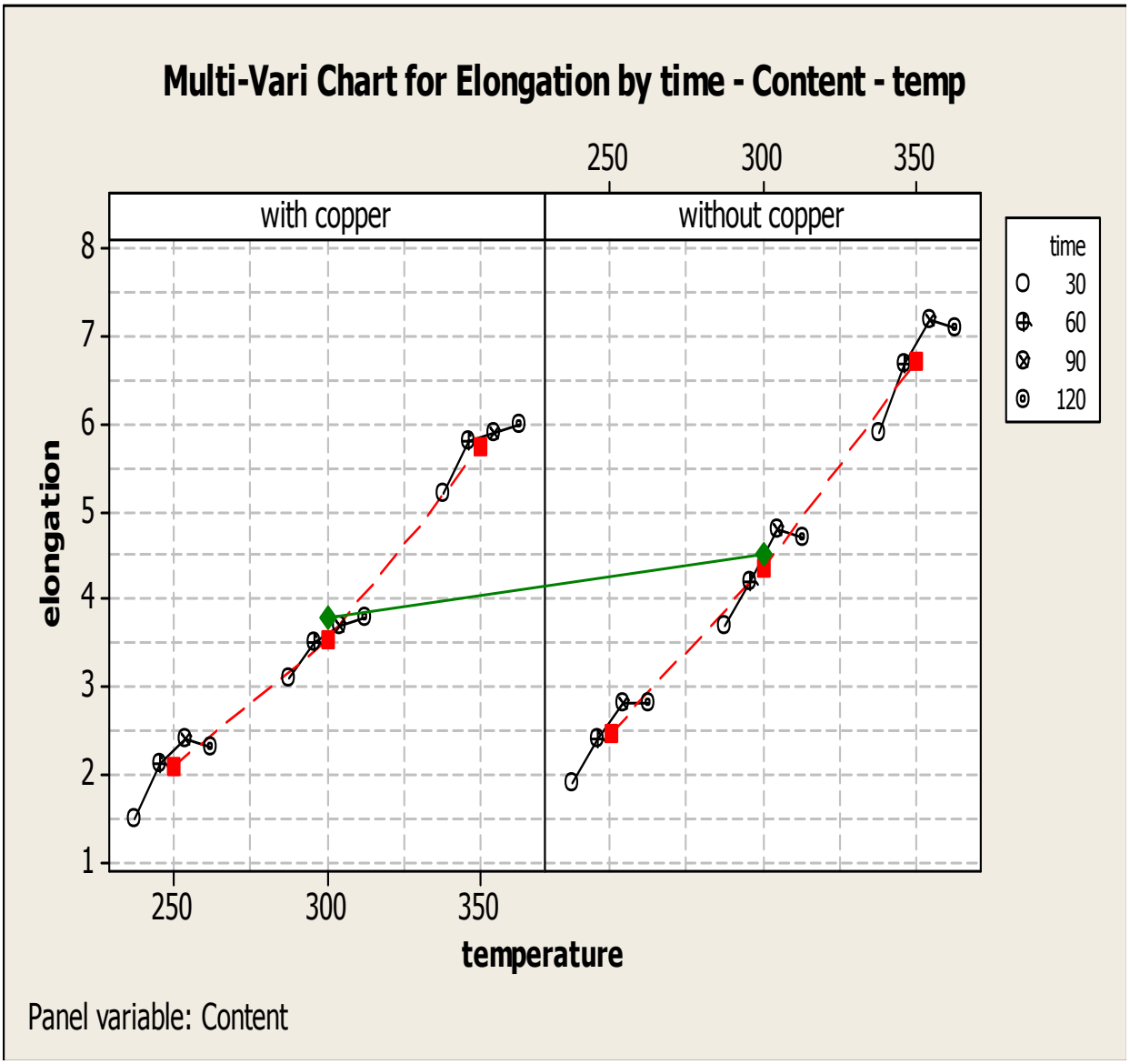

Figure 1: Effect of copper addition with different austempering temperature (°C) and time (minutes) on percentage of elongation (mm)

It is clear that elongation in both ductile irons increases with the increase in austempering temperature and time. But with the addition of copper and austempering at 250°C for 30 minutes the elongation decreases to 1.5% from 1.8% while at the same temperature with increase in austempering time up to 120 minutes elongation decreases to 2.5% from 2.8%. For the same materials at 350°C austempering temperature and 120 minutes austempering time elongation decreases to 6% with addition of copper from 7%. Based upon the results shown in Fig 1 general regression analysis has been checked out (Fig 2). For time as a variable, p value (0.000) is smaller than 0.05 and hence signifies its importance in elongation. Two separate equations are drawn to find out a linear relation between elongation and austempering temperature and austempering time.

Regression Equation

Content
with copper elongation = -8.8375 + 0.0101667 time + 0.0395 temperature

without copper elongation = -8.09583 + 0.0101667 time + 0.0395 temperature

Coefficients

Term	Coef	SE Coef	T	P
Constant	-8.46667	0.452551	-18.7088	0.000
Content	-0.37083	0.058424	-6.3473	0.000
time	0.01017	0.001742	5.8366	0.000
temperature	0.03950	0.001431	27.6013	0.000

Summary of Model

S = 0.286218 R-Sq = 97.66% R-Sq(adj) = 97.31%
PRESS = 2.32363 R-Sq(Pred.) = 96.69%

Figure 2: General Regression Analysis: elongation versus time, temperature, Content

The regression model is well fitted (as R sq adjusted value is around 97.66%) and speaks itself the vitalness of austempering temperature and austempering time in the decrease of elongation of the material. Hardness (RA) of the materials for the same percentage addition of copper and same process parameters is also calculated (Fig 3). Results obtained define hardness of the ductile iron increases with the addition of copper as mean line indicates positive slop.

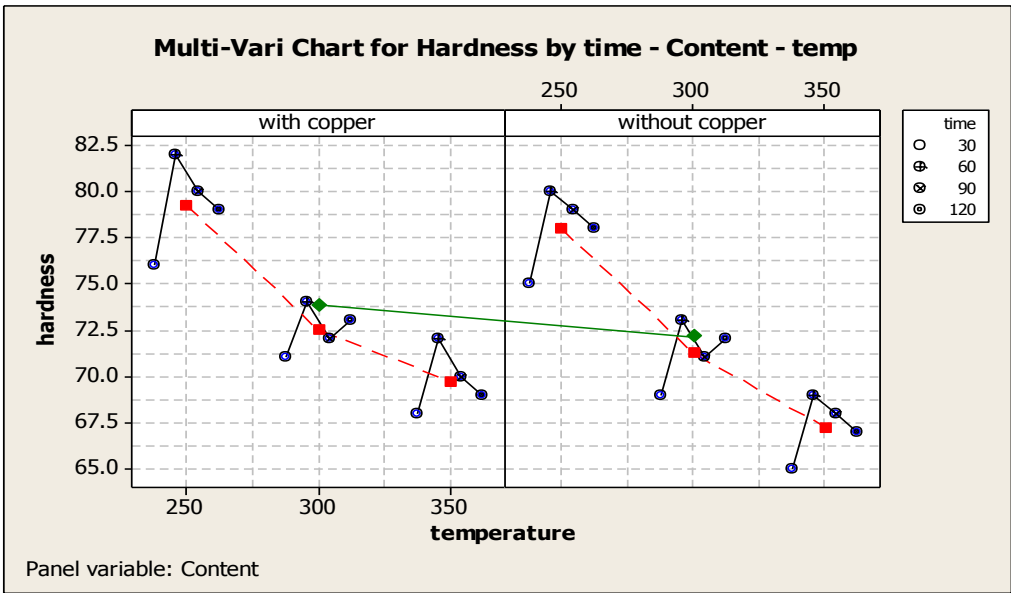

Figure 3: Effect of copper addition with different austempering temperature (°C) and time (minutes) on hardness (RA)

For both materials (with copper, without copper) at every stage of temperature hardness increases for first 60 minutes of austempering time and then starts decreasing. At austempering temperature 250°C and time 30 minutes hardness obtained is 76 RA with copper compared to 75RA without copper. While austempering at 350°C for 30 minutes hardness decreases to 68 RA with copper compared to 66 RA without copper. The general regression analysis of hardness versus austempering time and austempering temperature is also checked out (Fig 4). Two equations has been generated to find out the relation between hardness and austempering temperature and austempering time.

Regression Equation

Content

with copper hardness = 102.875 + 0.0177778 time - 0.10125 temperature

without copper hardness = 101.208 + 0.0177778 time - 0.10125 temperature

Coefficients

Term	Coef	SE Coef	T	P
Constant	102.042	3.01533	33.8410	0.000
Content	0.833	0.38928	2.1407	0.045
time	0.018	0.01161	1.5318	0.141
temperature	-0.101	0.00954	-10.6184	0.000

Summary of Model

S = 1.90706 R-Sq = 85.68% R-Sq(adj) = 83.53%
PRESS = 102.829 R-Sq(Pred.) = 79.76%

Figure 4: General Regression Analysis: hardness versus time, temperature, Content

The regression model is well fitted as R square value is 85.68% and p value is 0.00 less the 0.5 hence significant. The regression equations show linear relation between hardness of ADI and austempering temperature and time. Negative sign in the equations show with the increase in austempering temperature hardness of the materials decrease while austempering time has small positive effect on the same. Fig 5 represents variation of Ultimate tensile strength (UTS) with austempering temperature and time. Positive slope represents UTS of the ductile iron increases with the addition of copper but with the increase of austempering temperature and austempering time UTS of ductile iron decreases.

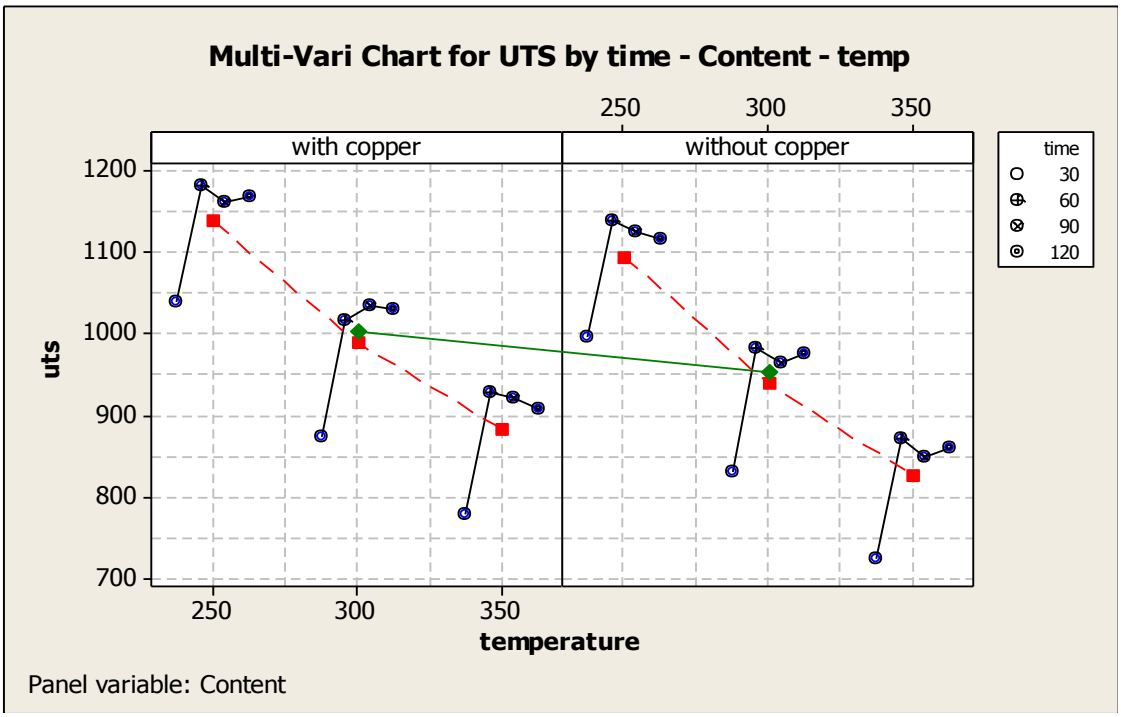

Figure 5: Effect of copper addition with different austempering temperature (°C) and time (minutes) on ultimate tensile strength (MPa)

From the observations maximum UTS achieved is around 1200 MPa with the addition of copper and austempering at 250°C for 60 minutes compared to 1150 MPa without copper for the same process variables. UTS of the materials shows same trend as observed in hardness. With the increase in austempering temperature from 250°C to 350°C UTS of the ADI decreases in both cases. The above shown results are further analyzed by general regression analysis shown in Fig 6. Again two separate equations have been formed to find out the linear relation of UTS with austempering temperature and time with confidence level.

Regression Equation

Content
with copper UTS = 1686.46 + 1.32444 time - 2.60875 temperature

without copper UTS = 1636.29 + 1.32444 time - 2.60875 temperature

Coefficients

Term	Coef	SE Coef	T	P
Constant	1661.38	74.2634	22.3714	0.000
Content	25.08	9.5874	2.6163	0.017
time	1.32	0.2858	4.6335	0.000
temperature	-2.61	0.2348	-11.1086	0.000

Summary of Model

S = 46.9683 R-Sq = 88.35% R-Sq(adj) = 86.61%
PRESS = 62903.7 R-Sq(Pred.) = 83.39%

Figure 6: General Regression Analysis: ultimate tensile strength versus time, temperature

The regression model is well fitted as R square value is 88.35% and P value is 0.00 less than 0.5. Negative sign in the equation show decrease of UTS with the increase of austempering temperature. Fig 7 represents variation of Yield strength (YS) with austempering temperature and time. Positive slope represents YS of the ductile iron increases with the addition of copper but with the increase of austempering temperature and austempering time YS of ductile iron decreases.

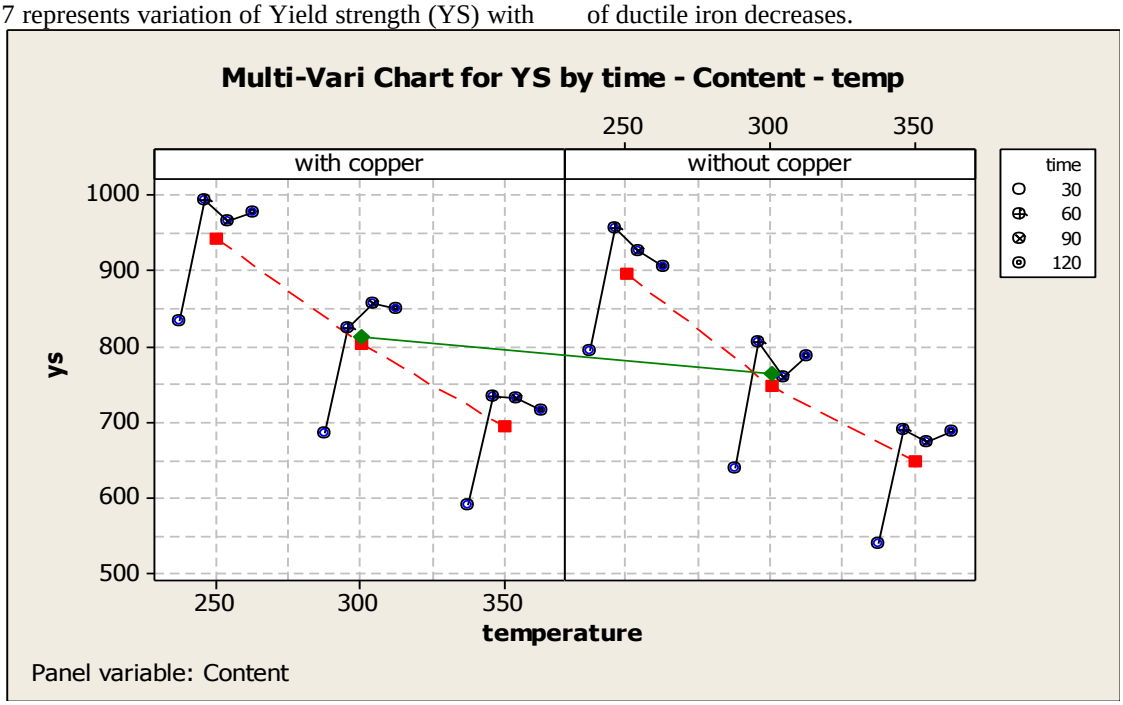

Figure 7: Effect of copper addition with different austempering temperature (°C) and time (minutes) on yield strength (MPa)

YS of the ADI also show the same trend shown by UTS. With the addition of copper yield strength of the ADI decreases from 1000 MPa to 600 MPa compared to 950 MPa to 550 MPa with increase of austempering temperature from 250°C to 350°C . The above shown results are further analyzed by general regression analysis shown in Fig 8. Again two separate equations have been formed to find out the linear relation of YS with austempering temperature and time with confidence level.

Regression Equation

Content
with copper YS = 1460.21 + 1.35389 time - 2.4925 temperature

without copper YS = 1410.12 + 1.35389 time - 2.4925 temperature

Coefficients

Term	Coef	SE Coef	T	P
Constant	1435.17	79.6643	18.0152	0.000
Content	25.04	10.2846	2.4349	0.024
time	1.35	0.3066	4.4154	0.000
temperature	-2.49	0.2519	-9.8940	0.000

Summary of Model

S = 50.3842 R-Sq = 86.04% R-Sq(adj) = 83.95%
PRESS = 72388.1 R-Sq(pred.) = 80.10%

Figure 8: General Regression Analysis: Yield strength versus time, temperature

The regression model is well fitted as R square value is 86.04% and P value is 0.00 less than 0.5. Negative sign in the equation show decrease of YS with the increase of austempering temperature.

IV. CONCLUSION

Quantitative analysis of the observations represents elongation is the only property that decreases with the addition of copper in ADI while hardness, YS and UTS increases. In both materials with and without copper at every stage of temperature with increase in austempering time elongation increases. Hardness, UTS and YS shows common behavior as with increase in austempering time the values obtained first increase for 60 minutes and then start decreasing. General regression models are well fitted as R square values obtained always greater than 80%.

REFERENCES

Thesis:

[1] Ranjit Kumar Panda, "Effect of copper on austempering behavior of ductile iron" Department of Metallurgical & Materials Engineering National Institute of Technology, Rourkela, 2011.

Journal Papers:

[2] Wikipedia, 2014, Alloy Steel, http://en.wikipedia.org/wiki/Alloy_steel.

[3] Setuo Takaki, 'Effect of Copper on Tensile Properties and Grain-Refinement of Steel and its Relation to Precipitation Behavior' Materials Transactions, 45 (7), 2004, 2239-2244

[4] G. G. Zalazinskii, L. I. Leont'ev, and T. L. Shchennikova, "Effect of Copper and Molybdenum Additions on the Microstructure and Mechanical Properties of Steel Shot", Russian Metallurgy (Metally), 2007 (4), 282–286.

[5] A.Yu. Yakovlev, I. P. Volchok, "The effect of copper on the structure and properties of graphitized steel", Metal Science and Heat Treatment, 50, 2008, 41 – 44

[6] DuctileIron Data for Design Engineers, http://www.ductile.org/didata/section4/4intro.htm

RESEARCH ARTICLE OPEN ACCESS

Desiccant Cooling System- A Novel Technique for Air Conditioning

Yashpalbajaj*, Swaty**
*(Mechanical Engineering, DCRUST, Murthal Email:yashpal.bajaj23@gmail.com)
** (Mechanical Engineering, DCRUST, Murthal Email:swatyp2@gmail.com)

ABSTRACT
Now a days, due to energy crisis/high energy costs, novel techniques for air conditioning are to be explored. In this paper various techniques that can be used for air conditioning or dehumidification purpose are investigated. These techniques improve the indoor air quality a lot with a considerable savings in energy consumption. The working of desiccant dehumidifier & conventional dehumidifier air conditioner is discussed along with the performance comparison is also done for better understanding.
Keywords— Air Conditioning, Dehumidification, Desiccant Cooling

I. INTRODUCTION

The average global air temperature of the Earth's surface is increasing day by day. It has been proved that the greenhouse gases are mainly responsible for it [1]. Residential energy accounts for 40% of the primary energy consumptions relative to the CO_2 emission in the EU, of this HVAC (heating, ventilation and air conditioning) systems consume approximately 50%, lighting accounts for 15% and appliances 10% [2].

With the increasing requirements for indoor cooling, sustainable cooling systems have recently gained prominence. These novel cooling systems utilize renewable energy gained from solar collector, cooling tower, ground thermal source etc, and avoid CFC and CO_2 emissions. Desiccant cooling system is one kind of innovative technologies which employs renewable energy to produce the desired air for comfortable working/living spaces [3]. These systems have little dependency on fossil-fuel energy and are environment friendly.

II. DESICCANT COOLING

Desiccant cooling consists in dehumidifying the incoming air stream by forcing it through a desiccant material and then drying the air to the desired indoor temperature.

To make the system working continually, water vapour absorbed must be driven out of the desiccant material (regeneration) so that it can be dried enough to absorb water vapours in the next cycle [4]. This is done by heating the material desiccant to its temperature of regeneration as shown in Figure1.

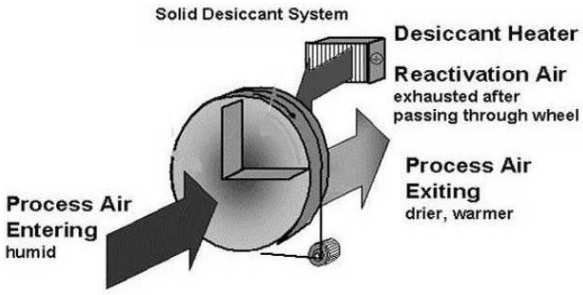

Figure1: Principle of Desiccant Cooling System

2.1 SOLID DESICCANT COOLING SYSTEM

A Solid desiccant cooling system comprises principally three components [4] as shown in figure 2

- Dehumidifier (desiccant material)
- Cooling Unit
- Regeneration Heat Source

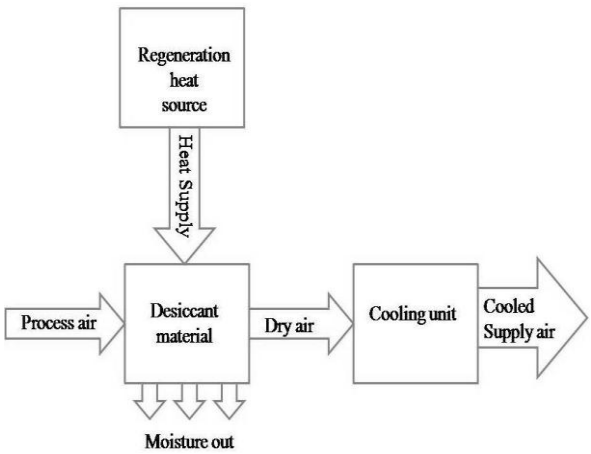

Figure 2: Solid Desiccant Cooling System

2.1.1 DEHUMIDIFIER(DESICCANT MATERIAL)

In the case where the desiccant is employed in its solid state, the desiccant dehumidifier is generally a slowly rotating desiccant wheel or a periodically regenerated adsorbent bed.

Solid desiccant dehumidification employs the porous and strong hydrophilic materials to absorb moisture from the air stream [4]. The generally used solid desiccants include silica gel, natural and synthetic zeolites, activated alumina, titanium silicate, synthetic polymers, lithium chloride etc.

2.1.2 COOLING UNIT

The cooling unit can be the evaporator of a traditional air conditioner, an evaporative cooler or a cold coil [4]. The role of the cooling unit is the handling of the sensible load while the desiccant removes the latent load.

2.1.3 REGENERATION HEAT SOURCE

The regeneration heat source supplies the thermal energy necessary for driving out the moisture that the desiccant had taken up during the adsorption phase. Because the thermal energy source is required, a variety of possible energy sources can be utilized [4].Those includes solar energy, waste heat, and natural gas heating, and the possibility of energy recovery within the system.

2.1.4 WORKING

Desiccant cooling systems can be operated in a recirculation mode, in ventilation mode, Dunkle cycle and wet-surface heat exchanger cycle.

In recirculation mode, also called recirculation cycle, the process inlet air is the return air from the space being conditioned and the regeneration air is the outdoor air.

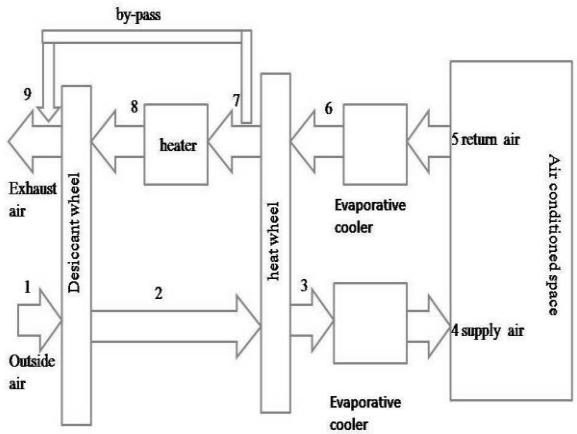

Figure 3: Solid Desiccant Cooling System with Evaporative Cooler

In the ventilation mode, the process inlet air is the outdoor air and the regeneration inlet air can be either the outdoor air (standard vent cycle) or the conditioned space exhausted air.

The system described here is in ventilation mode with regeneration air being returned from the conditioned space.

In the system presented in figure 3 the outdoor air stream is passed through rotary desiccant wheel. Its moisture is partly but significantly adsorbed by the desiccant material and the heat of adsorption elevates its temperature so that a warm and rather dry air stream exits at the state 2.The air stream is then cooled successively in the heat exchanger (heat wheel) from the state 2 to the state 3, and then in an evaporative cooler from the state 3 to the state 4.

This cool and dry air supplied to air conditioned space. There it takes heat and moisture so its humidity and temperature will be increased.

Another evaporative cooler is used to cool down the return air from the state 5 to the state 6 and the cold air stream serves as heat sink to cool the supply air in the heat exchanger. Consequently, its temperature is risen when exiting the heat wheel at the state 7 [5]. At this point, it is ready to undergo a complementary heating to reach a temperature high enough at the state 8 in order to be able to regenerate the desiccant material. A certain portion (about 20%) of the return air stream, at the state 7, bypasses the heating source in order to reduce the regeneration heat consumption.

2.2 Liquid Desiccant Cooling System

A liquid desiccant cooling system, therefore, comprises principally three components [9] as shown in figure 4

- Conditioner
- Regenerator
- Interchange Heat Exchanger (IHX)

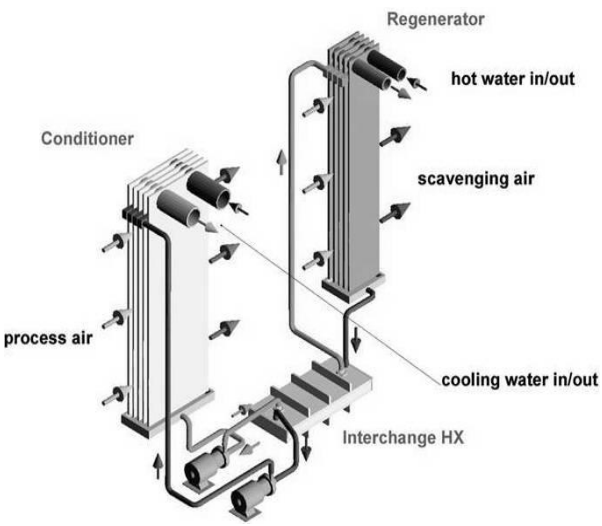

Figure 4: Liquid Desiccant Cooling System

2.2.1 CONDITIONER

The conditioner is a parallel-plate liquid-to-air heat exchanger. A coolant, typically cooling tower water flows within the plates and a very low flow of liquid desiccant flows down the outer surfaces of the plates [5]. Thin wicks on the plate surfaces create uniform desiccant films.

The air to be processed flows horizontally through the gaps between the plates. As this humid air comes in contact with the desiccant, water vapor is absorbed.The heat released by this absorption is transferred to the coolant. The air leaves the conditioner much drier, although its temperature may not significantly change**.**

2.2.2 REGENERATOR

The dilute desiccant that leaves the conditioner is pumped to the regenerator. The regenerator has the same configuration as the conditioner: a parallel-plate liquid-to-air heat exchanger.Again, very thin films of desiccant flow in wicks on the outer surfaces of the plates, and air flows in the gaps between the plates.

For the regenerator, however, a hot heat transfer fluid flows within the plates. This hot fluid can be supplied by a gas-fired boiler, solar thermal collectors, recovered heat from an engine or fuel cell, or other energy source.

2.2.3 INTEREXCHANGE HEAT EXCHANGER

The hot, concentrated desiccant that leaves the regenerator and the cool, dilute desiccant that flows to the regenerator exchange thermal energy in the interchange heat exchanger. This exchange increases the efficiency of the regenerator and decreases the cooling load on the conditioner.

Figure 5 shows another liquid desiccant cooling system in which strong and weak desiccant flows in the whole system.

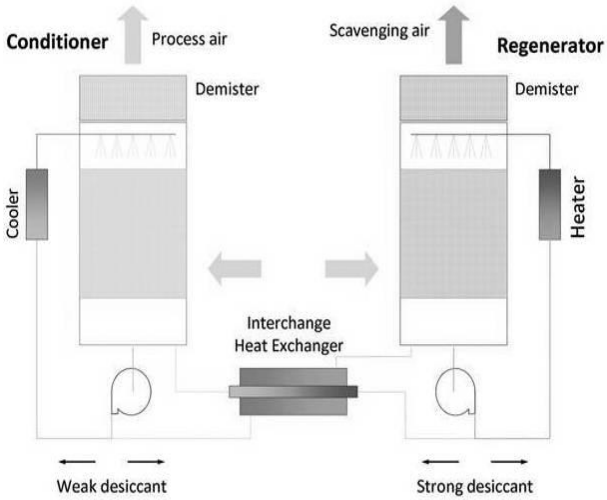

Figure 5: Liquid Desiccant Dehumidifier and Cooler

III. ADVANTAGES OF DESICCANT ENHANCED COOLING

- It extends the climatic applicability scope of the evaporative cooling to the hot and humid zones.
- The preheating being eliminated, energy(can reduce the power consumption by 24%-48% as compared to VCR) and costs can be saved.
- The regeneration heat can be supplied by free energy sources.
- The system is environmental friendly since doesn't use any Chlorofluorocarbon based refrigerant.
- The sensible and latent cooling loads can be handled independently.
- The evaporative cooler can be replaced by the evaporator of a significant downsized traditional air conditioner, depending on the sensible heat ratio (SHR) of the room being conditioned. This will be conducive to significant energy and cost savings.

Some of the solid desiccant material are Silica Gel, Indicating Silica Gel, Molecular Sieve, Calcium Oxide, Calcium Sulphate and Other Adsorbents whereas the Liquid desiccant material are Methyl Glycol (MEG), Lithium Bromide and Brine solution.

IV. PERFORMANCE COMPARISON

Both Desiccant Dehumidification & Conventional Dehumidification systems perform the same function, now question arises which one is the best. Choosing between the best, there are no simple answers, however there are some guidelines that help us in choosing the best system for our requirement.

- Both systems are much economical when used together.
- If electricity is cheaper & thermal energy is expensive in the region then conventional dehumidifier should be preferred to remove bulk of the moisture otherwise desiccant based system will be a right choice .
- Conventional dehumidifiers are best when used for higher temperatures & moisture levels. These are not suitable to dry air below 8°C dew point because condensation freezes on the coil, thus slowing the moisture removal process.
- Desiccant dehumidification is best suitable when air is cold (8°C or below) & humid or when low dew point is required.
- If dehumidified air with 100% RH (relative humidity) is required then solution is conventional dehumidification, on the other hand if desired result is conditioned air whose RH less than 100% then desiccant humidifier is the only solution.

- Generally desiccant dehumidification system is used for applications below 45% RH down to less than 1% RH.

V. CASE STUDY

5.1 CASE 1: PAINTBALL MANUFACTURING PLANT

Paintball manufacturing plant is Located in India on the north-west coast of Kandla about 600 km from Mumbai, this plant is one of a few in the world for the manufacture & export of color filled gelatin balls. The Gelatin balls called Paint Balls are in heavy demand for popular sport & recreation activities worldwide, particularly in Europe & US.

The plant is fully automatic and designed for producing large quantities of paint balls according to the highest quality standards in a climate control environment.

Problem:

The paintball paint, which is both water-soluble and biodegradable, is made at a specialty paint facility and then shipped to the encapsulating plant. Softened gelatin is loaded into the encapsulating machine, which automatically injects a precisely measured amount of paint into the cavity, encapsulating the paint. Since the gelatin is soft and warm, the balls must be cooled and hardened in a tumbling machine, then placed on shelves to dry. To ensure a safe flowing production in the above manufacturing process, climate control is crucial.

Solution:

Liquid desiccant units is used to transform the harsh ambient conditions of 29 ºC (84.2 ºF), 83% RH to stable, requested conditions of 22 ºC (71.6 ºF), 12 R.H.

5.2 CASE 2: FERTILIZER PLANT

The Fertilizer plant situated in Goa, India is a modern, fully automated facility. The plant has an annual installed capacity of 946,200 metric tons of fertilizers. It comprises a single stream ammonia plant, a urea plant, an NPK plant and a DAP plant along with related on-site and off-site facilities for handling raw materials end products as well as the generation of steam.

Problem:

The humidity level in Goa is high throughout the year. Due to the high humidity levels in the Packing Area, the bags have to be over packed since once they are shipped and humidity level changes and the gross weight of the bags declines. As a result, the plant is suffering significant losses due to the bag's over packing.

Solution:

To solve the problem, a liquid desiccant cooling unit was installed. The unit supplies dry air to the packaging area which enables correct weighing, improved product quality & improved productivity due to a better flow ability.

5.3 CASE 3: HOSPITALS

A hospital in the province of Milan, Italy recently built a new prestigious Dialysis Center.
In 2005, the Center installed a Radiant Partition Walls System for cooling and heating the Dialysis area as well as the adjacent premises including the waiting area, restrooms, medical premises and service rooms, a total of almost 4,000 square feet.

Problem:

The rise in humidity caused condensation buildup on the walls and ceilings of the Center, causing potentially hazardous conditions and patient discomfort.

Solution:

Liquid desiccant cooling Systems installed which supplies dry filtrated air to the Air Handling Unit (AHU) which treats the Dialysis Center, allowing both patients and staff to enjoy clean air and comfort without any condensation buildup in the Center.

VI. CONCLUSION

Desiccant cooling is one of the innovative technologies in the field of air conditioning and different case studies shows that it improves the indoor quality air weather it may be case of any industry, hospitals or any other refrigeration and air conditioning system. So desiccant cooling is an appropriate environmental friendly technology.

REFERENCES

[1] S. Liu, “A Novel Heat Recovery Desiccant Cooling System”, Technical Report, University of Nottingham, Nottingham, 2008.
[2] L.P. Lombard, J. Ortiz, “Building energy consumption information: A review”, Energy and Buildings, 40, 2008, 394-398.
[3] J. R. Watt, “Evaporative Air Conditioning Handbook”, Chapman and Hall, 1997.
[4] K. Daou, R. Z. Wang, Z. Z. Xia , “Desiccant cooling air conditioning: A review”, Renewable and Sustainable Energy, 10, 2006, 55–77.
[5] C. P. Arora, “Refrigeration and Air conditioning”, TMH, 2nd edition, 2001.

International Journal of Engineering Research and Applications (IJERA) ISSN: 2248-9622
National Conference on Advances in Engineering and Technology
(AET- 29th March 2014)

RESEARCH ARTICLE OPEN ACCESS

A Comparative Study of Aircraft Controlling Surfaces: Defense and Commercial Applications

Garima Choudhary*, Anirudh Katyal*, Vishal Sethi*, Shikha Khaneja** Sudhir Kumar Chaturvedi*
*Department of Aerospace Engineering, **Centre for Information Technology, University of Petroleum & Energy Studies, Dehradun-248007 (E-mail: sudhir.chaturvedi@ddn.upes.ac.in)

ABSTRACT
Aircraft Stability refers to the property of an aircraft to maintain its attitude or to resist displacement, and if displaced, to develop forces and moments tending to restore the original condition. On the other hand, aircraft control implies to direct the movements of an aircraft with particular reference to changes in attitude and speed. In the context of aircraft, stability plays a key role in the ability to maintain control. The opposite of stability is maneuverability. If an aircraft had infinite stability, it would have no maneuverability. In this case, there would be no way to change the flight path. A desirable middle ground must be designed, depending on the type of aircraft. Where an aircraft trainer or jet transport aircraft may require greater stability for safety and passenger comfort, a jet fighter needs maneuverability for combat situations. Positive stability means that when the aircraft is displaced it tends to return to the original attitude.
Neutral stability would result in the attitude remaining constant after displacement, neither returning nor continuing to displace. Negative stability would result in the attitude continuing to displace or diverge. Stability is also categorized as both static and dynamic. If, the pilot after increasing the pitch of an aircraft, releases the control yoke, the nose will return to level flight, demonstrating positive static stability. As a matter of fact, the nose of the aircraft does not simply return to level, but overshoots and enters a descent, followed by a series of shallower climbs and descents until level flight is eventually reached. These oscillations of smaller and smaller amplitude are a function of the aircraft's positive dynamic stability. If the aircraft had neutral dynamic stability, the oscillations would continue at the same amplitude indefinitely. If an aircraft had negative dynamic stability, the amplitude of the climbs and dives would get steeper and steeper. This paper focuses on the preliminary and comparative analysis of stability and corresponding control measures that are associated with different types of aircrafts. The result would prove the studied analytical concept of the various control surfaces used in the various aircrafts which can be used for commercial and fighter aircraft applications.
Keywords **–** Control, Maneuverability, Stability, Civil and Fighter aircrafts

I. INTRODUCTION

Flight dynamics deals principally with the response of aerospace vehicles to perturbations in their flight environments and to control inputs. In order to understand this concept of dynamics, it is necessary to characterize the aerodynamic forces and moments acting on the vehicle, and the dependence of forces and moments on the flight variables, including airspeed and vehicle orientation. This paper has an introduction to the engineering science of flight dynamics, focusing primarily of aspects of stability and control [1].

1.1 Static Stability

Aircraft stability and control involves controlling the attitude and flightpath of an aircraft. Stability and control analysis is concerned with the aircraft at several levels of integration. Aircraft fly by generating a lift greater than or equal to their weight. Aircraft do this by holding a wing at a certain angle of attack, or incidence. *Longitudinal control* is the study of how to set, maintain or change that angle of attack whereas *stability* is the study of whether and how that angle of attack will remain fixed when the aircraft is subjected to small perturbations, due to atmospheric turbulence [2].

The issue for the control of the aircraft is how it can maintain its incidence at a given speed. When it takes off or lands, it does so by rotating -raising or lowering its nose-in order to change the incidence of the wing, altering the relationship between speed and lift [3].

1.2 Equilibrium and stability

The requirements of an aircraft control system are that it must be able to bring the aircraft into some required equilibrium and also maintain that equilibrium stably. **Equilibrium** of a system occurs

when the sum of all the forces and moments acting on it are identically zero.

Static stability is all about the initial tendency of a body to return to its equilibrium state after being disturbed. To have a statically stable equilibrium point, the vehicle must develop a restoring force/moment to bring it back to the equilibrium condition.

Dynamic stability: a system is dynamically stable if, when disturbed from equilibrium, it does eventually return to the equilibrium configuration. It is basically concerned with the time history of the motion after the disturbance.

To investigate the static stability of an aircraft, can analyze response to a disturbance in the angle of attack: (a) At equilibrium point, expect moment about centre of gravity (c.g.) to be zero i.e. CMcg = 0
(b)If then perturb α up, need a restoring moment that pushes nose back down (negative)

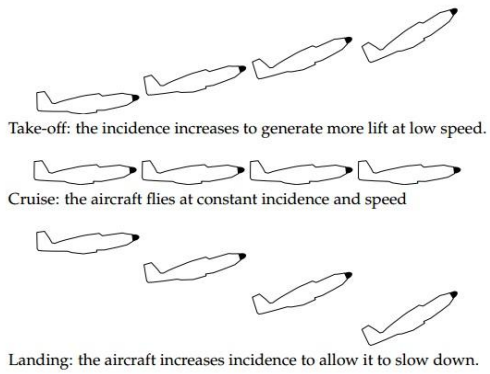

Fig.1 Phases of flight

Various Conditions for static stability:

- Cm = 0; $\frac{\partial Cm}{\partial \alpha} \equiv Cm_{\alpha} < 0$ (1)

Since $C_L = C_{L\alpha}(\alpha - \alpha_0)$ with $C_{L\alpha} > 0$, (2)

then an equivalent condition for static stability is that $\frac{\partial Cm}{\partial C_L} < 0$.

1.3 Functions of Aircraft Controls

The functions of an aircraft control system are to provide a means of changing the moments on an aircraft, to control, in this case, its incidence. There are many ways of doing this, but for the conventional aircraft we consider this is done by moving surfaces in order to change the aerodynamic forces on some part of the aircraft, thereby changing the overall moment [4].
The control surfaces are:

Elevator: It changes the total lift on the tail when it is deflected, causing a change in pitching moment on the aircraft. This allows the pilot to adjust the aircraft incidence;

Ailerons: These change the lift on each wing when they are deflected. They move in opposite directions—one goes up when the other goes down so that the lift on one wing increases and the other decreases. This generates a change in rolling moment and allows the aircraft to rotate about its axis to initiate turns, or allows it to oppose disturbances due to crosswind or gusts (Figure 1).

Rudder: It changes the side force on the vertical tailplane (or fin), generating a change in yawing moment, rotating the aircraft about a vertical axis. This can be used to resist yawing moments due to engine failure and crosswind and to aid in spin recovery and turn co-ordination.

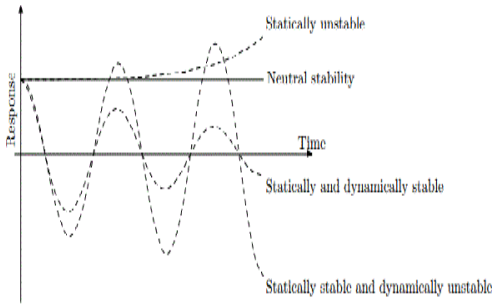

Fig.: 2 Terminology for study of stability

In steady level flight in still air, the rudder and ailerons will be deflected while the elevator will probably be at some deflection which depends on the aircraft loading. Under other conditions, or during a maneuver, all three controls may be used simultaneously. The controls can be operated directly by the pilot, through a system of mechanical actuators, possibly with aerodynamic or power assistance, or controls may be fully powered using a hydraulic or electrical system. These systems can be mechanically or electronically controlled (Figure 2).
The sign conventions for the controls and motions are shown in Figure 3.

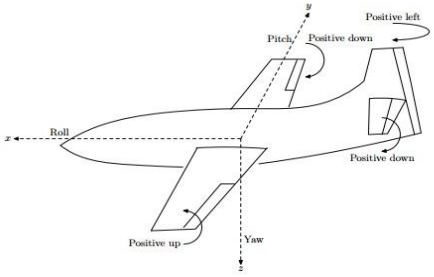

Fig. 3: Axes and sign conventions.

1.4 Trim and Stability

Figure 4 shows the basic configuration for the study of stability of an aircraft, labeled with the forces and moments and showing the corresponding sign conventions. The orientation of the aircraft is labeled with two angles, θ and α. The angle θ is the inclination of the aircraft which is the angle between the direction of flight and the horizontal; the angle α is the incidence, or angle between the direction of flight and the Zero Lift Line (ZLL). When α is zero, the Zero Lift Line is aligned with the flight direction and there is no lift acting on the aircraft, whatever might be is inclinationθ.

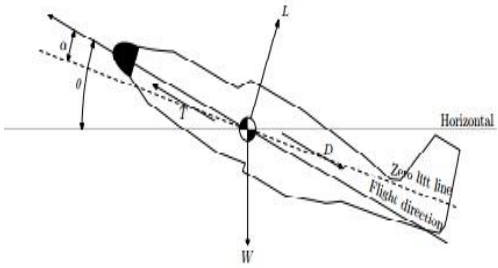

Fig. 4 Sign conventions for longitudinal stability

To examine the equilibrium and stability of the aircraft, we resolve forces parallel and perpendicular to the aircraft axis:

Parallel: $T - D - W \sin\theta = 0$, (3)

Perpendicular: $L - W \cos\theta = 0$, (4)

Moments about the c.g.: $Mcg = 0$. (5)

Moments about the centre of gravity (c.g.) cannot be due to the mass of the aircraft (by definition). This means that if Mcg = 0, the aerodynamic moments on the aircraft are in equilibrium and the aircraft is said to be trimmed or in trim. The basic problem of static stability is then: when an aircraft in trim is subjected to a disturbance which changes its incidence. This can be restated: if the aircraft pitches nose up, the change in aerodynamic moment about the centre of gravity ΔMcg should be negative in order to push the nose back down or, $\partial Mcg/\partial\alpha < 0$.

Figure 5 shows various ways Mcg can vary with α, including how it is possible to trim an unstable aircraft and how is possible for an aircraft to be stable without being able to trim at a useful incidence.

1.5 Aerodynamic centre and neutral point

The forces and moments acting on an aircraft depend on the shape of the aircraft and not on the position of the centre of gravity so we consider the aerodynamic loads separately from the gravitational.

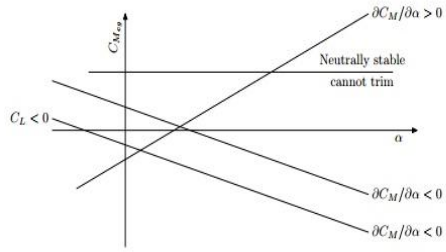

Fig. 5 Trim and Stability

Figure 6 shows a pressure distribution on an aerofoil section. The loads can be considered to act at a point, the centre of pressure, however, moves as the incidence varies, so it is not very useful as a reference point in calculations involving changing incidence.

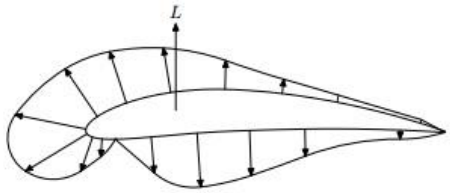

Fig. 6 Centre of Pressure

To make life easier, we can give up the requirement that the moment about our reference point be zero and, instead, allow it to have some finite value as long as the reference point is fixed and the moment is constant. We can do this by looking at the incremental pressure distribution, sketched in Figure 7.

If we think about the basic equation of stability, we can consider what happens to an aircraft which pitches slightly nose-up. Depending on the position of centre of gravity, relative to the aerodynamic centre, the aircraft will be stable, unstable or neutrally stable as shown in Figure 8.

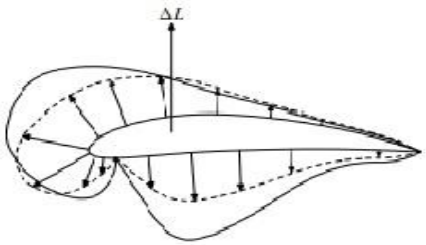

Fig. 7 Incremental Loads

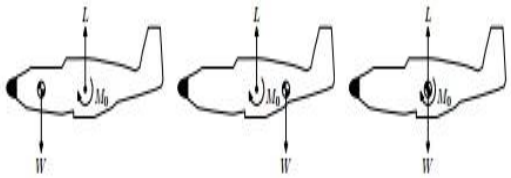

Fig. 8 Centre of gravity and aerodynamic centre Relationships

- If the centre of gravity is forward of the aerodynamic centre, $\frac{dM_{cg}}{d\alpha}$ is negative and the aircraft is statically stable.
- If the centre of gravity is aft of the aerodynamic centre, $\frac{dM_{cg}}{d\alpha}$ is positive and the aircraft is statically unstable.
- If the centre of gravity is at the aerodynamic centre, $\frac{dM_{cg}}{d\alpha}$ is zero and the aircraft is neutrally stable.

II. CONTROL AND STABILITY CHARACTERISTICS IN SUKHOI T-50 PAK FA

The aircraft has a fly by wire with adequate redundancy. This came in 2010 and now it expands its flight envelope. Depending on the flight conditions, signals from the control stick position transmitter or the FCS may be coupled to the remote control amplifiers. Now this aircraft perform sustained-altitude flat rotation manoeuvres and high angle of attack. Four T-50 prototypes have now flown and fifth one will come soon in the field and the production aircraft will enter service in 2016.

T-50 PAK FA (Perspektiyny Aviationny Kompleks Frontoyoy Aviatsii-Future Tactical Air System) Fighter is blended wing-body design, resembling the Su-27 in one key respect: the core of the structure is the "centroplane", a long chord, deep-section inner wing to which the rest of the airframe components-the forward fuselage and widely separated engine nacelles, wings and tail surfaces are attached. Compared to the Su-27, however, the centroplane is deeper between the engines, to accommodate weapon bays.

The flight control system has 14 effectors-12 moving flight surfaces and the engine nozzles. The leading edge flaps are use symmetrically to maintain lift at high angles of attack and adjust the profile to the Mach number. The ailerons are used only at low speed and take-off and landing, when the flaperons are used to increase lift.

The moving vertical tails sit on short fixed pylons that contain the actuators and the air intakes for engine compartment cooling and heat exchangers.

The vertical tail replaces the airbrake, moving symmetrically to increase drag with minimal pitch moment.

The centerline structure on the T-50 has to be quite shallow, so that designing it to resist peak wing bending loads will be a very difficult challenge. The solution on the T-50 is to design the "centroplane" section as a stiff, integrated structure with two sets of full-depth longitudinal booms, located at the outer edges of the nacelles and at the wing-to-Centro plane junction. These are connected by multiple (the patent drawing shows eight) spanwise spars that also carry the wing attachment fittings. The result is a structure that spreads the bending loads over the Centro plane and reduces the peak loads at the centerline.

It is believed that the target maximum speed of the T-50 is around Mach 2. The goal was originally Mach 2.35, but this was reduced to Mach 2.1 and then to the current figure, compared to Mach 2.25 for the Su-35S. The main reason for the difference is that the T-50 uses more composite materials in its primary structure than the Su-35S, which makes heavy use of titanium. The T-50 aircraft flying today are equipped with the izdeliye (Type) 117 engine, described by its designer in a 2011 interview as being more advanced than the 117S used on the Su-35S. The 117S appears to be an evolution of the AL-31 engine series with some technology from the 117. The 117 is claimed to have a thrust/weight ratio of 10:1.

2.1 Stability and Control characteristics of Boeing-737

The primary flight controls are intrinsically safe. In the event total hydraulic system failure or double engine failure, they will automatically and seamlessly revert to control via servo tab. In this mode, the servo tabs aerodynamically control the elevators and ailerons.

2.1.1 Roll

Ailerons are powered by hydraulic systems. If the aileron system jams, the co-pilots wheel can be used to move the spoilers. There are balance tabs and balance panels on both ailerons.

Aileron trim moves the neutral position via the feel and centering mechanism. There are two aileron trim switches to prevent spurious electrical signals from applying trim.

2.1.2 Spoilers / speedbreakes

Flight spoilers augment the ailerons and are powers by hydraulic systems. On landing, if armed, all spoilers will deploy when the thrust levers at idle and any two wheels have spun up or right gear is compressed. If not armed, the speed breakers will deploy as well.

2.1.3 Yaw

The rudder is moved by a PCU powered by hydraulic system. There is no manual reversion for the rudder. The yaw damper system can move the rudder a maximum of 2 degrees (-1/200), 3 deg (-3/4/500), 2 deg (NG flap up), 3 deg (NG flap down), either side of the trimmed position. Yaw damper

inputs are not fed back into the rudder pedals, which is why there is an indicator.

2.1.4 Pitch

The control column moves the elevators using hydraulics. If the elevator system jams, the stabilizer (trim) should still be available. There are balance tabs and balance panels on both elevators.
Pitch trim is applied to stabilizer. Trim can be applied by electric trim switches, autopilot or manual trim wheel. Speed trim is applied to the stabilizer automatically at low speed, low weight and most of take-offs.

2.1.5 Short-field Performance Enhancement Program

This package was developed in 2005/6 to allow GOL airlines to operate their 737-800s into the 1,465m (4,800ft) Santos Dumont airport. Various modifications enable weight increases of approximately 4,700kg (10,000lbs) for landing and 1,700kg (3,750lbs) for take-off from short runways. It includes the following changes:

- Flight spoilers are capable of 60 degree deflection on touchdown by addition of increased stroke actuators. This compares to the current 33/38 degrees and reduces stopping distances by improving braking capability.
- Slats only travel to Full Ext when TE flaps are beyond 25 (compared to the current 5). Autoslat function available from flap 1 to 25.
- Flap load relief function active from flap 10 or greater.
- Two-position tailskid that extends an extra 127mm (5ins) for landing protection. This allows greater angles of attack to be safely flown thereby reducing V*ref* and hence landing distance.
- Main gear camber (splay) reduced by 1 degree to increase uniformity of braking across all MLG tyres.
- Reduction of engine idle-thrust delay time from 5s to 2s to shorten landing roll**.**

III. CONCLUSION

The general equations and theory is almost same behind the manufacturing of all types of plane. Flight stability is the prime concern in which different axis stabilities as well as control measures are taken care in special concern. Flight dynamics is the science of air vehicle orientation and control in three dimensions. The three parameters are the *angles of rotation* in three *dimensions about the aircraft center of mass,* known as pitch, roll and yaw. Roll, pitch and yaw refer to rotations about the respective axes starting from a defined equilibrium state. We can conclude that mechanism is almost same in commercial and fighter aircraft only application of this concept if stability and control is applied in different ways.

REFERENCES

[1] Roy Langton, Stability and Control System of Aircraft System, Introduction to classical feedback Contro," *John Wiley & Sons Ltd*, 2006.
[2] David A. Caughey, "Introduction to Aircraft Stability and control*," Cornell Un iversity*, New York, Ithaca, 2011.
[3] John Anderson, "Introduction to flight," *McGraw-Hill, New York, Fourth Edition*, 2011.
[4] Elkin, B., and Reid, L., "Dynamics of Flight and control, Wiley & Sons," 1996.

International Journal of Engineering Research and Applications (IJERA) ISSN: 2248-9622
National Conference on Advances in Engineering and Technology
(AET- 29th March 2014)

RESEARCH ARTICLE OPEN ACCESS

Effects of Different Variables on Magnetic Abrasive Powder in Mechanical Alloying Method

Gurpreet Singh*, Sehijpal Singh**
*(Department of Mechanical Engineering, Baba Banda Singh Bahadur Engg. College, Fatehgarh Sahib, India
batth.gurpreet@gmail.com)
** (Department of Mechanical Engineering, Guru Nanak Dev Engg. College, Ludhiana, India
mech@gndec.ac.in)

ABSTRACT
The purpose of this study is to analyze the effects of different variables on magnetic abrasive powder in mechanical alloying process which are suitable for magnetic abrasive finishing process. The parameters such as milling time, ratio of abrasives, speed of agitated shaft plays vital role in manufacturing of magnetic abrasives. It has been observed from the experiments of the present investigation that for magnetic abrasive powders, optimum results are obtained when milling is carried out with milling time 60 min, ratio of abrasives is 40% in the iron powder and 250 rpm of the agitated shaft.
Keywords – Magnetic Abrasives, Magnetic Abrasive Finishing, Attrirtor, Mechanical Alloying, Ball Mill.

I. INTRODUCTION

The mechanical alloying (MA) process, using ball-milling techniques, has received much attention as a powerful tool for the fabrication of several advanced materials including equilibrium, non equilibrium and composite materials. The MA is a unique process in which a solid state reaction takes place between the fresh powder surfaces of the reactant materials at room temperature. It can be used to produce alloys and compounds that are difficult or impossible to obtain by the conventional melting and casting techniques. Basically the ball milling has evolved from being standard technique in milling of ores in mineral dressing and particle size reduction in powder metallurgy to important techniques for the preparation of materials with enhanced mechanical and physical properties either new phases or new engineering materials. Mechanical alloying may be defined as a method for producing composite metal powders with a controlled fine microstructure. It occurs by the repeated fracturing and re welding of powder particles mixture in a highly energetic ball mill [1]. As originally carried out, the process requires at least one fairly ductile metal to act as a host or binder. Other components can consist of other ductile metals, brittle metals, and inter metallic compounds or nonmetals and refractory compounds. The high energy involved in the MA process fragments and cold re-welds powder particles that form the initial mix. The powder particles are continuously trapped between colliding balls and balls container what raises the level of micro structural strain, enhancing its mechanical properties. Besides high energy milling can bring many changes to powders subject to such a process, including refinement of particle size and crystallite size, formation of amorphous phases, deformed bonds at surfaces and changes in boundary energies. Because of these changes the free energy of reactants and the kinetics reaction can be substantially modified. Mechanical alloying is the generic term for processing of metal powders in high-energy ball mills. However, depending on the state of the starting powder mix and the processing steps involved, different terms have been used in the powder metallurgy literature. Two different terms are most commonly used to describe the processing of powder particles in high-energy ball mills. Mechanical alloying describes the process when mixtures of powders (of different metals or alloys compounds) are milled together. Thus, if powders of pure metals A and B are milled together to produce a solid solution (either equilibrium or supersaturated), inter metallic, or amorphous phase, the process is referred to as MA. Material transfer is involved in this process to obtain a homogeneous alloy [2].

1.1 MAGNETIC ABRASIVE

Magnetic abrasive is a mixture of non-ferromagnetic abrasive and ferromagnetic iron particles used to do finishing operation with the aid of magnetic force. The iron particles in the mixture are magnetically energized using a magnetic field. The iron particles form a lightly rigid matrix in which the abrasives are trapped. This is called Flexible Magnetic Abrasive Brush (FMAB), when given

relative motion against a metal surface, polishes that surface. Some common types of magnetic abrasives are: sintered, bonded, adhesive based, unbonded, plasma based, others magnetic abrasives etc [3].

II. LITERATURE REVIEW

Previous literature available on mechanical alloying and different methods for manufacturing of magnetic abrasives mainly focused on the following broad areas:

- Development of various experimental set ups consists of provisions to give different-Parameters, capabilities.
- Optimization of process parameters of mechanical alloying using various experimental-set ups.

2.1 SINTERED MAGNETIC ABRASIVES

Lin et. al. (2007) prepared the magnetic abrasives by typically mixing iron powder (60 wt %) and Al_2O_3 (40 wt %) with average size of 5μm) and compressing mixture into the cylindrical shape. These compacts were sintered into a vacuum furnace. After sintering process, these cylinders were crushed to produce magnetic abrasives of average size 150 μm. The ball-shaped magnetic pole with special grooves was used with these magnetic abrasives. It was found that the design increased the finishing efficiency and created a good surface finish for the non-ferromagnetic material, SUS304. The best surface finish was obtained at a working gap of 2.5 mm, a feed rate of 10 mm/min, and an abrasive mass of two grams. The obtained maximum percentage improvement surface roughness was 60%. These abrasives were used for finishing of SS 304 material.

Zhang et. al. (2011) studied on magnetic abrasive finishing by sintering method and research on tests of magnetic abrasive finishing, analyses the effect of the sintering temperature, ratio of magnetic and abrasive particle size, sintering time and sintering characteristics of magnetic particles on magnetic abrasive during the finishing process, so as to achieve a better process and principle for magnetic abrasive finishing. The obtained maximum percentage improvement surface roughness was 65%. These abrasives were used for finishing of SS 304 material.

2.2 ADHESIVE BASED MAGNETIC ABRASIVES

Feygin et. al. (1998) prepared magnetic abrasives by mixing iron powder, Al_2O_3 and glue as adhesive (commercially known as an industrial crazy glue). Iron and abrasive particles were strongly bonded with each other by the glue. They reported that this method was simple as compared to the other methods for preparation of the magnetic abrasives. MRR was higher as compared magnetic abrasives prepared by other methods. The obtained maximum percentage improvement surface roughness was 49%. These abrasives were used for finishing of SS 304 material.

Kremen et. al. (1999) developed magnetic abrasives using an adhesive to bind magnetic component (iron powder) with abrasive component (diamond powder). All the three components were mixed thoroughly, dried and crushed into small particles of desired size for machining. Then by using glued magnetic abrasive powder and keeping magnetic flux density 0.4 tesla, machining time 5 minute and adding 4% of boric acid in water as cooling fluid, the effect of powder grain size on the surface roughness and MRR of a silicon wafer and tube was observed. The obtained maximum percentage improvement surface roughness was 45%. These abrasives were used for finishing of SS 316 material [4].

2.3 PLASMA BASED MAGNETIC ABRASIVES

Anzai et. al. (1989) developed NbC based magnetic abrasives by plasma powder melting (PPM) technique. NbC particles (65% by volume) were dispersed uniformly in the matrix of iron. The obtained maximum percentage improvement surface roughness was 51%. These abrasives were used for finishing of SS 304 material.

Yamaguchi et. al. (2008) developed spherical iron-based magnetic abrasive, which carries Al_2O_3 grains on the surface, made by plasma spray. First, they examined the feasibility of the plasma spray to make the existing magnetic abrasive more spherical, and suggested the conditions needed to produce the spherical magnetic abrasive. Secondly, they developed the new spherical magnetic abrasive made of separate particles: WA Al_2O_3 abrasive grains and iron particles in the ratio of 1:12, which carry the nonferrous abrasive on the outer surface alone. The obtained maximum percentage improvement surface roughness was 47%. These abrasives were used for finishing of brass material.

Handa et. al. (2008) fabricated fine spherical iron-based magnetic abrasives of diameter less than 10 μm by plasma spraying. Carbonyl iron powder with 7.2 μm average sizes was used as the magnetic matrix powder and diamond particles of average size 0.31 μm (10% by volume) were used as abrasive grains to produce a composite powder. The diamond particles were thermally diffused into the iron powder during plasma spraying. After the powder mixtures passed through the plasma flame, the powder mixtures were rapidly cooled and then were recovered in the powder

recovery vessel. The obtained maximum percentage improvement surface roughness was 50%. These abrasives were used for finishing of SS 316 material [5].

2.4 UNBONDED/LOOSELY BONDED/MIXED MAGNETIC ABRASIVES

Fox et al. (1994) used unbonded magnetic abrasive for finishing of ceramic. The obtained maximum percentage improvement surface roughness was 26%. These abrasives were used for finishing of ceramic rollers.

Shinmura & Yamaguchi (1995) prepared mixed type of magnetic abrasives by mixing of iron particles of various sizes and sintered magnetic abrasives. These mixed magnetic abrasives were used for internal finishing of SUS304 steel tubes and clean gas bomb shells. They found that the magnetic force of the mixed-type magnetic abrasives takes the median value between those of the magnetic abrasive and iron particles. The magnitude of magnetic force increases with increasing mixed weight percentage of iron particles but the number of the cutting edges gets reduced. The obtained maximum percentage improvement surface roughness was 30%. These abrasives were used for finishing of SS 316 material.

Yamaguchi & Shinmura (2000) used loosely bonded magnetic abrasives (2.4 gm iron of size 510 µm, 0.6 gm Al_2O_3 of size 80 µm and 0.36 ml straight oil type grinding fluid) for internal finishing of tubes using pole rotation system. They reported that with a weaker magnetic field on the abrasives and oversupply of the abrasives in the machining area result in jumbling of abrasives. The jumbling resulted in increased material removal but poor surface finish. This was caused by the aggressive contact of the abrasives against the surface. The obtained maximum percentage improvement surface roughness was 21%. These abrasives were used for finishing of brass material.

Jain et al. (2001) used loosely bonded magnetic abrasives (mixture of iron, Al_2O_3 and lubricant) for external finishing of stainless steel cylindrical rod of diameter 48-50 mm. It was reported that the improvement in the surface finish is 60.83% with MRR of 58.6 mg/min. These abrasives were used for finishing of SS 304 material.

Yamaguchi et al. (2001) used loosely bonded magnetic abrasives (0.56 gm iron of 330 µm, 0.14 gm Al_2O_3 of 80 µm and 0.2 ml soluble type barrel finishing compound) for finishing of SUS304 stainless steel elbows of radius of curvature R30, R46, R80 using pole rotation system. The obtained maximum percentage improvement surface roughness was 26%. These abrasives were used for finishing of SS 304 material.

2.5 MECHANICAL ALLOYING METHOD

Hakaru et. al. (1996) developed Si-M alloy powder by mechanical alloying process. In this process the crystalline powder of Si-M (Fe or Co) in the composition ratio varying from Si-M= 1:2 to 2:1 were mechanically alloyed by the laboratory ball mill in an inert atmosphere. The amorphization reaction between Si and M proceeded according to a second order reaction.

Halil et. al. (2005) produced Fe-Fe_3C composite powder by mechanical alloying process. The elemental iron powder containing 1 wt% carbon was carried out under Argon atmosphere by using a high energy ball mill for various milling time. In order to compare and determine the effect of MA on properties the same amount of powders were mixed by a conventional mixer up to 5 hr[6-7].

III. MANUFACTURING OF MECHANICAL ALLOYED MAGNETIC ABRASIVE

Mechanical alloyed magnetic abrasives (MAMA) have been developed for efficient finishing of internal surface of tubes & outer surface of rods. Mechanical alloyed magnetic abrasives (MAMA) consisting of iron powder and Al_2O_3 have been mixed in a suitable proportion in a stirred ball mill.

The main motive is to identify the best parameters of the mechanical alloying that produce a more homogeneous embedment of the abrasive particles in the iron particles. In this study the design expert approach has been used for the systematic variations of the mechanical alloying parameters. By using design expert approach we are able to manufacture eight samples of the magnetic abrasive powder. The MA step involves a large, and indeed combinatorial, number of mechanical alloying variables such as: Alloying time, RPM of agitate shaft, Ratio of Fe- Al_2O_3 powder, Base alloying powders size, Selection of grinding media, Ball mass to powder mass ratio. It is not possible to control all of these milling variables for this study, but the milling variables that are tested include the milling time, Fe & Al_2O_3 powder ratio, RPM of agitated shaft. A baseline milling condition is established, and each sample manufactured with a single variable and held the others fixed, with the help of design expert a relative comparison between the samples is considered.

3.1 SELECTION OF PROCESS PARAMETERS

In MAM, the machining is associated with many factors. Time of machining, quantity of abrasives, work piece- magnet gap, magnetic flux density and rotational speed of the work piece are responsible to great extent for smooth finishing in MAM. Mechanical alloying governs the strength and strong bonding of the abrasive layer inside the work piece.

Following parameters are taken into consideration for fine machining with mechanical alloyed magnetic abrasives in MAM.

- Effect of alloying time for magnetic abrasives on surface finish.
- Effect of Fe- Al_2O_3 ratio on surface finish.
- Effect of rpm of agitated shaft on magnetic abrasive powder.
- Effect on surface finish of zinc stearate ratio in magnetic abrasive powder.
- Effect on surface finish of spindle oil in magnetic abrasive powder.
- Effect of mechanical alloyed dry magnetic abrasives on surface finish.
- Effect of unbonded magnetic abrasive on surface finish.
- Effect of quantity of magnetic abrasives used during machining on surface finish.

The comparison of percentage wastage of abrasives is also calculated by comparing the quantity of abrasives wasted when used mechanical alloyed and unbonded abrasive. After studying the review literature we are able to fix the magnetic flux density to 1 tesla [8] [9].

IV. EFFECTS OF DIFFERENT VARIABLES

4.1. Effect of alloying time on finishing

Mechanical alloying time plays an important role in machining process. Several experiments are made to fix the time limit for alloying of magnetic abrasive powder.

In this study when time take 20 minutes for alloying time then we observed during the experimenation internal surface finish of brass pipe was very poor, because alloying time less then 30 minutes then not proper alloying done between the Fe- Al_2O_3 particles, the Al_2O_3 particles were not proper embedd in the iron particles and surface finish was poor inside the brass pipe. In this study when time take 60 minutes for alloying time then we observed during experimentation the surface finish was also good inside the brass pipe. In this study when alloying time taken 90 minutes then we observed during the experimentation the surface finish was also good. But unnecessary alloying were done size of Fe- Al_2O_3 particles were so fine and unnecessary power and time consumptions. Another problem observed, face the problem during paper magnet test. Because particles of Fe- Al_2O_3 are so fine these were not spread properly on the white paper. These were disabling for magnetic separation test.

4.2 Effect of Fe- Al_2O_3 ratio on surface finish

Ratio of Fe- Al_2O_3 particles plays a vital role in manufacturing of magnetic abrasive powder suitable for magnetic abrasive finishing process. Several experiments are conduct to set the ratio of Fe-Al_2O_3 particles.

Following table shows various observations made regarding the effect of relative proportions of iron and abrasive powder and their corresponding behaviour during machining.

As the quantity of the iron was 60% of the weight and the quantity of the abrasive was 40% of the weight then observed good machining rate. Because quantity of iron particles and abrasive particles were. When equal quantity of iron particles and abrasive particles were used then observed the machining rate is very poor because quantity of the iron powder was more then more magnetic forces and quantity of the abrasives are also more then more abrasion were done surface finish was poor.

4.3 Effect on surface finish of zinc stearate ratio in magnetic abrasive powder

Zinc stearate ratio in magnetic abrasive powder plays very important role in surface finish by the magnetic abrasive machining. The ratio of zinc stearate in magnetic abrasive powder was select according to the literature 5% weight of magnetic abrasive powder. In this study the quantity of magnetic abrasive powder is 4gm and quantity of the zinc stearate was .20gm in the magnetic abrasive powder. The effect of zinc stearate observed on the internal surface finish of brass pipe by magnetic abrasive machining was very good, Because zinc stearate very fine and soft powder so zinc stearate provide some softness to magnetic abrasive powder then abrade the very smoothly.

4.4 Effect of spindle oil on surface finish while add in magnetic abrasive powder

The ratio of spindle oil in the magnetic abrasive powder was select according to the literature 2ml in the magnetic abrasive powder. In this study the quantity of magnetic abrasive powder is 4gm. The effect of spindle oil observed on the internal surface finish of brass pipe by magnetic abrasive machining was very good, but comparatively to zinc stearate the surface finish was poor. Because the spindle oil leave the black oil layer on surface of the workpiece. After

machining then black color oil layer appeared on the surface of the workpiece.

4.5 Effect of mechanical alloyed dry magnetic abrasive powder on surface finish

In this study observed the effect of mechanical alloyed dry magnetic abrasive powder on surface finish was very poor. Because dry magnetic abrasive powder had no lubricant such as zinc stearate, spindle oil etc. then rough abrasion was done on surface of the workpiece. After machining abrasion lines were appeared on surface of the workpiece.

V. CONCLUSION

On the basis of Experimental results of the present work, following conclusions have been drawn regarding the internal finishing of brass pipe with MAF:

Amongst all the available varieties of magnetic abrasives, the mechanical alloyed magnetic abrasives give highest surface finish on most of the work materials. The best surface finish is obtained on brass pipe. It is concluded from the results the Percentage of improvement in surface finish was significantly affected by quantity of abrasives in iron, ball to powder ratio, speed of impellers mounted on agitated shaft and alloying time.

REFERENCES

[1] Anzai Masahiro, Yoshida Takumi, Nakagawa Takeo (1996) “Magnetic abrasive automatic polishing of curved surface” RIKEN, 12 (1), 15-16.

[2] Shinmura Takeo, Takezawa koya, Hantano Eiji Toshio, “Study on magnetic abrasive process” Bull Japan Society of Precision Engg., 18 (4), 1984, 347-349.

[3] L. Lu, M.O Lai, Mechanical Alloying, Kluwer Academic Publisher, 1998, Material, Butter worth’s London, 1974, 225-254.

[4] Wang A.C Lee S.J,“Study the characteristics of magnetic finishing with gel abrasive” International Journal of Machine Tools and Manufacture, 49 (1), 2009, 1063-1069.

[5] Yamaguchi Hitomi, Shinmura Takeo, () “Internal finishing process for alumina ceramic components by a magnetic field assisted finishing process” Precision Engineering, 28 (1), 2004, 135-142.

[6] Handa K., Yamaguchi H., Zhou H, “New spherical magnetic abrasives with carried diamond particles for internal finishing of capillary tubes” Diamond & related materials, 17 (7-10, 2008, 1434-1437.

[7] Benjamin, J. S., Volin, T. E. Metall. Trans. 5:1929–1934, 1974.

[8] Gilman, P. S., Benjamin, J. S. (1983). Annu. Rev. Mater. Sci. 13:279–300.

[9] Singh Dhirendra K. Jain V.K Raghuram V. (2005) “On the Performance Analysis of flexible magnetic abrasive brush” Machining Science and Technology, 9 (1), 601-619.

International Journal of Engineering Research and Applications (IJERA) ISSN: 2248-9622
National Conference on Advances in Engineering and Technology
(AET- 29th March 2014)

RESEARCH ARTICLE OPEN ACCESS

Doe: A Key to Optimize Friction Stir Welding of Dissimilar Aluminum Alloys

Rahul Singla*, Bikram Jit Singh**
*(Department of Mechanical Engineering, Geeta Institute of Management & Technology, Kanipla-Kurukshetra)
Email: errahulsingla@gmail.com
** (Department of Mechanical Engineering, Maharishi Markandeshwar University, Sadopur – Mullana)
Email: chann461@yahoo.com

ABSTRACT
The paper deals in emphasizing the importance of DoE in designing the experiments for Friction Stir Welding (FSW) of dissimilar aluminum alloys. DoE provides us series of runs in which purposeful alterations are made to critical process parameters (as input variables) of a system and the effect on response variables is measured. From the available literature, it has been observed that the effect of welding parameters on desired characteristics was determined by taking into consideration one parameter at a time or by using conventional methods like; Single Factor at a Time (SFAT) technique. So without ignoring the limitations of earlier researches, the main focus in this study has been kept on welding of dissimilar alloys (specifically AA-6061 and AA-5086) by using DoE which is quite rarely used Multi-Factor at a Time (MFAT) technique.
Keywords **-** Aluminium Alloys, Critical to Process parameters, Design of Experiments, Friction Stir Welding.

I. INTRODUCTION

Welding is a process of joining two or more similar or dissimilar materials with the application of heat and with or without application of pressure. Filler materials also may or may not be used. In order to join two or more pieces of metals through any welding process, the most essential requirement is heat. Pressure may also be employed but in many processes, it is not essential. There are two types of welding i.e. Fusion Welding and Solid State Welding. In Fusion Welding, there is no pressure applied but a filler material is always used. In Solid State Welding, pressure is applied along with heat but no filler materials are used.

In recent times, focus has been on developing fast and efficient processes that are environment friendly. The spotlight has been turned on ***Friction Stir Welding (FSW)*** as a joining technology, capable of providing welds that do not have defects normally associated with fusion welding processes [16] [10]. The joining does not involve any use of filler metal and therefore any aluminium alloy can be joined without concern for the compatibility of composition, which is an issue in fusion welding [5]. It has been found as one of the most significant welding process invention from the last two decades. Figure 1 shows Systematic Drawing and Process Principle of Friction Stir Welding.

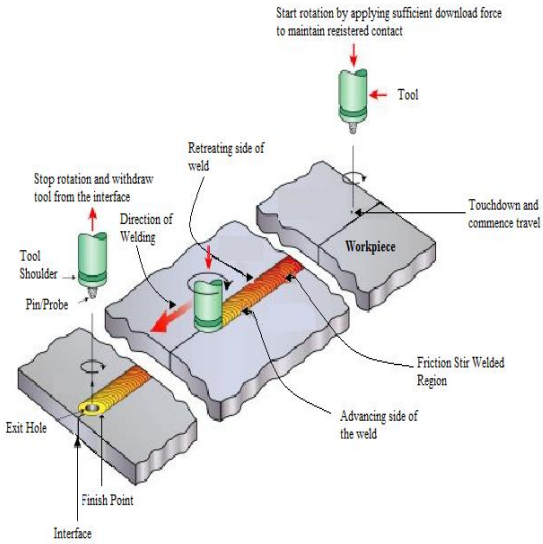

Figure 1: Systematic Drawing and Process Principle of Friction Stir Welding

II. FRICTION STIR WELDING EQUIPMENTS

The major equipments used in FSW are:

2.1 Tool

The tool used in FSW is cylindrical in shape with concave area with a pin which is coaxial with the axis of rotation of the tool. The tool consists of

two main parts i.e. a pin or probe and a shoulder. The function of a tool is mixing of the work piece material and heating by frictional hear and hence material selection of the tool is very important factor. The good tool material should feature following properties:

- Good wear resistance.
- High hardness elevated temperatures and should retain the hardness for an extended period.
- Good static and dynamic properties at welded temperature.
- Mechineability and fracture toughness.

2.2 Machine

A conventional Vertical Milling Machine can be used to carry out the FSW process. The machine must have the ability to apply significant pressure onto the workpiece, should offer wide range of tool rotation and feed rate speeds, provides enough space for its working table to holding the welding assembly and rigidly during the welding operation.

2.3 Fixture

The workpieces to be welded have to be securely clamped to prevent the joint phases from being forced apart. Fixture provides the medium in which workpieces are rigidly clamped. Special types of fixtures can be designed as per requirements. Workpieces are clamped on to fixture which is further mounted on the Vertical Milling Machine.

III. PROCESS PARAMETERS IN FSW

Following are some of the critical parameters of FSW which are detailed out in fig. 2.

3.1 Tool Rotation Speed

One of the crucial parameters that have significant impact on the quality of the weld in FSW is Tool Rotation Speed. The speed at which fixed tool rotates in vertical milling machine is referred to as tool rotation speed. Clockwise rotation can be viewed from above the tool, looking down onto the workpiece. Vertical milling machine offers different tool rotation speeds ranging from very low level to quite high levels. Appropriate selection of the tool rotation speed is very much necessary to cause extensive plastic flow of the materials to be welded.

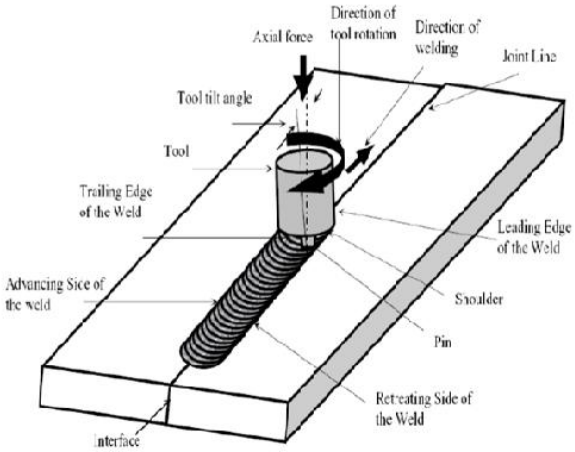

Figure 2: Process parameters in FSW

3.2 Travelling Feed/Feed rate

In vertical milling machine, tool is fixed but only rotates at its position and workpieces that are clamped on to fixture travels. By travelling feed/feed rate, we mean the speed with which workpieces that are clamped onto fixture travels. It may also be termed as welding speed i.e. speed at which welding occurs. The relation between travelling feed/feed rate and the generation of heat during welding is complex but it is generally said that raising the tool rotation speed and reducing the feed rate will result in increasing the temperature at weld surrounding which intern leads to production of successful weld.

3.3 Tool Tip Shape

The shape of the tool is another very important factor that can lead to improvement in both the quality of the weld and maximum possible welding speed. Optimizing tool shape for producing more heat and achieving more efficient stirring offers two main advantages: (i) Improved breaking and mixing of oxide layer. (ii) More efficient heat generation, yielding higher welding speeds and, afcourse, enhanced quality. Different tool tip shapes as used in FSW can be cylindrical, square, triangular, and trapezoidal.

3.4 Tool Tip Plunge Depth

The part of the tool, which paniterates in workpiece during welding is referred to as the probe or tip of the tool. The plunge depth needs to be correctly set, both to ensure that the necessary downward pressure is achieved and to ensure that the tool fully penetrates into the weld region. Plunge depth should be always less than the thickness of the workpiece.

3.5 Tool Tilt Angle

As the tool may in some circumstances be tilted through a small angle, part of the shoulder may

be embedded deeper into workpiece. This angle of tilt is referred to as 'tilt angle'. Tilting the tool by 2-4 degrees, such that rear of the tool is lower than the front, has been found to assist the forging of the material at the heat of the tool.

3.6 Shoulder Diameter

The part of the tool, which is pressed onto the surface of the workpiece during welding is referred to as 'shoulder'. Tool shoulders are designed to produce heat to surface and subsurface region of the workpiece. So one of the most important parameters of the shoulder is diameter because it has significant impact on the amount of frictional heat generated. Greater shoulder diameter increases the pressure force and the weld shape changes which depreciates the mechanical properties of the welds. So the choice of shoulder diameter requires due consideration.

IV. RELATED WORK

A brief account of literature search on existing research work in FSW carried out by other researchers in India and abroad is presented below.

4.1 Literature related to description and introduction of FSW

A detailed study shows that the readiness level of friction stir welding for aluminum is high with several industrial implementations. Recent advances in pin tool designs and optimized processing parameters have enabled friction stir welding applications in the marine, ground, transportation and automotive industries [1]. A brief review on Friction Stir Welding of aluminum alloys where in Friction Stir Welding process, its importance, various parameters (like traverse speed, rotating speed of motion of tool, axial force and till angles) effecting mechanical and microstructural characteristics has been explained. Main emphasis has been on tool geometry and its implication on mechanical and microstuctural characteristics of the weld [16].

4.2 Literature related to selection of critical to process (CTP) parameters in FSW

The effect of the tool shape on the mechanical properties and microstructures of 5-mm thick welded aluminum plates. The simplest shape (column without threads), the ordinary shape (column with threads) and the triangular prism shape probes were used to weld three types of aluminum alloys. It has been found for 1050-H24 whose deformation resistance is very low, a columnar tool without threads produces weld with the best mechanical properties; for 606l-T6 whose deformation resistance is relatively low, the tool shape does not significantly affect the microstructures and mechanical properties. For 5083-O, whose deformation resistance is relatively high, the weldablity is significantly affected by the rotation speed. For a low rotation speed (600 rpm), the tool shape does not significantly affect the microstructures and mechanical properties of the joints [7].

The work on welding of two dissimilar metal joints AA 6061 and SS 400 and to find optimum operating conditions of Friction Stir Welding is carried out. The parameters considered were tool rotation speed, transverse speed (Feed rate), and tool tilt angle. The impact value was used to evaluate the quality of dissimilar metal bute joints. ANOVA test was used to interpret experimental data [5].

In [11], the mechanical and metallurgical properties of dissimilar joints of aluminum alloy AA 6351-76 and Aa5083-A111 is presented. The technique used was Friction Stir Welding. To weld the joints, different welding speeds were used and then their effects on tensile properties were analyzed. The welding process parameters were -7001 Rotation speed in rpm, welding speed in mm/min and axial force in ton [11].

4.3 Literature related to optimization of FSW

The material flow in butt friction welding by combining traditional metallography as well as X-ray and computer tomography (CT) is elaborated [13]. The two and three-dimensional CT images are used in parallel with micrographs for visualization of the 1ow field. Two procedures for estimating the average velocities for material flowing through the shear layer are studied. The procedures depend on the configuration of marker material relative to the welding direction, i.e. longitudinal and transverse [13].

A detailed study on the effect of processing parameters on mechanical and micro structural properties of AA6056 joints produced by Friction Stir welding is performed [4]. Different samples were obtained by employing rotating speeds of 500, 800 and 1000 rpm and welding speeds of 40, 56 and 80 mm/mm. It was observed that the specimens welded at 56 mm/min showed the best behavior in the low cycle regime.

The author investigated on the mechanical and micro structural properties of dissimilar 2024 and 7075 aluminum sheets joined by friction stir welding. Mechanically properties have been evaluated by means of tensile and fatigue tests. The joints exhibit very good ductile properties after yielding and the UTS is settled at high levels. The specimens fracture surfaces after testing have been deeply analyzed by using a FEGSEM microscope, revealing the defects typology and location after the Friction Stirring

process and the microscopic mechanisms occurred during high stress deformations and final failure [3].

In [8], authors used Friction Stir Welding Technique to Aluminum alloy AA-5083 with variation in rotational and transverse speed of tool. During the experimentation, it was found that with increase in transverse speed, heat input generation decreases due to which the cavity or groove like defects were being produced. The Welding parameters considered were rotational speed, transverse speed, plunge depth, tool till initial heating time and tool down speed. The technique of radiography was carried out using digital radiography system.

In [10], authors proposed that with lower welding speed, the weld is perfect and no obvious defects are produced for analyzing defects, technique of radiography was used. With the increase in welding speed, the welding line at bottom is clear and clear flow lines are generated from bottom up to part of weld. Friction Stir welding approach was adopted for welding. As the tool rotation speed increases, the defect rate decreases. The welding parameters that were considered were downward for constant, welding speed constant and rotation speed. Four set of welding trials were made at the base material AA 7075. Tensile test was conducted to determine the tensile properties of weld material, and it was concluded that quality welds could be produced with the tool rotation speeds of 600-1200 RPM [10].

The influence of axial force on the mechanical and metallurgical properties of friction stir welded aluminium alloy AA6082-T651 joints is highlighted [15]. The axial force is varied from 3 kN to 8 kN on the surface of the base material. Tensile test, macrostructure and microstructure tests were performed on all the welded specimens. SEM was used to know the behaviour of the fractured surface of the tensile test specimens. It is found that the joint fabricated at 6 kN axial force has higher tensile strength and good metallurgical properties.

V. GAPS IN EXISTING RESEARCH WORK

The literature found on FSW has not taken into consideration following aspects:

- Most of the work has been conducted on similar alloys like (AA 6061, AA 5083 and AA 2219). Not much work has been done on dissimilar aluminum alloys.
- No significant work has been done on AA 5086 which is indeed very important alloy used in marine engineering and aerospace applications like ship building, fabrication of aircrafts.
- The literature survey indicates that majority of the studies have been conducted by taking into account one parameter/factor at a time (say; tool rotation, tool profile, tool shape, tilt angle etc.). Multi factors at a time have rarely been taken into account. Moreover it is hard to find papers defining impact of two or more factor-combinations or interactions at a time.
- Above literature search indicates that the technique of Design of Experiments (DoE) has not been used in a systematic way and the experiments have been conducted by using hit & trial methods. Prioritization of various CTP parameters is highly lacking.
- The literature surveyed also reveals that wherever DoE has been used, very few had deduced mathematical modeling of process parameters for future scope.

VI. PROBLEM FORMULATION

Without neglecting the limitations of the earlier researches, the main focus in this research has been kept on welding of dissimilar alloys, specifically, AA 6061 and AA 5086. These are two dissimilar aluminium alloys that are widely used in aerospace, ship building and other fabrication industries as these aluminium alloys have high corrosion resistance properties and offers high strength-to-weight ratio. As till now, the design of experiments using multiple parameters was primarily done using traditional approaches. So, in this work, Minitab 16 release software will be used to generate an orthographic matrix of designed experiments. The tool will not only be used to carry out the statistical analysis of experimentation and to generate graphical implications of achieved results but also it will be utilized to optimize the selected process parameters effectively.

Therefore keeping in view the background, literature review and gaps thereon, this research work aims at:

- Selection and prioritization of various Critical to Process (CTP) parameters.
- Identification of key characteristics (Desired Mechanical properties).
- Mathematical Modeling (equation formulation for various key characteristics).
- Optimization through DoE (by using Minitab 16 release version).
- Scope of present work in future.

VII. PROPOSED METHODOLOGY

Keeping in line with the objectives detailed in the Section VI, a step by step methodology of conducting the research work is given in figure 3.

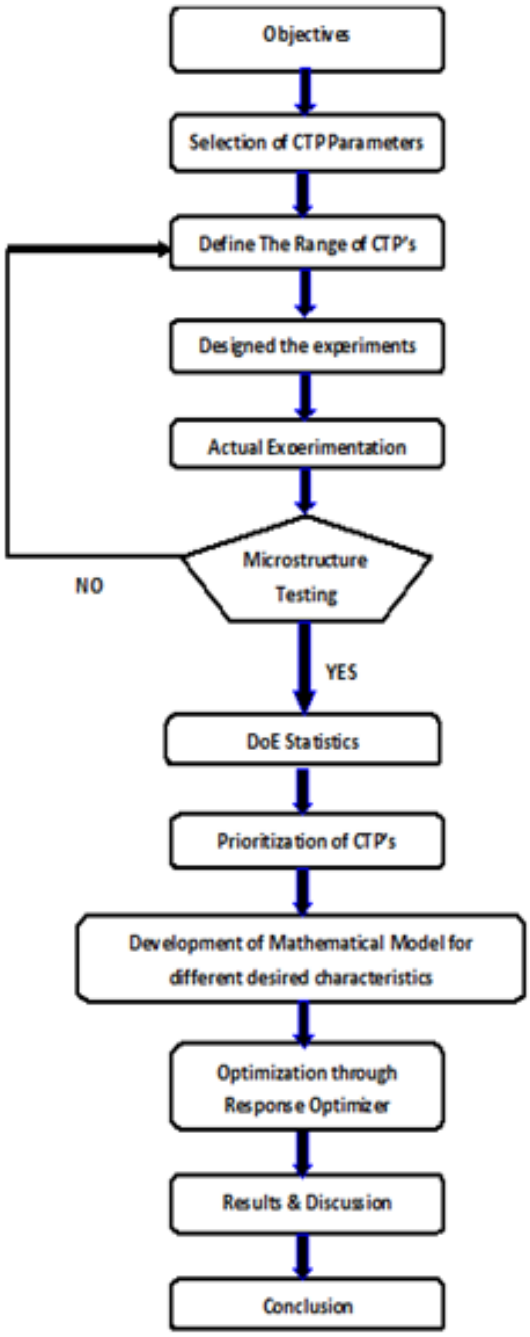

Figure 3: Flow Chart representing methodology that will be adopted to carry out research work.

VIII. CONCLUSION

Majority of the research studies on FSW as per literature review has been done by taking into account one factor at a time (OFAT).(i.e. Tool rotation speed, tool profile, tool tilt angle, welding speed etc.) Multi factors at a time have rarely been taken into account. Traditional methods of conducting mechanical experiments involves hit and trial methodology taking into consideration one factor at a time. The limitations of the traditional methods of designing experiments are overcome by the help of using DoE. These advantages includes assessing the impact of multi factors and their interactions to find out the effect on response variables; determining statistically significant factors which makes optimization process more accurate and presenting the graphical implications of different factors effecting response variables.

REFERENCES

[1] Arbegast, W.J., "Friction stir welding after a decade of development", Welding Journal; NFS center for friction stir processing; South Dekota School of Mines and Technology; 85 (4), 2006, 28-35.

[2] Banwasi, N., "Mechanical testing and evaluation of high-speed and low-speed friction stir welds", Master's Thesis, Wichita State University, 2005.

[3] Cavaliere, P., Campanile G. and Panella F. "Mechanical and microstructural behavior of aluminum alloy sheets joined by friction stir welding", International Journal of Machine Tools and Manufacture; 46 (1), 2006, 588-594.

[4] Cavaliere, P., Campanile G. and Panella F., "Effect of welding parameters on Mechanical and microstructural properties of AA6056 joints produced by friction stir welding", Journal of Materials Processing Technology, 180 (1), 2006, 263-270.

[5] Chen Thai Ping and Lin Wei-Bang, "A study on dissimilar friction stir welding process parameters in aluminum alloys and low carbon steel", International Conference on Smart manufacturing Application, 2008.

[6] Elangovan, K. and Balasubramanian, V., "Influences of tool pin profile and tool shoulder diameter on the formation of friction stir processing zone in AA6061 aluminum alloy", Elsevier, Materials and Design, 29 (1), 2008, 362 373.

[7] Fujjii, H., Lui, L., Maeda, M. and Nogi, V. "Effect of tool shape on mechanical properties and microstructure of friction stir welded aluminum alloys", Elsevier Materials Science and Engineering, A-419, 2006, 25-31.

[8] Joshi, V., Balasubramaniam, K. and Prakash, R.V., "Optimization of friction stir welding parameters for AA5083 by radiography and ultrasonic technique", IEEE – International Ultrasonic Symposium Proceedings; 978-1-4577-1252-4/11, 2011, 1920-1923.

[9] Mehra, S., Dhanda, P., Khanna, R., Goyat, N.S. and Verma, S., " Effect of tool on tensile strength in single and double sided friction stir welding", International Journal of Scientific and Engineering Research, 2012, 3 (1), 1-6.

[10] Muruganandam, D., Sreenivasan, K.S., Kumar R.S., Das, S. and Rao V.S., "Study of process parameters in friction stir welding of dissimilar aluminum alloys", Proceedings of the 2011 International Conference on Industrial Engineering & Operations Management; 2011, 22-24.

[11] Palanivel, R. and Mathews, P.K., "Mechanical and microstructural behavior of friction stir welded dissimilar aluminum alloy", IEEE- International Conference on Advances in Engineering Science and Management, ISBN 978-81-909042-2-3, 2012, 7-11.

[12] Saini, P., Tayal, S.P., Kumar, A. and Kaushik, V., " Experimental study of hardness by friction stir welding of 6061-T6 aluminum pieces", International Journal of Current Engineering and Technology, 3 (3), 2013, 792-794.

[13] Schmidt, H. N., Dickerson, T.L. and Hottel, J.H., "Material flow in butt friction stir welds", Acta Materialia, 54 (1), 2006, 1199-1209.

[14] Singh, A., Sandhu, M. P., Singh, G. and Girdhar, K,.B. (), "Effect of rotational speed on tensile strength & micro hardness of friction stir welded AL2014 and AL5083-aluminium alloy", International Journal of Advance Research In Science and Engineering, 2 (9), 2013, 129-133.

[15] Singh, G., Singh, K. and Singh, J., "Effect of axial force on mechanical and metallurgical properties of friction stir welded AA6082 joints", Journal of Advanced Materials Research, 383-390, 2011, 3356-3360.

[16] Sivashanmugam, M., Ravikumar, S., Kumar, T., Seshagiri R.V. and Muruganandam, D., "A review on friction stir welding for aluminum alloys", IEEE, 978-1-4244-9082-0/10, 2010, 216-221.

RESEARCH ARTICLE OPEN ACCESS

Morphological Characteristics and UTS of Al 5083 after FSW

Neeraj Sharma*, Rajesh Khanna**, Rajat Gupta***, Deepak****
*(Department of Mechanical Engineeering, R.P.Inderaprastha Institute of Technology, Karnal, Haryana Email: neeraj.sharma@live.com)
** (Department of Mechanical Engineeering, Maharishi Markandeshwar University, Mullana, Ambala Haryana Email: raajeshvkkhanna@rediffmail.com)
***(Department of Mechanical Engineeering, R.P.Inderaprastha Institute of Technology, Karnal, Haryana Email: rajatrpiit@gmail.com)
****(Department of Mechanical Engineeering, Geeta Institute of Management and Technology, Kurukshetra, Haryana Email: mithudeepak21@gmail.com)

ABSTRACT
Friction-Stir Welding (FSW) is a solid-state, hot-shear joining process. This process has been utilized in aerospace parts joining process. In this research Al 5083 has been joined and micro-graph has been analysed to study morphological properties. It has been found that onion type ring has been formed during the joining. The heat affected zone (HAZ) is evaluated and the ultimate tensile strength of specimens fabricated from aluminium alloy has also been investigated.
Keywords –AL 5083, FSW, Morphology, tool pin, UTS

I. INTRODUCTION

Friction-Stir Welding (FSW) is a solid-state, hot-shear joining process. The process utilizes a bar-like tool in a wear-resistant material (generally tool steel for aluminum) with a shoulder and terminating in a threaded pin. This tool moves along the butting surfaces of two rigidly clamped plates placed on a backing plate. The shoulder makes a contact with the top surface of the plates to be welded as shown in Fig 1. The heat generated by friction at the shoulder and to a lesser extent at the pin surface and it softens the material being welded [1].

In [3], authors analyzed the FSW on AA5086-O and AA6061-T6 aluminum alloys and found that tool rotational speed significantly affects the amount of maximum tensile residual stress while traverse speed mainly changes the distribution of transverse residual stresses. In [4], authors compared the fatigue strength of FSW with the conventional arc-welding methods: MIG-pulse and TIG. The fatigue strength of FS welded AA 6082 is higher than that of MIG-pulse and TIG welds of the same material. In [5], authors have joined the Al 6013-T4 alloy and X5CrNi18-10 stainless steel and fatigue properties of FS joints were found to be approximately 30% lower than that of the Al 6013-T6 alloy base metal. The hardness value slightly decreases in the thermo-mechanical affected zone (TMAZ) at the advancing side (Al 6013-T4 alloy side).

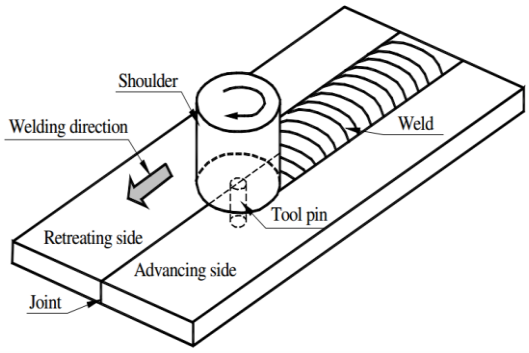

Fig.1: A Schematic representation of FSW [2].

In [6], authors optimized the welding parameters of AZ31 magnesium alloy by friction stir welded to get the best conditions for defect-free weld. The experimental results showed that faster the welding speed is, larger the pore is. In [7], authors made lap joints by FSW of AA 5754 and investigated that increasing tool rotation for a fixed tool pin diameter reduces fatigue strength of joints. Increasing tool pin diameter for a fixed tool rotation, decreases fatigue strength of joints.

Study the friction stir welding (FSW) on AA6082- T6 is made [8], with the conventional tensile tests and local indentation tests to investigate mechanical properties of dissimilar zones of FSW welded joint.

II. EXPERIMENTATIONS

Vertical Milling Machine is used for friction stir welding. 5083 and 6082 aluminium alloy is used for experimental purpose. Al 5083 is an aluminium alloy with magnesium and traces of manganese and chromium. It is highly resistant to attack by seawater and industrial chemicals. Alloy 5083 retains exceptional strength after welding.

The various process parameters used for the friction stir welding are:

Work-Piece	: 6 mm thick AA 5083
Tool pin length	: 5.8 mm
Tool pin diameter	: 6 mm
Tool tilt angle	: 2^0
Axial force	: Constant
Tool Material	: High Carbon Steel
Tool Rotation Speed	: 1950 RPM
Shoulder Diameter	: 20 mm
Welding Speed	: 25 mm/min

(a)

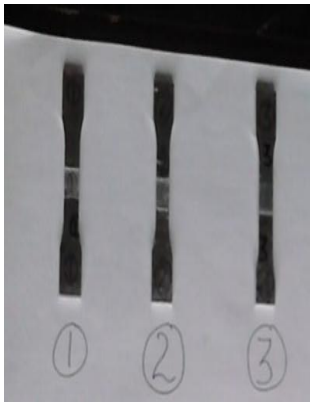

(b)

Fig 2: Specimens (a) after FSW (b) for testing

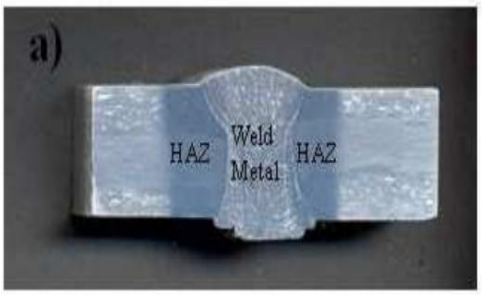

Fig. 3: Principal zones in welding of aluminum

Figure 2 shows the specimen after welding. After a fusion welding process two principal zones are identified in the welded joints named: Fusion Zone (FZ) and Heat Affected Zone (HAZ) whereas in the case of FSW three different zones are formed: stirred zone (nugget), Thermo-Mechanical Affected Zone (TMAZ) and the. These zones are showed in the macrographs of Figure 3.

III. MORPHOLOGY

Cross-sections of the weld joints under the various FSW conditions were observed. Neither cracks nor porosity was visible, showing a good quality. Optical microscopic images of stir zone of FSW specimens are shown in figure 4.

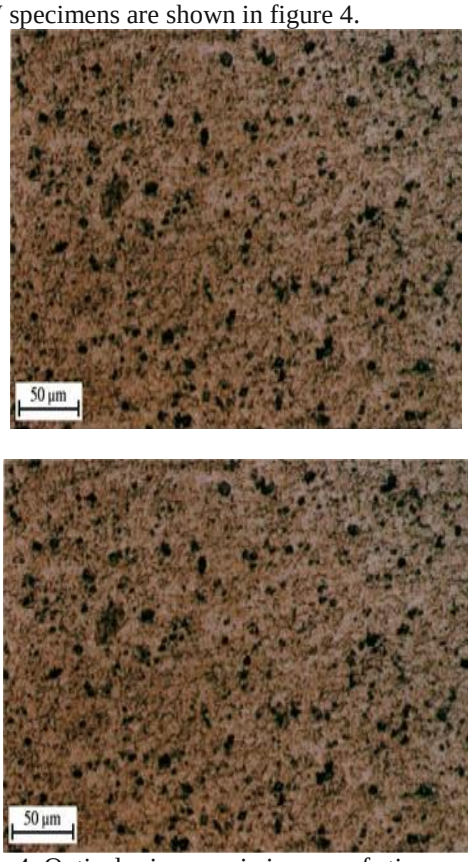

Fig 4: Optical microscopic images of stir zone of FSW specimens (AA 5083)

The microstructure of the welded joint is formally divided into four zones: base material, heat affected (HAZ), thermo-mechanically affected (TMAZ) and stirred zone. The weld nugget is composed of fine-equi-axe-drecrystallized grains, which are formed under the high temperature and high rate of deformation in the weld nugget due to the pin stirring and the size of the crystal grain is about 8ìm in different welding parameters (figure 4). From the testing, the ultimate tensile strength and percentage elongation was measured for the three specimens which were welded with the cylindrical tool pin.

From specimen (1) cylindrical pin profile tool, specimen (2) square pin profile and the specimen (3) trapezoidal tool pin profile tool, the ultimate tensile strength shown in table 1. The maximum tensile strength was obtained for the cylindrical pin tool.

Table 1: UTS according to Tool pin profile

Sr. No.	Tool Pin profile	Ultimate Tensile Strength (MPa)
1	Cylindrical	200.12
2	Square	180
3	Trapezoidal	152.86

IV. CONCLUSION

In this research work, it is observed that quasi-static mechanical properties decrease in a dramatic manner in FSW. The micro-structural transformation in the heat affected zone of very fine needle shape β'' precipitates to coarse bar shape β' precipitates produced by the thermal effect during the welding process (thermodynamic instability).

The experimental result showed that for the parameter under study, the cylindrical tool pin provides the better ultimate tensile strength as compared to square and trapezoidal tool pin structure.

REFERENCES

[1] T Fukuda, Friction stir welding process, *Welding International , 15*, 2001, 611-615.

[2] N T Kumbhar amd K Bhanumurthy, Friction Stir Welding of Al 6061 Alloy, *Asian J. Exp. Sci., 22*, 2008, 63-74.

[3] H J Aval, S Serajzadeh and A H Kokabi, Experimental and theoretical evaluations of thermal histories and residual stresses in dissimilar friction stir welding of AA5086-AA6061, *Int J Adv Manuf Technol, 61*,2012, 149–160.

[4] M Ericsson and R Sandstrom, Influence of welding speed on the fatigue of friction stir welds, and comparison with MIG and TIG, *International Journal of Fatigue, 25*, 2003,1379–1387.

[5] H Hu Uzun, C D Donne, A Argagnotto, T Ghidini and C Gambaro, Friction stir welding of dissimilar Al 6013-T4 To X5CrNi18-10 stainless steel, *Materials and Design, 26*, 2005, 41–46.

[6] H Zhang, S B Lin, L Wu, J C Feng and S L Ma, Defects formation procedure and mathematic model for defect free friction stir welding of magnesium alloy, *Materials and Design, 27*, 2006, 805–809.

[7] M K Kulekci, A Şik and E Kaluç, Effects of tool rotation and pin diameter on fatigue properties of friction stir welded lap joints, *Int J Adv Manuf Technol, 36*, 2008, 877–882.

[8] G Borino, L Fratini and F Parrinello, Mode I failure modeling of friction stir welding joints, *Int J Adv Manuf Technol, 41*,2009,498–503.

International Journal of Engineering Research and Applications (IJERA) ISSN: 2248-9622
National Conference on Advances in Engineering and Technology
(AET- 29th March 2014)

RESEARCH ARTICLE OPEN ACCESS

Effect of Rare Earth Elements on Lead Free Solder Alloys

Prerna Mishra*, S.N. Alam**, Rajnish Kumar***
* (Department of Metallurgical & Materials Engineering, NIT Rourkela, Rourkela-769008 Email: er.prernamishra@gmail.com)
** (Department of Metallurgical & Materials Engineering, NIT Rourkela, Rourkela-769008 Email: syedn@nitrkl.ac.in)
*** (Department of Metallurgical & Materials Engineering, NIT Rourkela, Rourkela-769008 Email: rajnishkumar.me@gmail.com)

ABSTRACT
Sn-Pb solders have been widely used as interconnecting material in electronic packaging and assembly. However, due to environmental and health concern we need to eliminate the usage of Pb bearing solders due to the inherent toxicity of Pb which has led to the development of Pb free solders. Researchers found that the properties of Pb free solders have been improved by doping it with trace amounts of rare earth (RE) elements. This work aims to summarize the effects of addition of RE elements on the wettability, mechanical properties, melting behaviour and microstructure of lead free solder alloys.

Keywords – Sn-Pb, lead free solder, wettability, mechanical properties, melting behavior, microstructure, rare earth elements

I. INTRODUCTION

Environmental related resolutions such as restriction of certain hazardous substances (RoHS) and the waste electrical and electronic equipment (WEEE) have been introduced by many countries [1] [2]. However, legislation that mandates the removal of lead from electronics was introduced by countries such as japan and those in the European Union during the last 15 years. As cited by Environmental Protection Agency (EPA), Pb and Pb containing compounds is one of the top 17 chemicals causing negative impacts to both environment and human body due to which a major change in direction of research into science and engineering of soldering has taken place [3] [4] [5]. 1 July 2006 has been officially designated as the date when the directive on the restriction of hazardous substances in electrical and electronics equipment will require "the use of lead, cadmium, mercury, hexavalent chromium and halogenated flame retardants" be phased out [6]. Electronic manufacturers now have two choices either attaining 100% recycling of Pb or using lead free solder alloys. Recycling rate of electronic devices is very low due to high cost of recycling processes especially for high technology products such as computers so the other alternative is to develop lead free solder alloys [2] [7]. For developing a new solder alloy, one needs to think of various properties such as melting temperature, wettability, mechanical properties, microstructure, cost, availability and reliability of solder joint [8] [9]. Researchers developed a large number of lead free solder alloys. These solders have been tin rich ones with various alloying elements such as Bi, Ag, Cu, In, Zn and Sb. Binary lead free solders such as Sn-Ag, Sn-Cu, Sn-Zn, Sn-Bi and Sn-In cannot fulfill the requirements in electronic packaging and assemblies, additional alloying elements were added to enhance the performance of these alloys. So this led to the development of ternary and even quaternary lead free solders [10] [11] [12] [13]. RE elements has been considered as "vitamins" of metals which means that trace amounts of these elements can significantly improve the properties of metals. In this paper the effects of addition of RE elements on various properties of lead free solder alloys has been summarized.

II. STATE OF ART

2.1 Effects of RE addition of Sn-Bi and Sn-Bi-Ag lead free solder alloys

On addition of trace amounts of RE elements to Sn-Bi and Sn-Bi-Ag has significantly improved the wettability of the solder [16]. The spreading area increases by approximately 50% on addition of RE elements to the solder alloys as shown in Fig. 1.

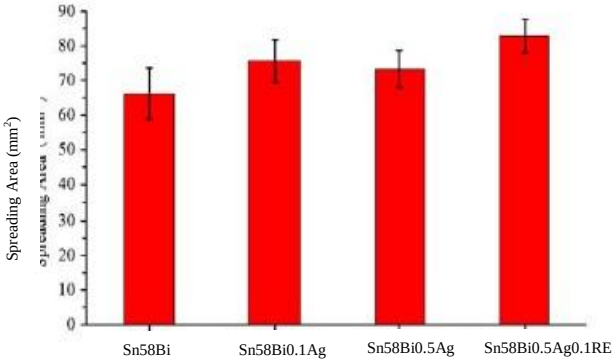

Fig 1: Spreading area of Sn-58Bi based solder alloy

Shear strength of the solder joints increases on addition of RE elements and Ag in both as reflowed condition and after thermal aging. Shear strength of all the solder joints decrease after high temperature aging for 168 hrs. (Aging temperature is 80°C). After aging shear strength of the RE doped solder joints decreased only slightly (less than 2%) as compared to the joints without RE doping (reduced by 7%) as shown in Fig 2.

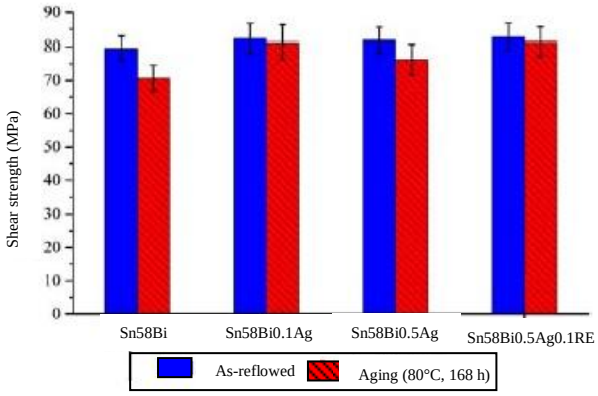

Fig.2. Shear strength of Sn58Bi based solder joints

Microstructure of Sn-58Bi solder is much coarser as compared to other three solders. Addition of trace amount of RE elements and Ag has refined the microstructure [Refer Fig. 3]. Micrographs show that addition of RE elements depressed the rate of coarsening after aging as shown in Fig. 4. Microstructure of RE doped solder is more uniform and width of eutectic colony is thinner.

Two types of intermetallic compounds Cu_6Sn_5 and Ag_3Sn were observed. Addition of RE elements refine intermetallic particles as well as decreases the thickness of interfacial intermetallic whereas high temperature aging an increase in the intermetallic thickness of the solder joint as shown in Fig.5, Fig 6, and Fig 7.

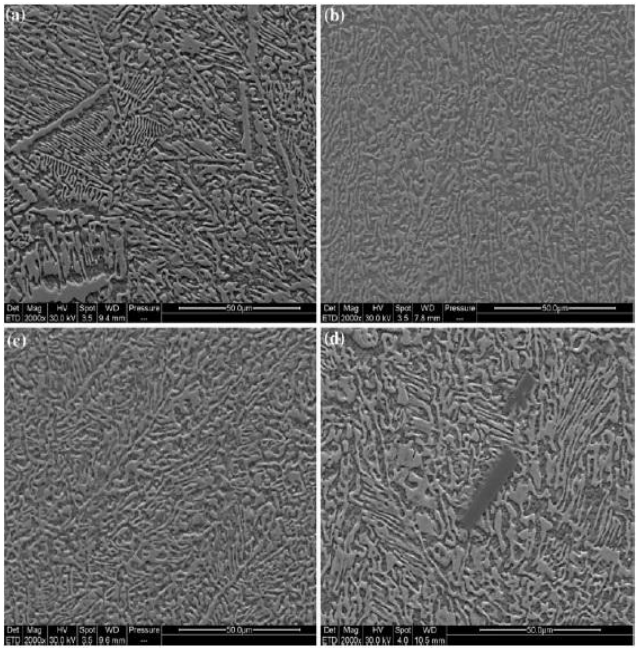

Fig.3. Microstructure of the solder alloys in the as-reflowed state: (a) Sn-58Bi, (b) Sn-58Bi-0.1RE, (c) Sn-58Bi-0.5Ag, and (d) Sn-58Bi-0.5Ag-0.1RE.

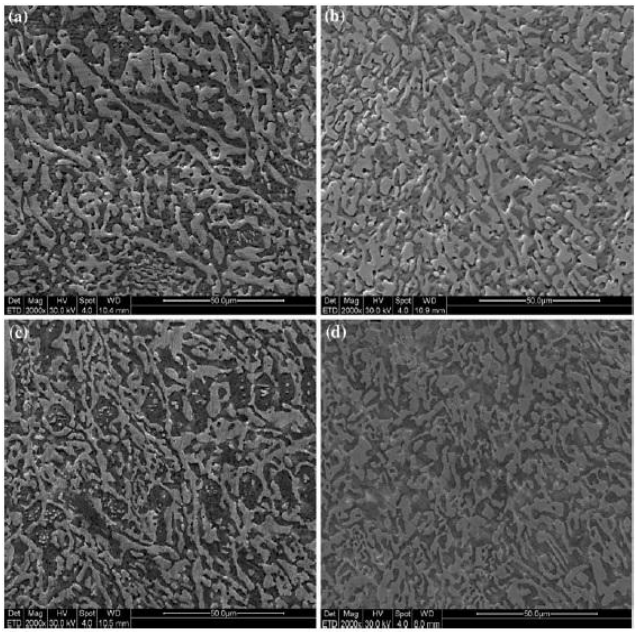

Fig.4. Microstructure of the solder alloys after aging: (a) Sn-58Bi, (b) Sn-58Bi-0.1RE, (c) Sn-58Bi-0.5Ag, and (d) Sn-58Bi-0.5Ag-0.1RE

There is little influence on melting temperature and micro hardness of the solder on addition of RE elements [16].

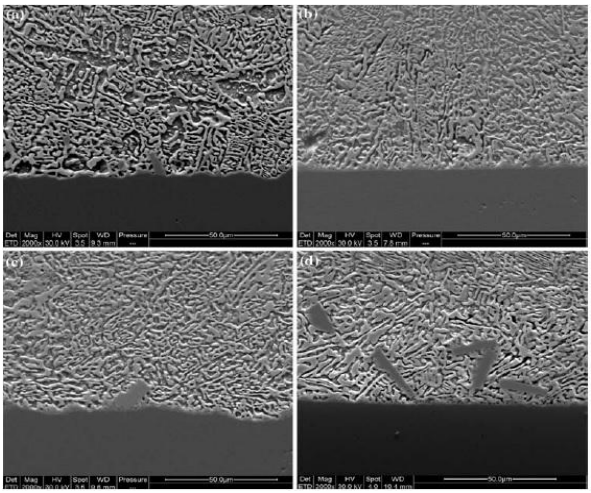

Fig.5. Microstructures at the solder/Cu substrate interface in the as-reflowed state: (a) Sn-58Bi, (b) Sn-58Bi-0.1RE, (c) Sn-58Bi-0.5Ag, and (d) Sn-58Bi-0.5Ag-0.1RE.

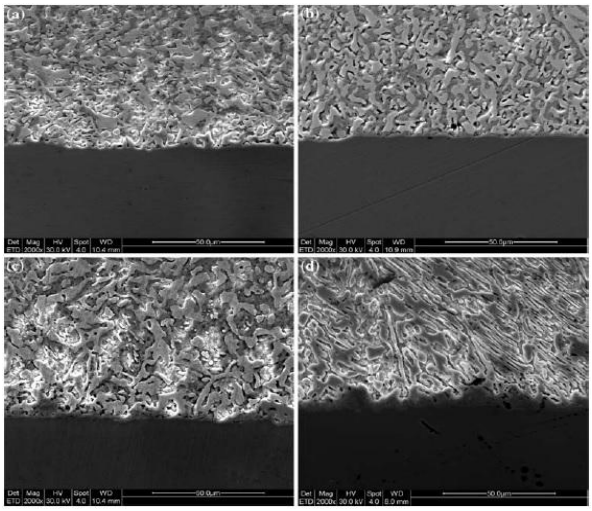

Fig.6. Microstructures at the solder/Cu substrate interface after aging: (a) Sn-58Bi, (b) Sn-58Bi-0.1RE, (c) Sn-58Bi-0.5Ag, and (d) Sn-58Bi-0.5Ag-0.1RE.

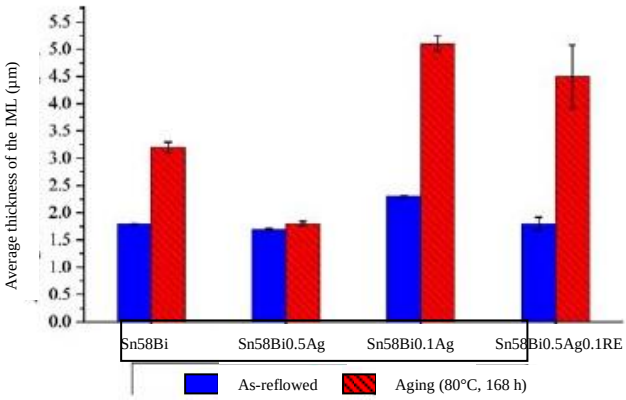

Fig.7. Average thickness of the Intermetallic layer (IML) at the solder/Cu interface.

2.2 Effects of RE on Sn-Zn lead free solder alloy

With 0.05% RE elements the coarse β-Sn grains disappear and the Sn rich phase becomes finer. Microstructure of the solder is uniform as shown in Fig 8 [17].

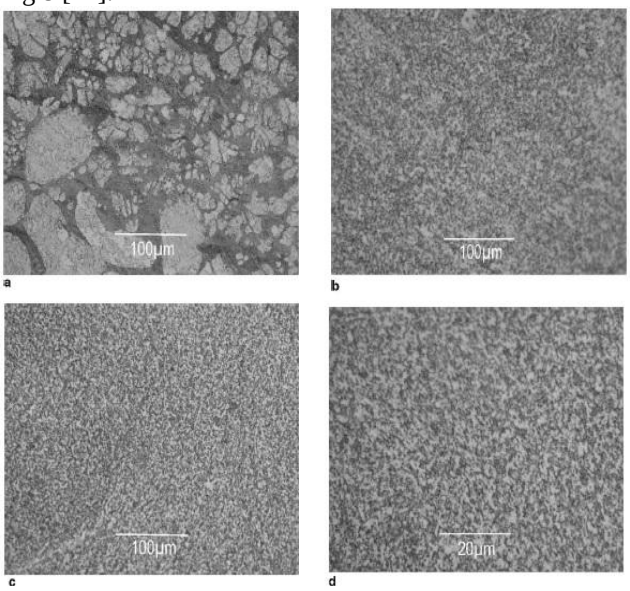

Fig.8. Optical micrographs of chill-cast samples of (a) Sn-9%Zn, (b) Sn-Zn-0.05RE, (c) Sn-Zn-0.5RE, and (d) Sn-Zn-0.5RE (high magnification).

A. On addition of 0.1% Re elements tensile strength is improved by 20% and it increases to 30% on addition of 0.5% RE to the solder alloys whereas elongation is decreased. Proof stress is improved by 0.2% in RE doped solder alloys as shown in Fig 9

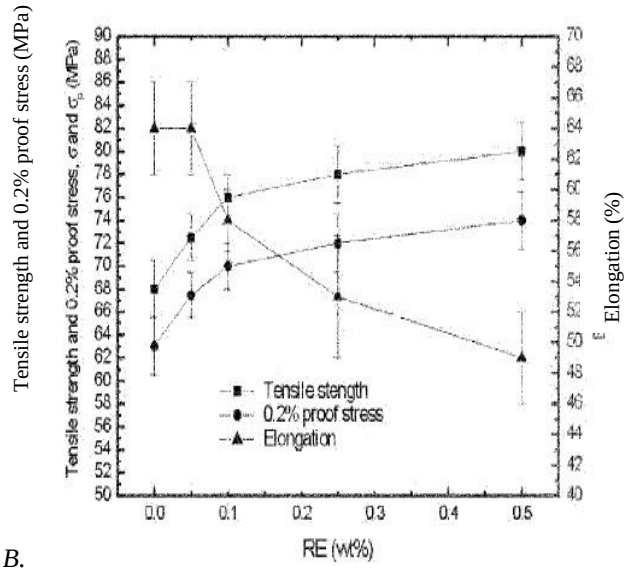

B.

Fig.9. Tensile properties of Sn-Zn, Sn-Zn-0.05RE, Sn-Zn-0.1RE, Sn-Zn-0.25RE, and Sn-Zn-0.5RE alloys

With 0.05% and 0.1% RE addition the wetting properties were significantly improved with RA flux as shown in Fig 10 and Fig 11 [18].

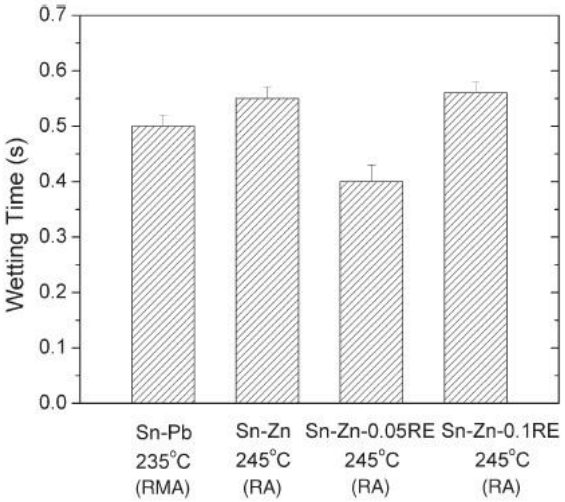

Fig.10. Variation of wetting time with amounts of RE elements at 245°C.

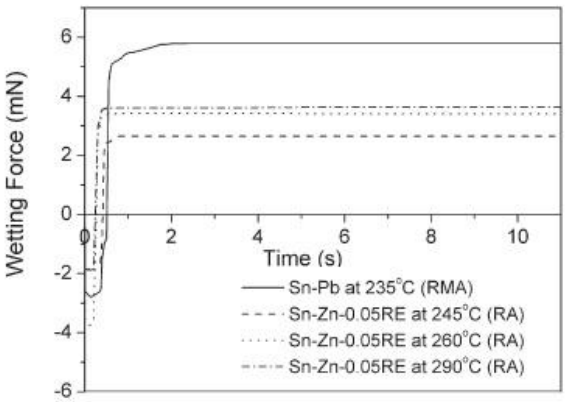

Fig.11. Wetting curves of Sn-Zn-RE solders compared with Sn-Pb.

Micro hardness increases by 13% on addition of 0.05% and 0.1% RE elements to the solders as shown in Fig 12 [18].

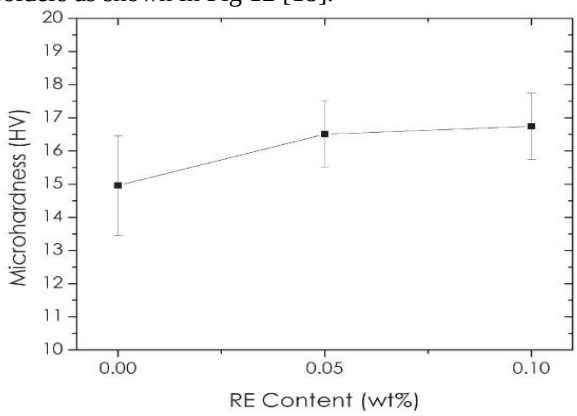

Fig.12. Variation of micro hardness with RE content.

Adding Re elements to the solders has very little influence on the melting temperature as shown in Fig 13 [18].

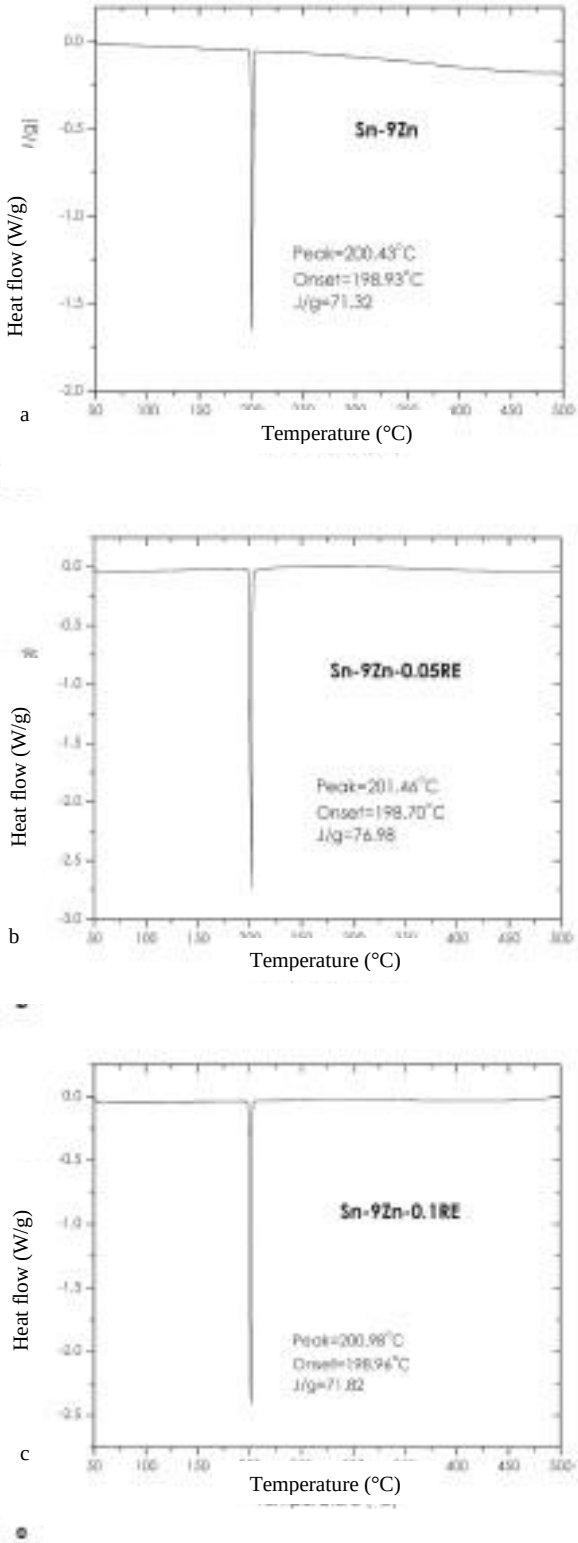

Fig.13 The DSC curves (a) Sn-9Zn, (b) Sn-9Zn-0.05RE, and (c) Sn-9Zn-0.1RE.

2.3 Effect of RE on Sn-Cu lead free solder alloys

On addition of RE elements, about one-third to half of the β-Sn grains have been transformed into smaller grains and the grains are refined as shown in Fig 14 [19].

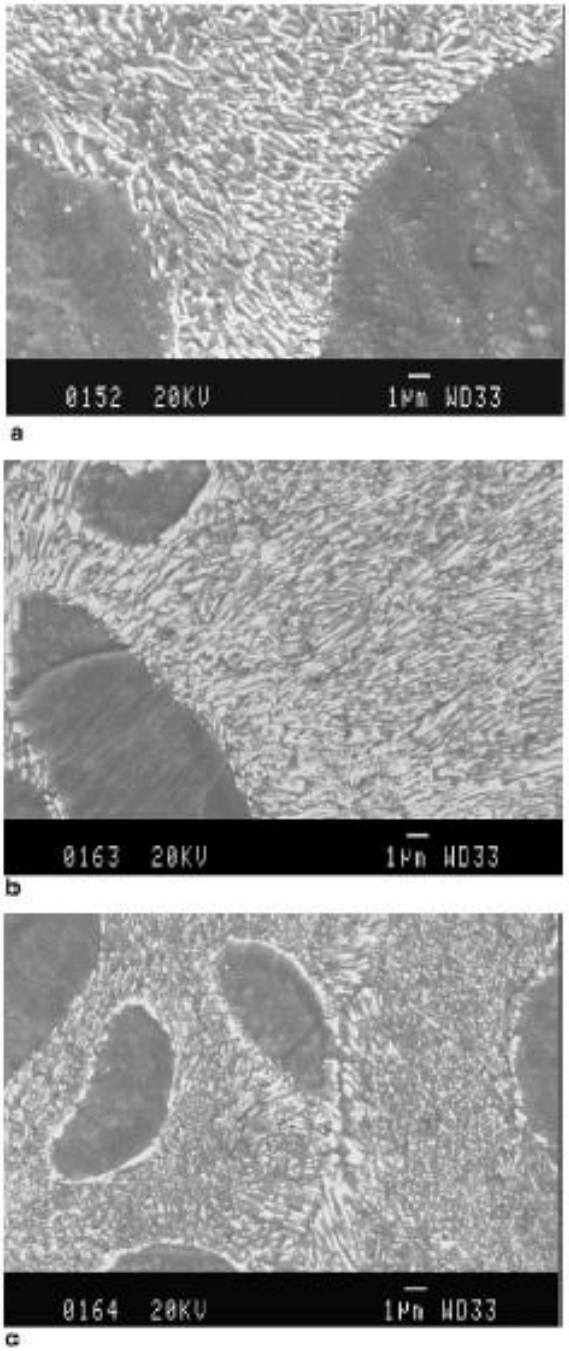

Fig. 14 SEM micrographs for (a) Sn-0.7%Cu, (b) Sn-0.7%Cu-0.25%RE, and (c) Sn-0.7%Cu-0.5%RE.

In the eutectic band Cu-Sn intermetallic were found in the β-Sn matrix. Addition of RE elements decreases the flake size of Cu_6Sn_5 intermetallic and become finely dispersed in the eutectic networks [19].

To study the stability of microstructure the Sn-Cu-RE alloys were aged at 150°C for 20 hrs and it was found that after aging of Sn-Cu, the intermetallic Cu_6Sn_5 particle become coarse and there dispersion was not uniform and also the eutectic colonies were no longer noticeable. The microstructure of Sn-Cu-RE alloys after aging was uniform and the precipitates were fine uniformly dispersed as shown in Fig 15 [19].

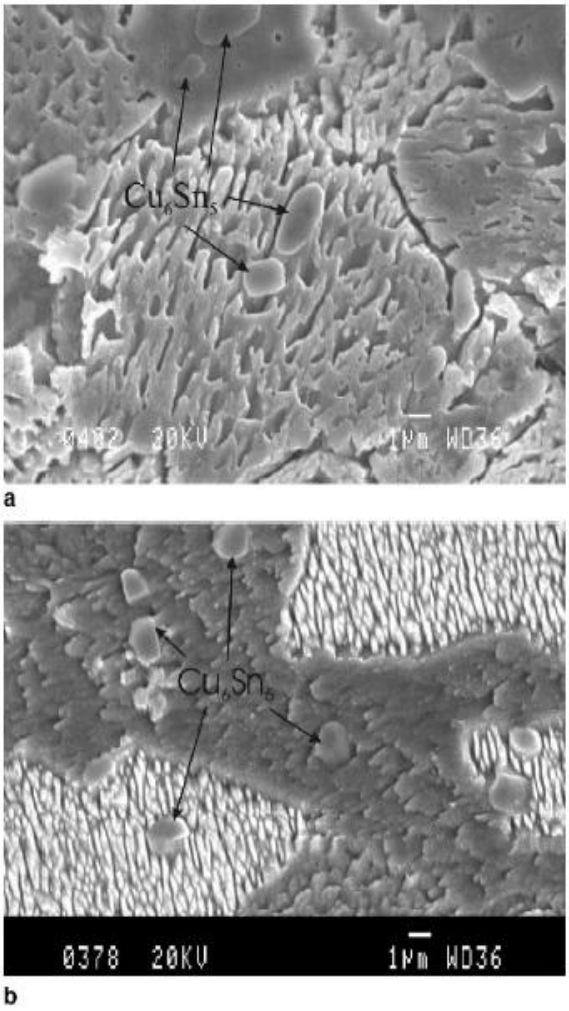

Fig.15 SEM microstructure after aging at 150°C for 20 h: (a) Sn-0.7%Cu and (b) Sn-0.7%Cu-0.5RE.

On addition of 0.25% and 0.5% Re elements increases ultimate tensile strength by 20% and 27 % but there is decrease in elongation as shown in Fig 16 [19].

qqqqqqqqqqqqqqqqqqq

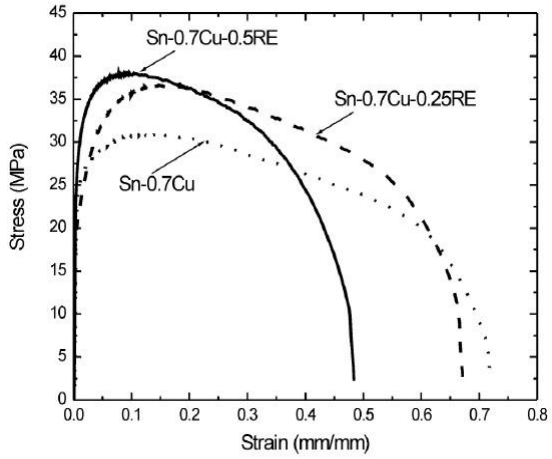

Fig.16. Comparative tensile stress-strain curves for Sn-0.7%Cu, Sn-0.7%Cu-0.25%RE, and Sn-0.7%Cu-0.5%RE solder alloys.

Adding RE elements to the solder increase the hardness for both 10g and 50g load tests as shown in Fig 17 [19].

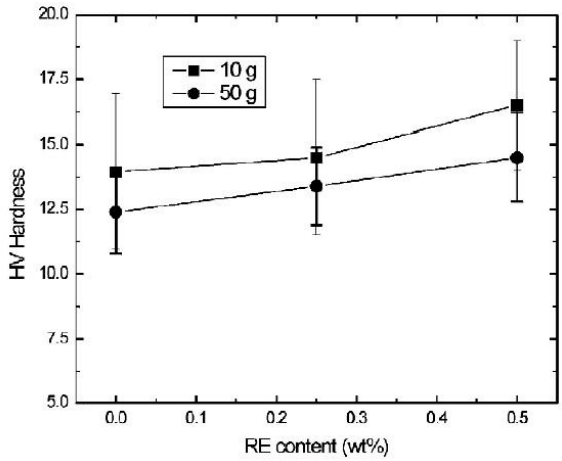

Fig.17. Micro hardness data for Sn-0.7%Cu, Sn-0.7%Cu-0.25%RE, and Sn-0.7%Cu-0.5%RE using 10 g and 50 g loads.

III. CONCLUSION

Addition of trace amounts of rare earth (RE) elements enhances the properties and reliability of lead free solder alloys making the resulting alloys a better alternative for Sn-Pb solder replacement.

The micro structure, tensile strength and hardness of the Pb solder containing RE elements is significantly improved without too much loss in ductility and also the thickness of inter metallic layer is decreased.

Wettability of the solder contain RE elements has been greatly improved because RE have surface active properties which decreases the interfacial surface tension between the solder and the substrate, thus accelerating wetting of the solder alloys.

Addition of RE elements to Pb free solder alloys should be up to a certain range otherwise it would deteriorate the microstructure and other properties.

REFERENCES

[1] Wu, C. M. L., and Y. W. Wong, "Rare-earth additions to lead-free electronic solders", Journal of Materials Science: Materials in Electronics, 18(1-3), 2007, 77-91.

[2] Hwang JS, "Implementing lead-free electronics", McGraw-Hill, New York, 2004.

[3] Allenby BR, Ciccarelli JP, International Proceeding of surface mount international conference, 1–28, 1992.

[4] Wu, C. M. L., et al., Properties of lead-free solder alloys with rare earth element additions, J. Materials Science and Engineering: R: Reports, 44 (1), 2004, 1-44.

[5] E.P. Wood, K.L. Nimmo, "In search of new lead-free electronic solders", J. Electron. Mater., 23(8), 1994, 709-713.

[6] P. Biocca, "Global update on lead-free solders", Surf. Mount Technol. 13 (6), 1999, 64–67.

[7] Ma, Hongtao, and Jeffrey C. Suhling., "A review of mechanical properties of lead-free solders for electronic packaging", Journal of materials science, 44, 2009, 1141-1158.

[8] Kim, Young-Sun, Keun-Soo Kim, Chi-Won Hwang, and Katsuaki Suganuma, "Effect of composition and cooling rate on microstructure and tensile properties of Sn–Zn–Bi alloys", Journal of alloys and compounds, 352, 2003, 237-245.

[9] NCMS, Lead-free Solder Project Final Report, National Center for Manufacturing Sciences, Michigan, Report 0401, RE 96, 1997.

[10] M. Abtew, G. Selvaduray, Lead-free solders in microelectronics, Mater. Sci. Eng. Rep., 27 (5–6), 2000, 95–141.

[11] I.E. Anderson, J.C. Foley, B.A. Cook, J. Harringa, R.L. Terpstra, O. Unal, "Alloying effects in near-eutectic Sn–Ag–Cu solder alloys for improved microstructural

stability", J. Electron. Mater, 30 (9), 2001, 1050–1059.

[12] M. McCormack, S. Jin, G.W. Kammlott, H.S. Chen, "New Pb-free solder alloy with superior mechanical properties", Appl. Phys. Lett., 63 (1), 1993, 15–17.

[13] A.Z. Miric, A. Grusd, "Lead-free alloys", Soldering Surf. Mount Technology, 10 (1), 1998, 19–25.

[14] Z.G. Yu, M.B. Chen, "Rare Earth Elements and their Applications", Metallurgical Industry Press, 1995, 138-273.

[15] Dong, Wenxing, Y. Shi, Z. Xia, Y. Lei, F. Guo., "Effects of trace amounts of rare earth additions on microstructure and properties of Sn-Bi-based solder alloy", Journal of Electronic Materials, 37 (7), 2008, 982-991.

[16] Wu, C. M. L., D. Yu, C. Law, L. Wang, "The properties of Sn-9Zn lead-free solder alloys doped with trace rare earth elements", Journal of electronic materials, 31 (9), 2002, 921-927.

[17] Wu, C. M. L., D. Yu, C. Law, L. Wang, "The Wett ability and Microstructure of Sn-Zn-RE Alloys", Journal of electronics materials, 32 (2), 2003.

[18] Wu, C. M. L., D. Yu, C. Law, L. Wang, "Microstructure and mechanical properties of new lead-free Sn-Cu-RE solder alloys", Journal of electronic materials, 31 (9), 2002, 928-932.

[19] Liang Zhang, S. Xue, L. Gao, G. Zeng, Z. Sheng, Y. Chen, S. Yu, "Effects of rare earths on properties and microstructures of lead-free solder alloys", J Mater Sci: Mater Electron, 20, 2009, 685–694.